Master of Science Thesis

Developing a data based method to quantify the effects of flight track, aircraft weight and engine setting on the received aircraft noise levels

S. de Blok BSc

13 May 2015

Faculty of Aerospace Engineering · Delft University of Technology

TU Delft Delft University of Technology

Challenge the future

Developing a data based method to quantify the effects of flight track, aircraft weight and engine setting on the received aircraft noise levels

Master of Science Thesis

For obtaining the degree of Master of Science in Aerospace Engineering at Delft University of Technology

S. de Blok BSc

13 May 2015

Faculty of Aerospace Engineering · Delft University of Technology

Delft University Of Technology
Department Of
Control & Operations, Air Traffic Performance and the Environment

The undersigned hereby certify that they have read and recommend to the Faculty of Aerospace Engineering for acceptance a thesis entitled **"Developing a data based method to quantify the effects of flight track, aircraft weight and engine setting on the received aircraft noise levels"** by **S. de Blok BSc** in partial fulfillment of the requirements for the degree of **Master of Science**.

Dated: 13 May 2015

Head of department: ______________________
Prof. Dr. D.G. Simons

Supervisor: ______________________
Dr. Ir. M. Snellen

Reader: ______________________
Ir. M. A. Brouwer

Abstract

To provide continuous growth of Amsterdam Airport Schiphol (AAS), the department Stakeholder Strategy and Development (SSD) of Amsterdam Airport Schiphol (AAS) introduces Noise Abatement Measures to create quieter aircraft operations and hence to be able to fly more frequent within the current environmental law related to aircraft noise. However, SSD faces difficulties with the evaluation regarding whether or not an implemented Noise Abatement Measure (NAM) really contributes to a quieter aircraft operation. To evaluate this, often the maximum loudness level L_{max} in decibels is considered. L_{max} is the maximum sound level during a measurement period or a noise event. Nevertheless, L_{max} of aircraft noise is influenced by many factors, for example: flap setting, engine setting, meteorological conditions and landing gear-up/landing gear-down. Therefore, SSD found that it is very difficult to determine the specific contribution of a NAM to the aircraft noise level L_{max}. Hence, AAS demands a technique in improving the distinctive capabilities between noise measurements.
Much information is encapsulated in a noise measurement. Not only are the noise measurements of the Noise Monitoring System (NOMOS) influenced by, for example, aircraft type, configuration and engine setting, but also practical influences as, for example, additional instructions by Air Traffic Control (ATC) to a pilot or departures with de-rated thrust to save fuel influence the noise measurements as conducted by NOMOS significantly.
The goal of this research is to determine the contribution of the implemented NAM to the measured noise level, as to be able to investigate if an implemented NAM contributes to a decrease in exposed noise level.
Besides the ability to quantitatively determine the specific contribution of a NAM to the measured noise level, this research could also be of interest to other industries. For example, the effect of changes in the design of an aircraft to the emitted noise level can be studied by aircraft builders but also this study can be used for law enforcement purposes, as to monitor airports whether or not they comply with the noise restrictions, while this is done now a days by means of theoretical models and not by means of actual noise measurements.

The purpose of the research presented in this report is the determine/estimate two additional aircraft parameters/characteristics and to add this information to the original scattered dataset.

The ultimate goal of this MSc research is to distil the change in noise level resulting from differences in operational procedure in an operational environment.
The method used to quantify the contribution of the predictors to variances in noise level is Multivariate Linear Regression Analysis (MLRA). Predictors are variables that can be used to predict the values of other variables (as in statistical regression). A MLRA model is constructed to calculate noise levels from two predictors: the engine power setting $N1$ and the actual aircraft mass m. However, it appeared to be very difficult to determine m from aircraft performance theories. Nevertheless, the speed at which an aircraft pilot starts pulling the stick to rotate the aircraft during take-off, abbreviated as V_{rot}, was found to be determined by the chosen aircraft flap setting and the actual aircraft mass. Hence, the speed at which the aircraft lifts-off from the ground, abbreviated as the lift-off speed V_{lof}, is determined by the aircraft flap setting and actual aircraft mass as well. Also, V_{lof} can easily be determined from RADAR data as V_{lof} is the speed at which the aircraft gains height for the first time. For this reason, V_{lof} is chosen as aircraft mass representative. From aircraft performance theories it follows that V_{lof} is related quadratically to the aircraft mass, which resulted in V_{lof}^2 to be used as predictor in the MLRA model.
The research limitations are characterized by the fact that this MSc research only focusses on departures as to be able to quantify the aircraft mass representative V_{lof}^2. Hence, V_{lof}^2 can not be used when arriving aircraft are considered. Also, only one aircraft type is studied from which the configuration with regards to the flap setting and flown operational procedure is known. Besides, only two airlines are studied: airline A and B. The amount of measurements of airline A is significantly less compared to the amount of measurements of airline B which limits the statistical substantiation. Also, the noise measurements of only one NOMOS station are used which is situated in a inhabited area for informative purposes with regards to the exposed noise level in that area. In some cases, this limits the quality of the noise measurements/full time series. This research focusses on the addition of two predictors and hence this limits the validity of the results to only those two predictors.

For this study use has been made of a dataset consisting of 263 noise measurements (conducted by NOMOS station 10) and RADAR tracks. This dataset consists of two airlines (A and B) departing from runway 18L (the 'Aalsmeerbaan'), solely Boeing 737-800 aircraft and 7 routes which are divided into two route combinations (southern & western routes combination and eastern routes combination).
The following results were obtained in this MSc research:

- A module is designed linking *four* different information systems of AAS to each other, therefore enabling the user to gather aircraft performance, aircraft track, aircraft noise and aircraft properties in no less than just in few minutes. This module also corrects the 'L_{max} over time'-plot for the actual $N1$ setting and aircraft mass m representative V_{lof}^2 to improve the distinctive capabilities between noise measurements.
- A *N1* Determination Algorithm which is able to determine the flown $N1$ setting from an the associated noise measurement.
- An algorithm able to determine the lift-off speed as used during the take-off of a flight.

- A Multivariate Linear Regression Analysis model is designed, predicting L_{max} levels based on $N1$ and V_{lof}^2.

The following conclusions can be drawn based on this research:

- Aircraft mass m is very difficult to determine from aircraft performance theories;
- $N1$ is uncorrelated with L_{max};
- V_{lof}^2 is uncorrelated with L_{max};
- $N1$ is uncorrelated with V_{lof}^2;
- V_{lof}^2 is not a good aircraft mass m representative;
- $N1$ and V_{lof}^2 as predictors explain only 7% of the total variation in L_{max};
- $N1$ and V_{lof}^2 as L_{max} predictors do not improve the distinctive capabilities between noise measurements.

Future research is needed in order to:

- Improve position data of aircraft and hence improve the Doppler corrected spectrograms to be able to determine $N1$ better;
- Enlarge the dataset to be able to increase significance and to be able to gain more insight into the quality of $N1$ and V_{lof}^2 as predictors;
- Use other aircraft noise measurement sources to improve the quality of L_{max} and the associated spectrograms;
- Use more predictors in the MLRA model to further improve distinctiveness between noise measurements;
- Use data from which $N1$ and m are known so that the algorithms can be checked extensively on their quality and to be able to draw fundamental conclusions regarding $N1$ and m/V_{lof}^2 as predictors for L_{max}.

[Page intentionally left blank]

Preface

This report is my Master thesis in order to obtain my master degree in Aerospace Engineering. The past two and a half years were dedicated to completing various courses of the master track 'Air Traffic Performance and the Environment' from which I continued to the topic 'Aircraft Noise and Climate Effect' to fulfil my graduation period.
There are many topics to be studied in the field of aircraft noise from which I chose to dive into the sophisticated area related to aircraft noise classification. My MSc thesis forms only a small part of aircraft noise classification in which I studied the capabilities to improve distinctiveness between noise measurement, by using additional obtained information regarding the aircraft mass and engine setting, so-called 'predictors'.

In this preface I would like to thank a number of people who have been of great support to me, not only during my graduation period, but also throughout my entire academic study at the faculty of Aerospace Engineering. The first person who really has been of great support regarding the content of my graduation research is my supervisor at Delft University of Technology: Mirjam Snellen. She gave me excellent guidance throughout the project and made me dive into every single detail, which improved my knowledge regarding the main topic of interest, significantly. Also, I would like to thank her for the many hours she spend to guaranty the quality of my work.
Second, my second supervisor and mental supporter at Schiphol Group: Mark Brouwer. Mark showed to be one of the best psychologist when I had a hard time. Not only did he force me to stay focussed, but also showed his compassion related to my private matters in the past months.
Also, I am thankful to my graduation professor Dick Simons for his time, enthusiasm and critical view which only improved my work even more. At the start of this project, professor Simons immediately showed his great interest in the topic of this research and was always very curious about the results which motivated me enormously.
I would like to show my gratitude to the department Stakeholder Strategy and Development (SSD) at Schiphol Group for all the fun times we had and for their time and effort to get the best out of me and my graduation project. I would certainly recommend all graduate students to fulfil their master thesis project at SSD since SSD will give you the warmest welcome you have ever got.
Furthermore, my family who always showed their interest with respect to my entire academic study and who were always willing to support me wherever possible.

Especially my mother Sonja Overduin and dad Joop de Blok: Sonja and Joop always believed in me and Sonja jokingly called herself my 'financial sponsor'. I thank her for making it possible for me to study. Joop heard many theories I had to learn during my study and always tried to understand them, thus showed his compassion and interest. A special thanks goes out to my little brother Ricardo de Blok, as he often gave me the privilege to assist him learning theories and techniques I acquired during my study, as he did a technical study as well. I thank my grandfather Willem Overduin, who unfortunately passed away during my study, for the relaxing card games after me having finished a difficult exam that day. Grandmother Hinke Overduin for all the fun times, good discussions and lovely meals we had when I studied at her place. It meant to world to me, as well as it benefited my study results. My girlfriend Lara Hartman who showed her be loving and care and never underestimated the amount of work that had to be done at certain moments in time. She understands the most important things to me in life and supports me to achieve my goals.
Last, to all those people that I forgot to mention: I sincerely thank you.

It has been a great pleasure studying the classification of aircraft noise measurements. I hope that my work forms the basis for a significant breakthrough in this field of interest and is an inspirational reading to those whom continue the research on this topic.

I hope you enjoy reading this MSc thesis the much as I enjoyed studying the thesis its topic of interest!

Stefan de Blok BSc
April 29, 2015

Contents

List of Figures

[Page intentionally left blank]

List of Tables

[Page intentionally left blank]

List of Abbreviations

$L_{A_{max}}$	Maximum A-weighted noise Level
N1 DA	*N1* Determination Algorithm
AAS	Amsterdam Airport Schiphol
ADS-B	Automatic Dependent Surveillance-Broadcast
AGL	Altitude above Ground Level
AIP	Aeronautical Information Publication
ANOMS	Airport Noise & Operations Monitoring System
AoA	Angle of Attack
ATC	Air Traffic Control
BPF	Blade Passing Frequency
CAA	Civil Aviation Authority
CDA	Continuous Descent Approach
CISS	Central Information System Schiphol
DFT	Discrete Fourier Transform
DR	Down Range
FFT	Fast Fourier Transform
FMS	Flight Management System
FT	Fourier Transform
GA	General Aviation
IAF	Initial Approach Fix
ICAO	International Civil Aviation Organization

KLM	Koninklijke Luchtvaart Maatschappij
KNMI	Koninklijk Nederlands Meteorologisch Instituut/Royal Netherlands Meteorological Institute
LSPF	Least Squares Polynomial Fit
LVNL	LuchtVerkeersLeiding Nederland
MDA	Mass Determination Algorithm
MLRA	Multivariate Linear Regression Analysis
MTOW	Maximum Take-Off Weight
NADP1	Noise Abatement Departure Procedure 1
NADP2	Noise Abatement Departure Procedure 2
NAM	Noise Abatement Measure
NMT10	NOMOS Station 10
NOMOS	Noise Monitoring System
OASPL	Overall A-weighted Sound Pressure Level
OSPL	Overall Sound Pressure Level
PFM	Peak Find Method
RMSE	Root Mean Square Error
RPM	Revolutions Per Minute
SEL	Sound Exposure Level
SID	Standard Instrument Departure
SIL	Sound Intensity Level
SIS	Schiphol Information System
SPL	Sound Pressure Level
SR	Slant Range
SSD	Stakeholder Strategy and Development
TOGW	Take-Off Gross Weight
UTM	Universal Transverse Mercator
WGS84	World Geodetic System 1984

Chapter 1

Introduction

Airports in The Netherlands are subjected to tangent environmental laws to restrain pollution and noise nuisance. Amsterdam Airport Schiphol (AAS) is one airport dealing with this regulatory framework but nevertheless they are resolute to continue growth with respect to aircraft movements. To cope with the law related to aircraft noise, the department Stakeholder Strategy and Development (SSD) of AAS is responsible for the implementation of Noise Abatement Measures (NAMs). NAMs are used to minimize aircraft noise as to be able to maximize the number of aircraft movements within the environmental law as set by the Dutch government.
SSD demands to be able to visualize the effect of a NAM by measuring aircraft noise with its Noise Monitoring System (NOMOS). NOMOS measures aircraft noise in the vicinity of AAS and has an informative role with respect to the local residents. However, in practice it appears that the effect of a NAM to the exposed noise level can not easily be determined since the total set of measurements show a high degree of scattering. This is caused by the fact that many other parameters are contributing to the exposed noise level as, for example, engine setting, flap setting and aircraft configuration. Therefore, AAS has difficulties evaluating the effectiveness of implemented noise reducing measures with the measured noise levels by NOMOS.
For evaluation-, persuasion- and policy purposes it is important to be able to evaluate a change in operational procedure with respect to the effect on the exposed noise level. This is not only the case for a NAM but can also be important to evaluate, for example, a change in the design of an aircraft not only from theory, but also in practice.
Additionally, the data presented in this research is retrieved within an operational environment, where other research often focus on a more conditioned environment, for example wind tunnels and aircraft noise prediction models.

The purpose of the research presented in this report is to determine/estimate two additional aircraft parameters/characteristics and to add this information to the original scattered dataset. Hence, the purpose is to build a system which effectively contributes to a quantitatively higher correlation between the noise measurements, hence decrease the level of scattering of the total dataset.
The ultimate goal of this MSc research is to distil the change in noise level as contributed

by a difference in operational procedure. The method quantifies the contribution of the two predictors to variations in the noise level, also referred to as the Multivariate Linear Regression Analysis (MLRA) model. Predictors are variables that can be used to predict the values of other variables (as in statistical regression). The two predictors used in the MLRA model are: the engine power setting $N1$ and aircraft mass m.
The research limitations are characterized by the fact that this MSc research only focusses on departures and not on arrivals. Hence, the MLRA model based on the two predictors used in this research can not be constructed when arriving aircraft are studied. Besides that, it appeared to be very difficult to determine the actual aircraft mass m from aircraft performance theories directly and hence an aircraft mass representative has been identified. The aircraft mass representative is chosen to be the lift-off speed during take-off V_{lof} at which the aircraft first gains height and appeared to be quadratically related to m, hence V_{lof}^2 is used as second predictor for the MLRA model. Thus, no conclusions directly related to the relation between aircraft mass m and the exposed noise level can be drawn from this thesis research. Also, only one aircraft type is studied from which the configuration with regards to the flap setting and flown operational procedure is known, although the proposed method can also be applied to other aircraft types from which the flap setting during take-off is known. Besides, only two airlines are studied: airline A and B. The amount of measurements of airline A is significantly less compared to the amount of measurements of airline B which limits the statistical substantiation. Also, only the noise measurements of one NOMOS station are used which is situated in a inhabited area for informative purposes with regards to the exposed noise level in that area. In some cases, this limits the quality of the noise measurements/full time series. This research focusses on the addition of two predictors and hence this limits the validity of the results to only those two predictors.

This report consists of the following chapters. This chapter introduced the topic of interest, the purpose of this report and the method and limitations of this research. The project plan is defined in chapter 2 and AAS, the environment in which the aircraft noise measurements are conducted, is introduced in chapter 3. Background information regarding the methods and theories is given in chapter 4 and the dataset used in this research is set in chapter 5. Subsequent, chapter 6 and chapter 7 explain how the two predictors aircraft engine setting $N1$ and aircraft mass representative V_{lof}^2, respectively, are determined. The results of this research, including the statistical method, are stated in chapter 8 on which conclusions & recommendations are drawn in chapter 9. Last, the sources underpinning the statements made in this thesis are summed in the Bibliography.

Chapter 2

Project Plan

As a guideline for this MSc research the project plan is set out in this chapter. First the problem definition of this research is stated. Second, the main aim of this research is given, third the objective will be stated and the research questions to be investigated are mentioned as fourth. Last, an overview will be given regarding the content of this thesis.

2.1 Problem definition

With new NAMs implemented SSD wants to be able to determine possible differences to decide whether a NAM effectively contributes to the reduction of nuisance.
Nevertheless, due to many different aircraft types, aircraft configurations and noise records obtained by the noise stations of AAS the measurements of noise metrics show a lot of scatter, also for a single procedure.
Therefore, AAS demands to be able to uniquely distinguish the measurements before the implementation of the NAM from the measurements after the implementation of the NAM to study its contribution to the exposed noise level. AAS expects that knowing the aircraft mass m_{ac} provides enough information in order to successfully assess the relation between noise measurements and the operational procedure.

Hence, AAS demands a technique in classifying noise measurements based on aircraft mass to be able to increase noise measurement distinctiveness over multiple time periods.

2.2 Research aim

This research focusses on the effect on measured noise levels by a difference in flown operational procedure. The hypothesis is that in addition to operational procedure, also aircraft mass m and aircraft engine setting $N1$ contribute to a great extent to the measured noise level. It is expected that constructing a model containing m and $N1$ as sound level predictors, can ultimately be used to statistically proof the effect of a difference in operational procedure.

Therefore, the aim of this research is to build a model based on $N1$ and m to be able to subtract the variation in noise levels as contributed by these predictors and hence to be able to obtain the direct effect on the exposed noise level by a difference in operational procedure.

2.3 Research objective

The objective of this MSc research is to determine an algorithm able to identify the two predictors of interest (m and $N1$) and to use these predictors as input for the model to predict noise levels as contributed by these parameters.
Thus, the research objective can be subdivided into three individual objectives:

1. Develop an algorithm to determine $N1$ from the available data resources;
2. Develop an algorithm to determine m from the available resources;
3. Develop a model based on the previous two predictors to be able to subtract their contribution to noise level variations from the total noise level.

2.4 Research questions

The following research question are answered during this MSc research:

- What is the context of the problem?
  - How did the initial problem arise?
  - Which individual elements contribute to the total noise level?
    - How does $N1$ contribute to the total noise level?
    - How does m contribute to the total noise level?
  - How are the latter elements identified from a noise measurement?
- How can aircraft noise be measured?
  - What different noise measurement stations are currently used?
  - What information is provided by these noise measurement stations?
  - Which noise measurement station is useful for this MSc research?
  - What information is provided by this noise measurement station?
  - Which studies related to noise measurements have already been conducted at AAS?
- How can m and $N1$ be determined from the available data resources?
- Which assumptions have to be made for the algorithms of both predictors?
- How can the results at the end of this research be evaluated as to statistically guarantee the reliability of the results.

2.5 Research overview

Figure 2.1 provides a general overview to the reader as content description of this MSc research thesis.

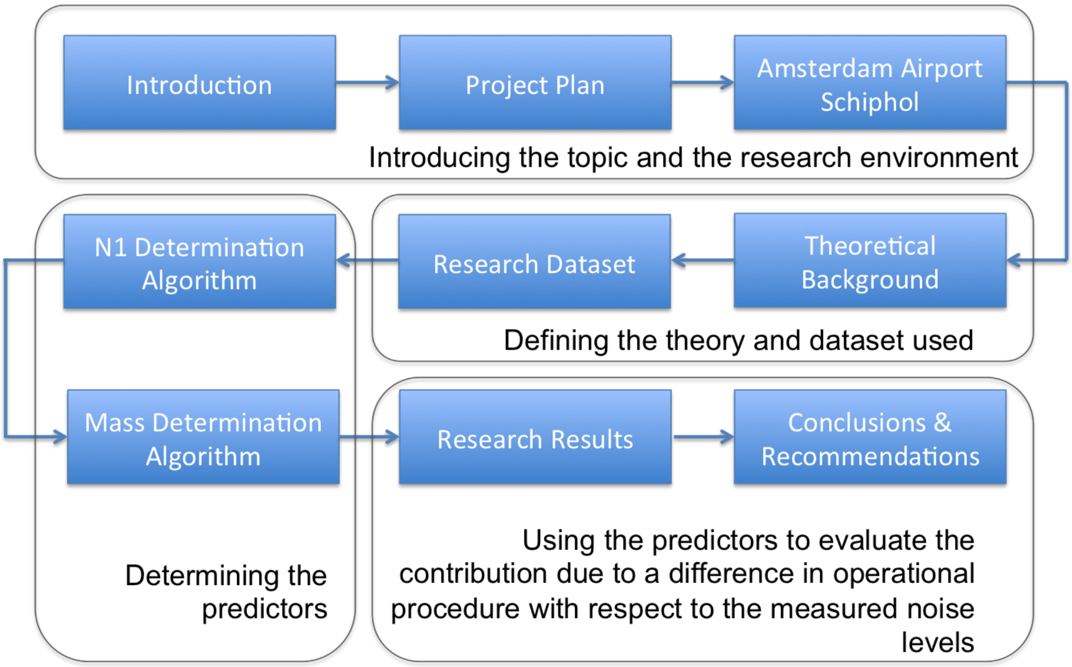

Figure 2.1: Research overview for the reader of this MSc research thesis

[Page intentionally left blank]

Chapter 3

Amsterdam Airport Schiphol

The MSc graduation project is initiated and facilitated by Amsterdam Airport Schiphol as supplier of the required data and, together with Delft University of Technology, supervisor during the complete graduation phase. Therefore, this chapter presents relevant information and the current lay-out of Amsterdam Airport Schiphol as background information of the project.

3.1 Runway lay-out

AAS maintains six runways: five main runways and one General Aviation (GA) runway (the 'Schiphol Oostbaan'). The runway lay-out of AAS is shown in Figure 3.1. Note that in Figure 3.1 the red crosses indicate the direction in which/from which it is not allowed to departure/land.

For safety, availability and traffic volume purposes not all five main runways are used at the same time. Instead, AAS uses five different periods to handle traffic volume, namely:

1. S - Start peak: 2 runways used for take-off, 1 runway used for landing,
2. L - Landing peak: 1 runway used for take-off, 2 runways used for landing,
3. O - Off peak: 1 runway used for take-off, 1 runway used for landing,
4. N - Night: 1 runway used for take-off, 1 runway used for landing,
5. D - Double peak: 2 runways used for take-off, 2 runways used for landing.

These periods are not associated to fixed times during the day, rather to the slots issued by AAS.
The active runways are shown in Figure 3.2. The regulatory bodies in The Netherlands decided that during the Night period (N), which is the period between 22:30 hour and 06:30 hour, only one runway for departures and one runway for arrivals may be used. In addition, during the night only runway 06 ('Kaagbaan'), 18R ('Polderbaan') and 36C ('Zwanenburgbaan') can be used for departures and 36L ('Polderbaan'), 24 ('Kaagbaan') and 18C ('Zwanenburgbaan') for arrivals.

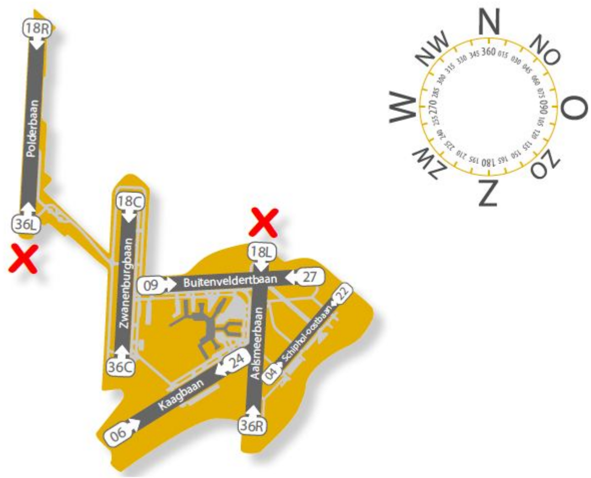

Figure 3.1: The current runway system of AAS

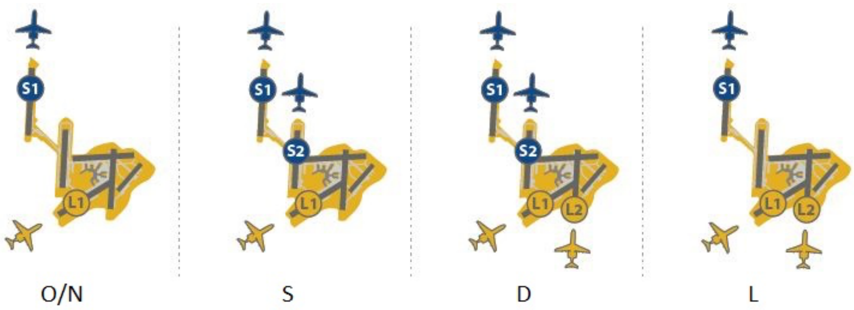

Figure 3.2: The current peak-period system of AAS with northern wind and good visibility

3.2 Air Traffic Management System

Arriving and departing air traffic follow routes to an Initial Approach Fix (IAF) or one of the outbound sectors respectively. Air traffic is assigned to one of the five outbound sectors to separate aircraft from each other and to minimize air traffic density per area for Air Traffic Control (ATC) workload purposes.
The direction from which an aircraft is *approaching* AAS and the active runway combination (runways used by ATC at that moment) determine, in almost all cases, the Initial Approach Fix (IAF) assigned to that particular aircraft. An IAF is a route in the sky which leads to a specific runway and hence provides the pilot guidance and direction during the approach to a runway and limits the workload of an air traffic controller by vectoring aircraft to a certain point in the sky from which each aircraft only need to be monitored instead of guided throughout the approach.
In case an aircraft *departures* from AAS a so-called Standard Instrument Departure (SID) is requested by the pilot of an aircraft from which ATC determines the runway to be departed from. An example of possible Standard Instrument Departures (SIDs) from runway 18L/36R (the 'Aalsmeerbaan') is shown in Figure 3.3.
A SID ultimately leads to one of the five sectors. Aircraft are guided to an area in the sky called a sector which leads to the "exit" of the Dutch airspace. This facilitates ATC in keeping aircraft separated from each other, hence improving safety and decreasing work-

load.

The above mentioned routes are designed as such to, on the one hand, cause the least amount of noise and pollution to the environment and, on the other hand, be the safest and most optimal path to the relevant runway. The environment refers noise and pollution as nuisance. The less nuisance with respect to noise and pollution is achieved as such to let aircraft follow a route which crosses the less densest areas. Nevertheless, aircraft flying these well-designed routes still cause nuisance to the environment in the sense of noise and pollution.
To connect the government, local residents and airlines with AAS a negotiating body has been established in 2006. This body represents all above-mentioned stakeholders and discusses sensitive issues related to nuisance caused by AAS. This body is called: *'The Alderstafel'*.

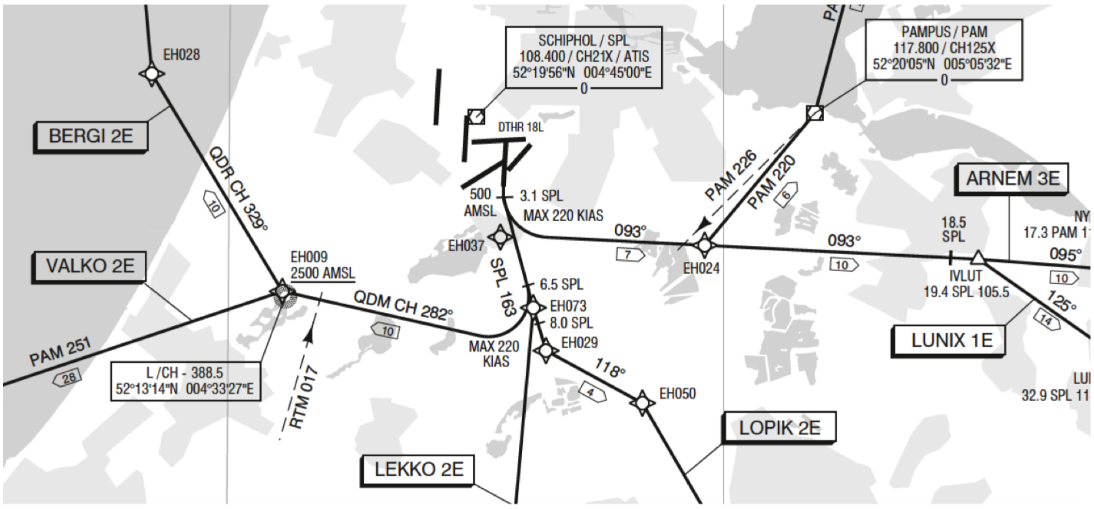

Figure 3.3: Standard Instrument Departures from runway 18L/36R of AAS

3.2.1 The Alderstafel

The Alderstafel is a negotiating body, established in 2006, providing an advisory role to the government of The Netherlands about the development of AAS, together with airports Eindhoven and Lelystad. The parties attending the Alderstafel try to find an optimum between the quality of the network of AAS and the quality of the environment [4].
The result of these negotiations is the Alders Agreement on three main topics related to:

1. Noise reduction,
2. Environmental quality,
3. Duty of mainport Schiphol.

This agreement is handed over to the Minister of Infrastructure and the Environment whom then anchors this into the Air Traffic Law. This means that AAS has to set up its operation as such to comply with this law.
The regulatory framework also captures theoretical models which must be used for all calculations and quantitative proof of AAS to ensure compliance. One of these compliances is for example to fixed maximum L_{den} contours. L_{den} is a European measure of

average noise during one day. The noise contours of equal L_{den}, as determined with a theoretical model, are illustrated in Figure 3.6. Note that L_{den} is an abbreviation of Level day, evening, night.

3.2.2 Stakeholder Strategy and Development

Stakeholder Strategy and Development (SSD) is a department of Schiphol Group responsible for the timely realization of sufficient and supported environmental capacity for the mainport Schiphol, with support from different stakeholders from politics and the environment [3].
SSD aims at providing maximum environmental space for air traffic growth at AAS. One of the techniques used to create more space with respect to environmental capacity is the implementation of Noise Abatement Measures (NAMs). Recently (15th April 2014), SSD managed to implement Noise Abatement Departure Procedure 2 (NADP2). This procedure will be clarified in subsection 4.6.1.

The produced noise by air traffic, also incorporating any NAM, is modelled by SSD, from which an example is presented in Figure 3.4. This modelling is carried out by incorporating solely aircraft noise theories and is not based on measurements retrieved from NOMOS, because measurements contain, among others, environmental conditions and measurement errors which can influence the outcome of an experiment significantly. Hence, use is made of theoretical models from which the outcome can be reproduced.

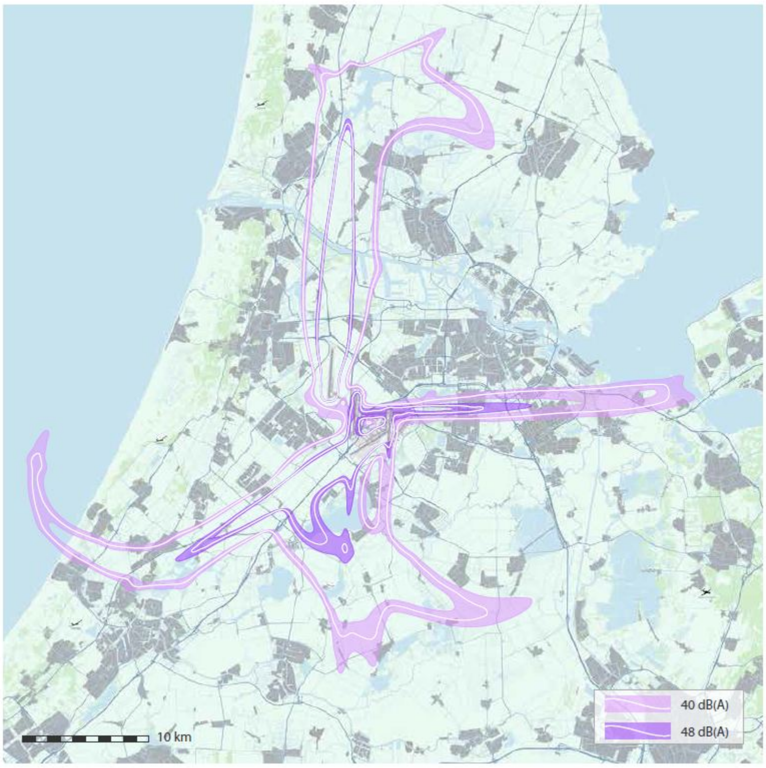

Figure 3.4: Noise map example produced by Stakeholder Strategy and Development

3.3 Noise Monitoring System

The Noise Monitoring System (NOMOS) is the noise measuring system of AAS and measures aircraft noise at residential areas around AAS since 1993. NOMOS provides a wide variety of, real-time and past, acoustic information to anyone having access to the internet. Among others, possible parameters that can be obtained via NOMOS are: $L_{max}, L_a, L_{a_{max}}, L_{den}$ and Sound Exposure Level (SEL). Next to these noise measures, also noise events from the past month can be downloaded from individual NOMOS stations, since NOMOS automatically saves the data files for each noise event detected by the system.

All available noise measurements of NOMOS are conducted using 31 measurement stations as shown in Figure 3.5).

The noise level as measured by NOMOS is coupled to the associated aircraft by using flight track data from RADAR. This coupling is carried out by software at the servers of Bruel&Kjaer (Manufacturer Airport Noise & Operations Monitoring System (ANOMS)) and all data is automatically saved on a server.

NOMOS serves as an informative system to the environment and local residents. No regulatory framework is based upon the measurements of NOMOS. However, SSD always seeks to find the effects of a NAM in practice and not only by theory because, at the end, it comes to the effectiveness of a NAM underpinned by means of a quantitative analysis from practice.

3.4 Airport Noise and Operations Monitoring System

The Airport Noise & Operations Monitoring System (ANOMS) is the flight tracking system used by AAS and automatically used by NOMOS as previously mentioned.
ANOMS provides real-time tracking of aircraft in the European skies. Besides the open-source features, AAS uses its own Central Information System Schiphol (CISS) to provide all sorts of information. This for example also includes additional recorded information of every aircraft equipped with Automatic Dependent Surveillance-Broadcast (ADS-B), provided by antenna equipment of the LuchtVerkeersLeiding Nederland (LVNL).
Regarding the main topic of the MSc thesis project, necessary data related to specific aircraft parameters (for example aircraft velocity V, height h and destination) can be retrieved if necessary. Position information of aircraft is derived from either TAR1 (ground RADAR) or TAR4 (terrestrial RADAR) with a sampling frequency of 1 Hz and 0.25 Hz, respectively. TAR1 RADAR shows all aircraft with a height less than 1000 feet within the defined RADAR range and TAR4 RADAR defines all aircraft with a height more than 1000 feet within the defined RADAR range. This range is the maximum distance at which the RADAR is able to determine the position of aircraft within an acceptable uncertainty.

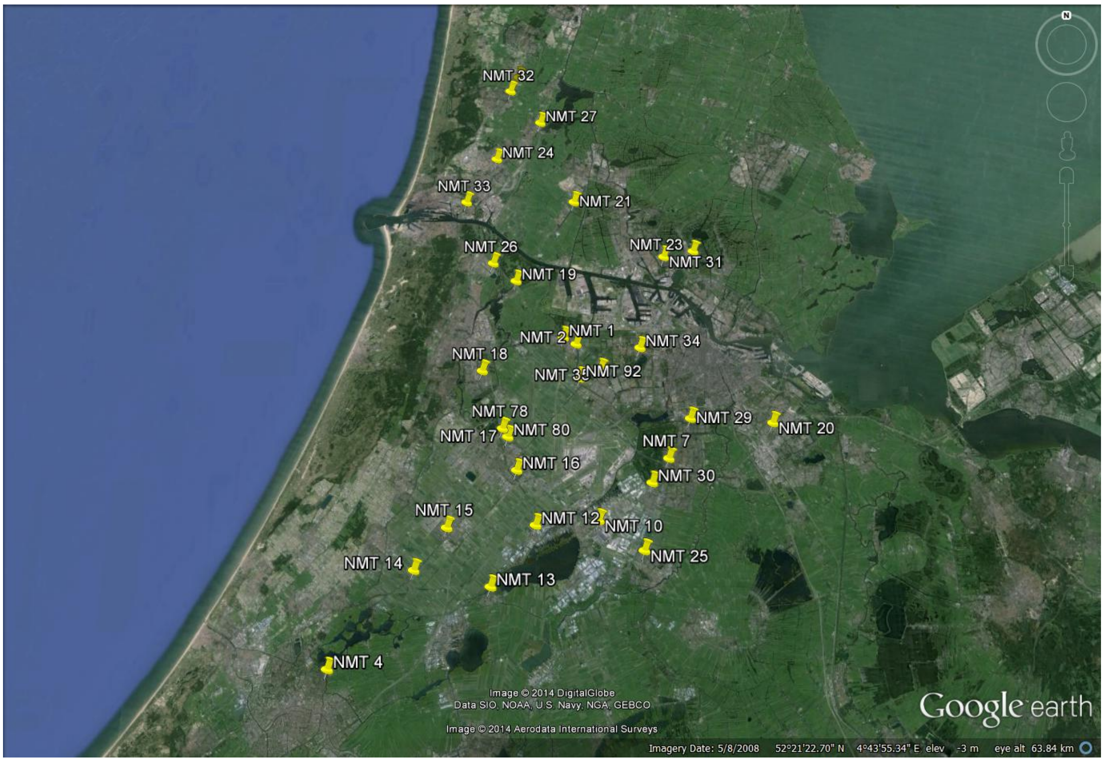

Figure 3.5: Locations of noise monitoring stations of AAS. Retrieved from [17]

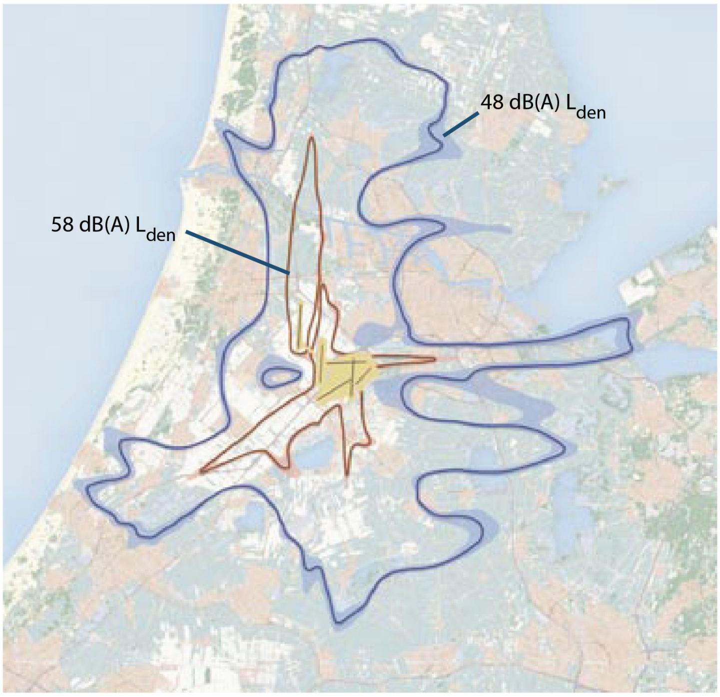

Figure 3.6: Noise contours of equal L_{den} constructed with a theoretical model of AAS. Retrieved from [2]

Chapter 4

Theoretical Background

This chapter provides a theoretical background as fundamental basis for the thesis research. It provides knowledge about the content to be explained in the next chapters.

4.1 General

Aircraft noise is commonly considered as nuisance by the community. This nuisance has to be minimized radically, as stated by International Civil Aviation Organization (ICAO). Over the past 40 years, ICAO aimed at reducing the noise at the source, while in 2001 a so-called "balanced-approach" has been agreed on to aircraft noise management [19]. Also, airports are restricted at noise quota, established by the local Civil Aviation Authority (CAA). The need for reduction is clear, however the method of reducing aircraft noise by a single measure is not readily available.

4.2 Aircraft noise sources

There are several contributors to the total aircraft-produced noise level.
Arntzen [6] states that the major airframe noise sources are the: tailplane, spoiler, wing, flap side edge, trailing edge devices, leading edge devices, nacelle, landing gear and fuselage. The engine noise sources are divided into four major noise sources, being: jet noise, fan exhaust noise, turbine & core noise and fan inlet noise. Filippone [14] categorized the noise sources as shown in Table 4.1. The components will be treated consecutively, together with the major aircraft engine noise sources identified by Arntzen [6].

Landing gear

Landing gear noise has been of renewed interest in the past 20 years. Empirical evidence with limited physics dominated this field of interest for a long time, even though the results of earlier research are often lacking statistical evidence [14].
Landing gear noise is ranked as a major airframe noise source with a broadband frequency range. Its cause is related to the interaction between the landing gear with high-lift

Table 4.1: Contribution to total noise level per aircraft component

Component	Contribution
Landing gear	High
Fuselage	Low
High lift devices	Medium
Engines	High

surfaces, upstream as well as downstream, causing a wake as shown in Figure 4.1.
Landing gear noise is considered to be numerically too complex to model, and so semi-empirical equation are common to be used in landing gear noise prediction models [11].
Landing gear noise is generally referred to as airframe noise. Besides the landing gear, also the wings, slats, flaps and tailplane sections are airframe noise sources. The baseline model used for airframe noise predictions is the model of Fink [15]. The model of Fink determines the overall noise trends for full aircraft studies, rather than the individual source generating mechanisms [6].

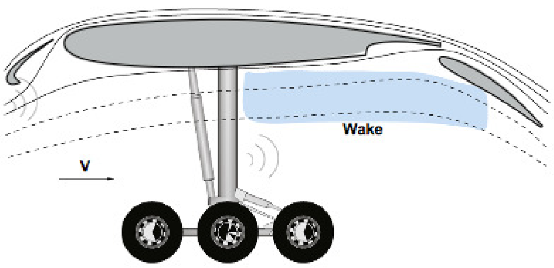

Figure 4.1: Interaction of landing gear with high-lift devices, upstream as well as downstream. Retrieved from Ref. [14]

Fuselage

Noise caused by the fuselage is commonly neglected in aircraft noise prediction models. It is believed that fuselage noise is 10 dB below that of the high-lift devices, although Liu and Dowling [23] proved that this might not be the case for a certain range of frequencies. Liu and Dowling identified two main sources contributing to fuselage noise: [1] The effect of a turbulent boundary layer over a rough surface and [2] the effect of vibrations amplifying the former effect due to perturbations to the boundary layer itself.
Besides this, many studies focus on the effect of fuselage noise to the internal perceived cabin noise.

High-lift devices

Noise caused by high-lift devices are considered to include: trailing-edge noise, flap-edge noise and leading-edge slat noise. High-lift devices are attached to the wings of the aircraft and are called "high-lift" surfaces because they largely provide the total lift of the wings.
Many research has been carried out concerning noise caused by high-lift devices, nevertheless the outcome suffers from some important gaps. The two major shortcomings

are that the geometrical details of the leading-edge slats and trailing-edge flaps are often classified as confidential and therefore unknown to, for example, researchers. Hence, no accurate computational methods are applicable and, partly as a result of the previous shortcoming, the current noise prediction methods are based on empirical evidence and rely on a limited set of parameters [33]. The turbulence in the air flow caused by the high-lift devices is illustrated in Figure 4.2.

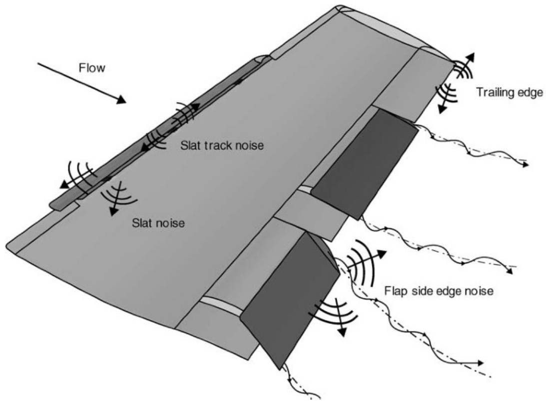

Figure 4.2: Turbulent airflow caused by the high-lift devices. Retrieved from Ref. [33]

Traditionally, the engines has been the most prominent noise source. However, at low engine power settings the airframe has a significant contribution to the overall sound level that cannot be ignored. For example, the "dirty configuration" (extended flaps, slats and gears) during the approach phase lead to a significant higher noise level.

Engines

Arntzen [6] identified the following major aircraft engine noise sources: jet noise, fan exhaust noise, turbine & core noise and fan inlet noise.

Fan blades at the front suck in air. Most of the air flows around the outside of the engine. All the air (turbojet) or only a portion of the incoming air (turbofan) entering the intake passes through the gas generator, entering the combustion chamber. The remainder passes through a fan, or low-pressure compressor, and is ejected directly as a "cold" jet or mixed with the gas-generator exhaust to produce a "hot" jet [24].

Jet noise is one of the primary noise sources of aircraft. Jet noise is caused by mixing. Mixing takes place when the engine bypass air mixes with the ambient air as well as when the engine bypass air mixes with the core air. Also, 'large scale' mixing occurs with the ambient fluid in the merged region behind the engine. This merged flow region is the primary cause of low frequency sound from a jet engine, because large turbulent structures are present. In fact, jet noise is in general not a single source but rather caused by many acoustic sources along the jet plume.
A model often used to predict jet noise is the empirical model created by Stone [28]. This empirical model predicts the Overall Sound Pressure Level (OSPL) normal to the engine symmetry axis, i.e. at a directivity angle of 90°, using jet velocity and other relevant

parameters. As a final step, frequency dependent directivity patterns are applied to the results [6].

Fan noise is caused by the primary objective of a gas turbine: namely generating propulsive forces. These propulsive forces, generated by the gas turbine, increases the momentum of the airflow. This increase in momentum is gained through different stages of the gas turbine. Each stage contains, more or less, a cylindrical disk of blades. The engine fan is generally referred to as being the first stage of the engine.
According to Arntzan [6], "Heidmann's model forms the fan noise prediction basis in the most aircraft noise prediction tools and has not yet been surpassed by other empirical methods". Therefore, Heidmann's model [18] is often used to predict fan noise.

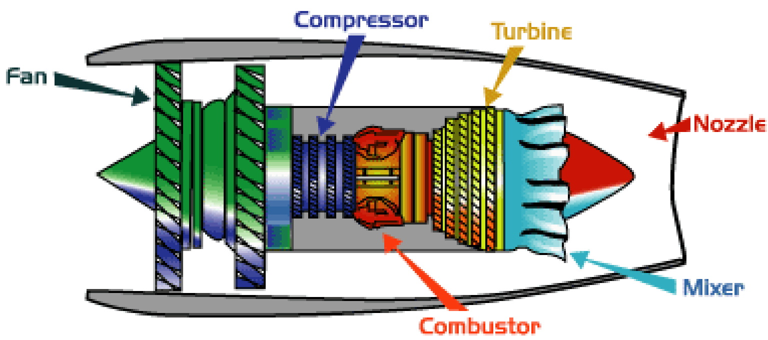

Figure 4.3: Schematic diagram illustrating the operation of a 2-spool, high-bypass turbofan engine, with LP spool in green and HP spool in purple. Retrieved from Ref. [31]

Aircraft engines radiate noise at the front and at the back of the engine. To suppress noise at the inlet as well as the exhaust, the engine nacelles are usually treated with acoustic lining material [6].
However, rotor-stator interaction causes discrete tones in the spectrum [25]. The wake of the rotor blades generate unsteady forces which hit the stator blades. The interaction between rotor and stator blades repeats itself with every blade passage. Hence, this particular pressure is repetitive and proportional to the number of blades and the fan rotational speed. The so-called Blade Passing Frequency (BPF) is the fundamental frequency at which this process repeats [6]. The Blade Passing Frequency (BPF) is determined by:

$$BPF = \frac{b \cdot \Omega}{60} \tag{4.1}$$

With b equal to the number of fan blades and Ω equal to the rotational speed per minute of the fan blades.
When the Fourier Transform (FT) is applied, multiple sine functions are used to approximate the signal. Hereby, harmonics of the BPF are constructed. These harmonics are indicated by k with $k = 1, \ldots, n$. The lowest BPF is called the fundamental frequency, i.e. the first harmonic ($k = 1$).
The BPF is related to the amount of thrust as delivered by the engines. The amount of thrust delivered by the engines increases when the BPF increases. However, the parameter directly related to the engine setting is the speed of the generator section $N1$. This

research uses the engine setting $N1$, directly above the noise measurement station, as a predictor. Therefore, $N1$ has to be determined.

Equation 4.1 is used to determined $N1$. For $N1 \neq 100\%$, the BPF settles at a frequency which is equal to:

$$BPF(N1) = N1 \cdot BPF_{N1=100\%} \tag{4.2}$$

In this fashion the thrust setting can retroactively be determined.

Unsteady inflow of the engine, turbulence in the boundary layer and turbulence in the blade wakes generate noise at a broad range of acoustic frequencies, referred to as broadband noise.

Another engine noise source is combustion noise, caused by the combustion chamber of the gas turbine, where heat energy is added to the flow by burning fuel. Sound waves are produced by two phenomena [6]: [1] sound waves are produced due to the expansion of the gas mixture in the combustion chamber and [2] non-uniformities through the pressure gradients in the turbine gives rise to acoustic waves.

4.3 Measuring aircraft noise

Aircraft noise can be measured in different ways. Usually, when aircraft noise related to airports is concerned, use is made of a continuous noise monitoring system with microphones placed at fixed locations surrounding the airport. This provides the possibility to monitor the noise in that area as caused by aircraft. However, while NOMOS makes use of a single microphone placed on a pole 10 meters above the ground, use can also be made of a microphone array.
A microphone array consists of multiple microphones placed in line (linear) or at multiple positions, depending on the expected directivity of the sound as radiated by the aircraft to be measured. For example, Boone *et al.* [8] found that with microphone arrays background noise can easily be suppressed and these arrays are insensitive to turbulence noise as caused by winds.

4.3.1 L_{max} determined by NOMOS

This research makes use of the L_{max} levels as measured/determined by NOMOS. Therefore, it is important to know the working principle of determining L_{max} levels.
To determine L_{max} levels, NOMOS operates as follows:

1. Each year during a couple of weeks NOMOS measures the noise not caused by aircraft (i.e. background noise);
2. An average background noise level is determined at the end of this period and another 10 dB is added to this noise level. This noise level is set as the threshold for aircraft noise event measurements;

3. NOMOS measures noise on a continuous basis. It measures noise by means of measuring pressure. When the noise level, converted from the measured pressure, exceeds the predetermined threshold, NOMOS starts recording a noise event;
4. During each second of this event an average pressure is determined and hence an average noise level per second is set;
5. When the average noise level is less than the predetermined threshold, NOMOS stops recording the noise event and this event is saved on the server of the station;
6. Each station sends its data to a mainframe where noise measures, as $L_{max}, L_{A_{max}}$ and SEL are calculated;
7. L_{max} is determined by taking the maximum noise level of the whole event (illustrated by Figure 4.4) as L_{max} for that particular event;
8. All single noise measures are then transferred from the mainframe to the internal servers of AAS.

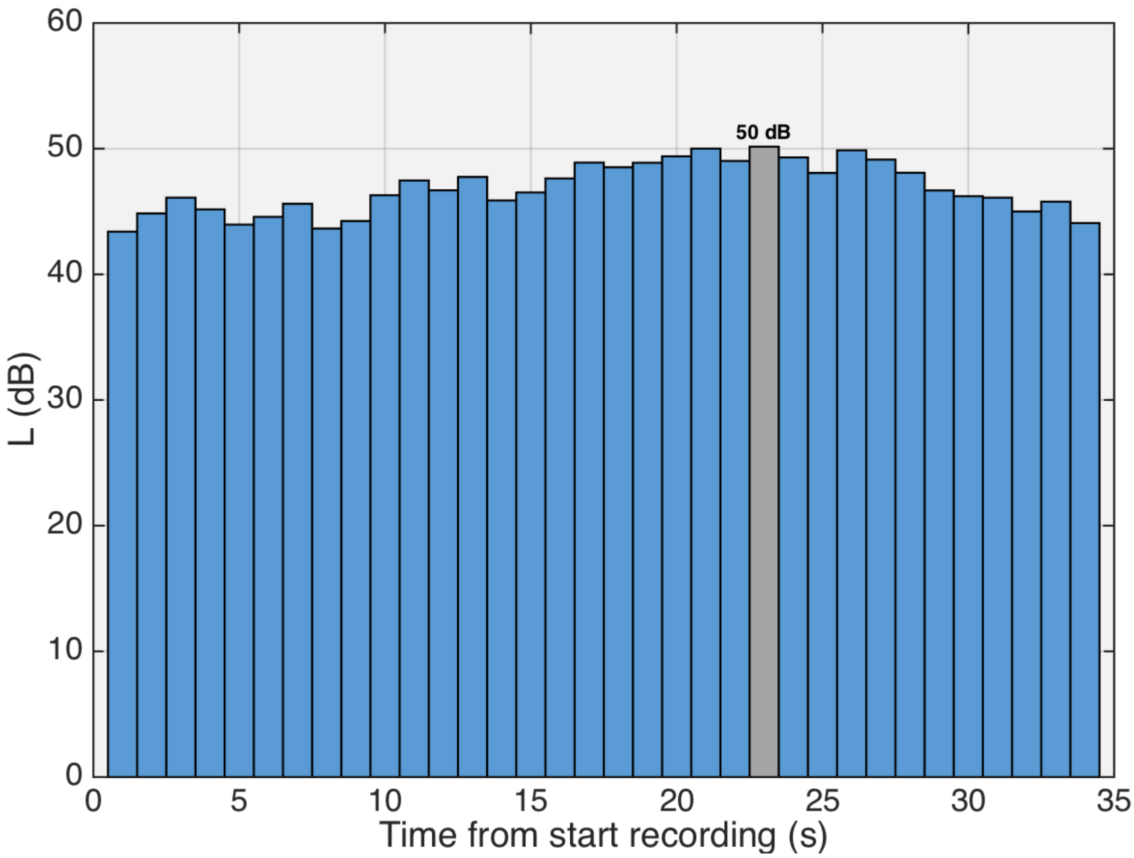

Figure 4.4: Working principle of NOMOS to determine L_{max}

4.4 Visualizing aircraft noise

Aircraft noise can be visualized in a spectrogram. A spectrogram typically contains time t on the x-axis, frequency f on the y-axis and sound intensity P by means of a color. Each aircraft component emits noise at a different intensity and frequency, of which all this information is embedded in the spectrogram.
Each component of an aircraft previously discussed emit noise at a certain frequency

range. The visualization of aircraft noise by a spectrogram requires the following steps which will be treated consecutively:

1. Determining the desired resolution in time and frequency domain;
2. Windowing;
3. Transformation of the acoustic data to the frequency domain;
4. Visualizing acoustic data in a spectrogram.

4.4.1 Resolution in time and frequency domain

The resolution in time and frequency domain has to be chosen such that it on the one hand avoids blurry data due to a changing relative velocity between aircraft and observer (microphone) and on the other hand provides sufficient resolution in the frequency domain. Time and frequency resolution is determined by the duration of a time block T and the sample frequency F_s. The size of a frequency bin Δf and T are inversely related:

$$\Delta f = T^{-1} \tag{4.3}$$

Note that T **does not** represent the time difference between two time steps, but rather determines the number of samples per block used for the Fast Fourier Transform (FFT). Capital T represents the time block, where lower case t represents a moment in time.

The number of samples per time block N_s follows from $N_s = T \cdot F_s$, so that the frequency resolution Δf becomes $\Delta f = T^{-1} = \frac{F_s}{N_s}$.
In other words, the number of samples per block N_s has to be chosen as such that both the resolution in the time-, i.e. number of blocks, as well as the frequency domain is sufficient when transformed to the frequency domain.

4.4.2 Windowing

Windowing suppresses the effect of overshooting. Overshooting occurs at the approximation of a signal via Fourier series. This overshoot is also referred to as the Gibbs phenomenon. The transitions of the signal from zero to one or visa versa causes the Fourier series to overshoot the signal.

Applying a window function before transformation to the frequency domain causes the square wave to smooth into a more harmonic shape, thus suppressing the Gibbs phenomenon.
Many window functions exist and all of them are symmetric. Each window affects the spectrum in a slightly different way, hence each application has its own best-suitable window function for each specific application and has to be chosen carefully [22].

4.4.3 Transforming acoustic data to the frequency domain

Once the data has been digitized and the window function has been set, the acoustic data has to be transformed to the frequency domain by using the Fourier Transform (FT). For continuous signals, the FT is expressed as:

$$X(f) = \int_{-\infty}^{\infty} x(t)\mathrm{e}^{-i2\pi ft}\,\mathrm{d}t \tag{4.4}$$

$$x(t) = \int_{-\infty}^{\infty} X(f)\mathrm{e}^{i2\pi ft}\,\mathrm{d}f \tag{4.5}$$

For $-\infty < f < \infty, -\infty < t < \infty$ and $i = \sqrt{-1}$. Where the uppercase $X(f)$ and lowercase $x(t)$ represent the frequency-domain function and the time-domain function, respectively.

Since NOMOS samples the aircraft noise into a digital recorded noise signal, the Discrete Fourier Transform (DFT) must be used. A common way to efficiently calculate the DFT for spectrogram purposes is the Fast Fourier Transform [7], which will also be used in this research.

4.4.4 Visualizing acoustic data

With the FFT carried out, frequency f over time t is known as well as the amplitude A of each frequency bin Δf. This information can now be visualized by means of a spectrogram. For illustration purposes, an example spectrogram of a Boeing 737-800 is shown in Figure 4.5.

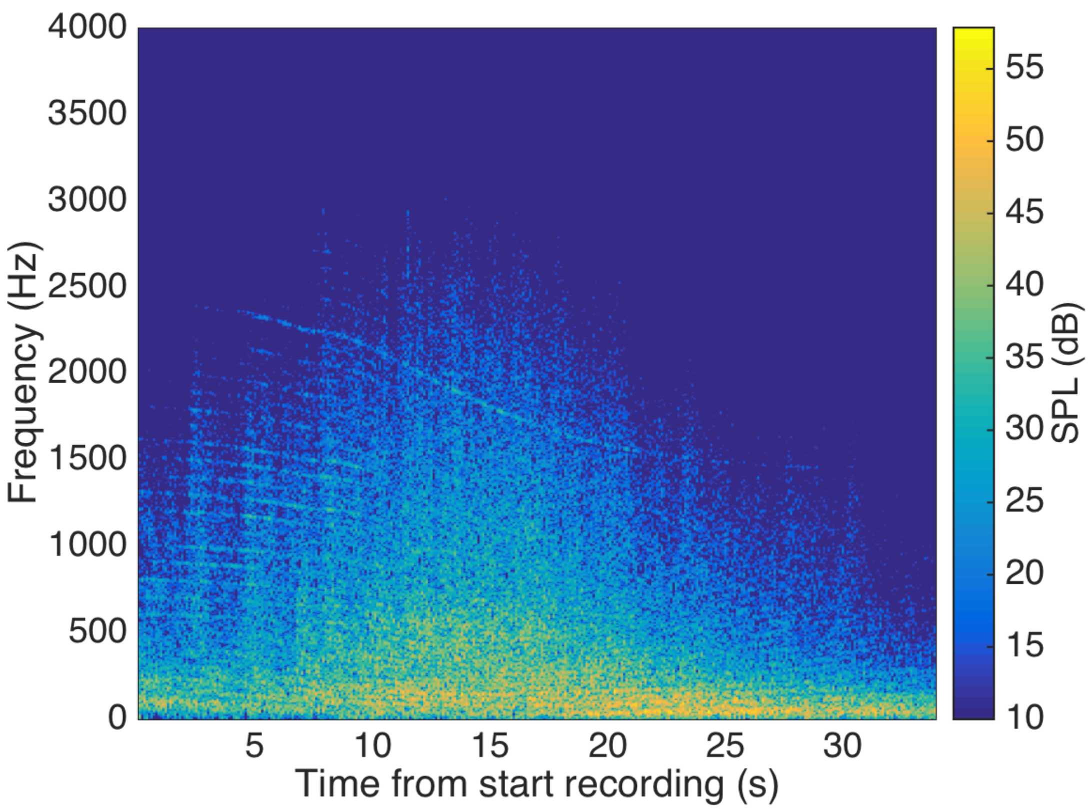

Figure 4.5: Example spectrogram of a Boeing 737-800

The BPF is embedded as a tonal component in the spectrogram. For Figure 4.5 the BPF component is visible between approximately 1600 Hz and 2400 Hz. The weaker "harmonics" above and below the BPF are actually no harmonics, but rather referred to as buzz-saw noise.
Origins of these buzz-saw tones are a series of non-uniform shock waves that develop upstream of the fan rotor whenever the relative rotor tip Mach number is larger than one. Buzz-saw noise is radiated mainly in the forward arc and its frequency range can vary between individual engines and even, for the same engine, between different fly-overs [27]. As Equation 4.1 already indicated, the BPF is constant for constant Ω. However, noise measurements are subjected to phenomenon as, for example, the Doppler effect, atmospheric attenuation and background noise, causing frequency and intensity shifts. The Doppler effect causes the BPF to be visible at higher and lower frequencies, depending upon the position of the source (aircraft) relative to the observer (NOMOS station). To determine the BPF from the spectrogram, which will be used for determining the engine setting $N1$ later on, the theoretical BPF has to be corrected for the Doppler effect.

4.5 The Doppler effect

While the NOMOS station has a fixed position during the measurements, nevertheless the aircraft is moving with respect to the receiver. The observed wavelength or frequency of a waveform thereby changes, as compared to that emitted by the aircraft. This change in observed wavelength or frequency due to the source motion is called the Doppler effect. A schematic overview of this phenomenon is shown in Figure 4.6.

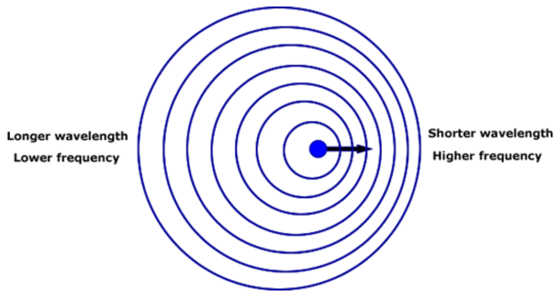

Figure 4.6: Representation of the Doppler effect

The frequency shift due to the source motion can be calculated by the following formula:

$$\frac{f'}{f} = \frac{1}{1 + \frac{\mathrm{d}r/\mathrm{d}t}{c}} \tag{4.6}$$

With f' being the observed frequency, f the actual frequency at the source, the change in Slant Range over time given by $\mathrm{d}r/\mathrm{d}t = \dot{r}$ and c the speed of sound.
c and $\mathrm{d}r/\mathrm{d}t$ have to be known in order to determine the BPF subjected to the Doppler effect.

4.5.1 Speed of sound c

The speed of sound c is mostly dominated by temperature and relative humidity. Wong and Embleton [32] derived that c can be approximated very accurately by the following equation:

$$c = c_0 \cdot [1 + h(C_0 + C_1 T_{temp} + C_2 T_{temp}^2 + C_3 T_{temp}^3 + C_4 T_{temp}^4)] \tag{4.7}$$

With c_0 the speed of sound in dry air at a temperature of 288.15 K. h the relative humidity and T_{temp} the temperature in °C. The constant C_0, C_1, C_2, C_3 and C_4 are equal to $9.66 \cdot 10^{-4}, 7.2 \cdot 10^{-5}, 1.8 \cdot 10^{-6}, 7.2 \cdot 10^{-8}$ and $6.5 \cdot 10^{-11}$, respectively.
The speed of sound c in Equation 4.6 is used to correct the spectrograms for the Doppler effect. But, since the measurements are retrieved at a period over time with changing temperature and humidity, Equation 4.7 is used to calculate c at the moment the measurement was conducted by NOMOS Station 10 (NMT10).

4.5.2 Position of aircraft relative to receiver

The change in Slant Range (SR) over time, also known as the relative velocity between two sources, can be calculated by:

$$V_{rel} = \frac{\mathrm{d}r}{\mathrm{d}t} \tag{4.8}$$

The SR is defined by parameter r and is equal to the length of the skywave path between the aircraft and the NOMOS station, not to be mistaken by the distance as measured along the Earth's surface (the so called Down Range (DR)) (see Figure 4.7).

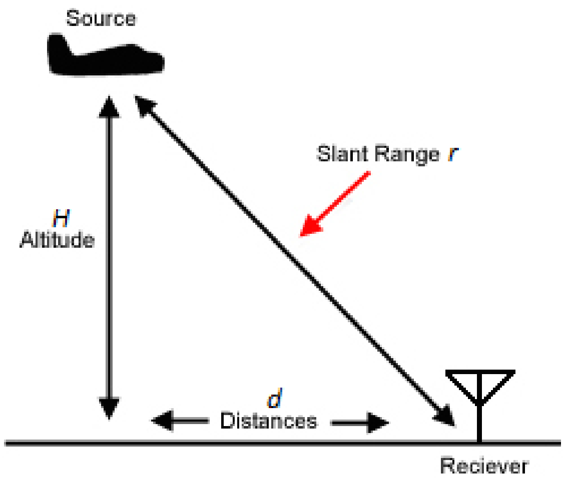

Figure 4.7: The Slant Range

Calculating the SR requires the DR d as well as the altitude H to be known, so that r can be calculated by using the Pythagorean theory:

$$r = \sqrt{d^2 + h^2} \tag{4.9}$$

Note that the distance between the NOMOS station and the aircraft remains small ($d <$ 10km) so that the curvature of the earth can be neglected in the calculation of d, hence

a flat-Earth is assumed.
Once d and h are known and converted to meters, r can be calculated with Equation 4.9. Now, using Equation 4.8 results in the relative velocity V_{rel} between the aircraft and the NOMOS station (see Figure 4.8).

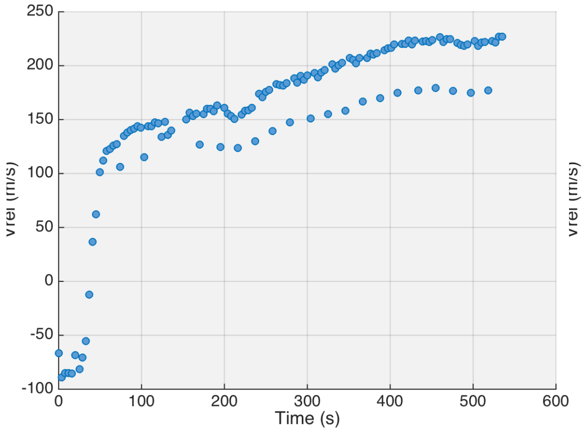

(a) Boeing B737-800

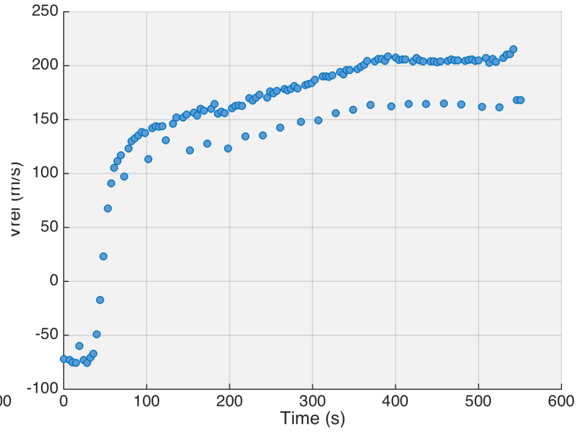

(b) Fokker 70

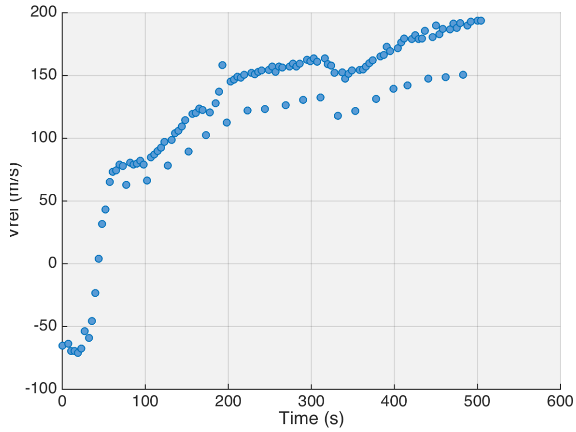

(c) Avro RJ-100

Figure 4.8: Relative velocity between different aircraft and NOMOS station 10

When the aircraft approaches the NOMOS station $r_{i+1} < r_i$ so that $r_{i+1} - r_i < 0$ and thus $V_{rel} < 0$, hence at first the relative velocity is negative until the aircraft passes the NOMOS station so that $r_{i+1} - r_i > 0$ and consequently $V_{rel} > 0$. Ground velocity V can never become negative by convention since the aircraft can not fly backwards and hence $r_{ground_{i+1}} - r_{ground_i} > 0$ and therefore $V > 0$ for all r_{ground}.

Figure 4.8 looks like there are two relative velocity profiles since many outliers lying on a continuous line are present. This phenomenon of outliers is mostly caused by the fact that TAR4 RADAR becomes less accurate when the distance between the aircraft and the RADAR increases. Besides this, also the data available from TAR4 RADAR is rounded to the nearest second hence rounding errors occur. Positioning data obtained further away from the TAR4 RADAR station are therefore subjected to measurement and rounding

errors.
However,only a small interval of the complete V_{rel} track is required since the noise sample encompasses only tens of seconds. This part of the track is situated mostly in the first 100 seconds. Hence, the outliers of Figure 4.8 *do not* influence the relative velocity profile used to correct the spectrogram for the Doppler effect. The cut-off of the relative velocity profile will be further elaborated in subsection 6.3.1.

The radar tracks and NOMOS samples come from two different data sources, hence the start- and end times of the radar tracks have to be synchronized with the start- and end times of the NOMOS data samples. The radar tracks have starting times earlier than those of the NOMOS samples since radar starts recording the tracks when the aircraft starts its take-off. NOMOS starts recording the noise samples when it notices the presence of the aircraft in its vicinity.
Synchronizing is done by cutting of the difference in starting times from the radar tracks so that the starting times become equal. End times are simply determined by calculating the duration of a noise sample and cutting of the end of the radar track longer than this duration.
It is assumed that the distance r is the smallest when the sound level of the NOMOS sample is at its maximum L_{max}. Using the time at which L_{max} occurs, together with the time that the minimum r is set, gives two synchronized times which can be shifted so that the beginning of a NOMOS sample coincides with the location at that time of the associated aircraft.

Using these begin- and end times results in the relative velocity profile as shown in Figure 4.9.

One of the major shortcomings of the earlier mentioned assumption is that there exist a small time step dt in which the sound "travels" towards NMT10 and hence synchronizing these times is not exact. Nevertheless, it is assumed that dt is very small and can be neglected.

It also stands out that the relative velocity track after cut-off (the right side of Figure 4.9) is not symmetrical. This is caused by the fact that the aircraft position before fly-over is also not symmetric with respect to the position after fly-over. Routes going to the south and the west are turning slightly to the south-east and routes going to the east even turn drastically to the west after passing NMT10. This causes the relative velocity profile to be unsymmetrical.

Once $\frac{\mathrm{d}r}{\mathrm{d}t}$ and c have been determined, Equation 4.6 can be used to calculate the Doppler factors. These Doppler factors can then be used to correct the noise measurements for the Doppler effect.

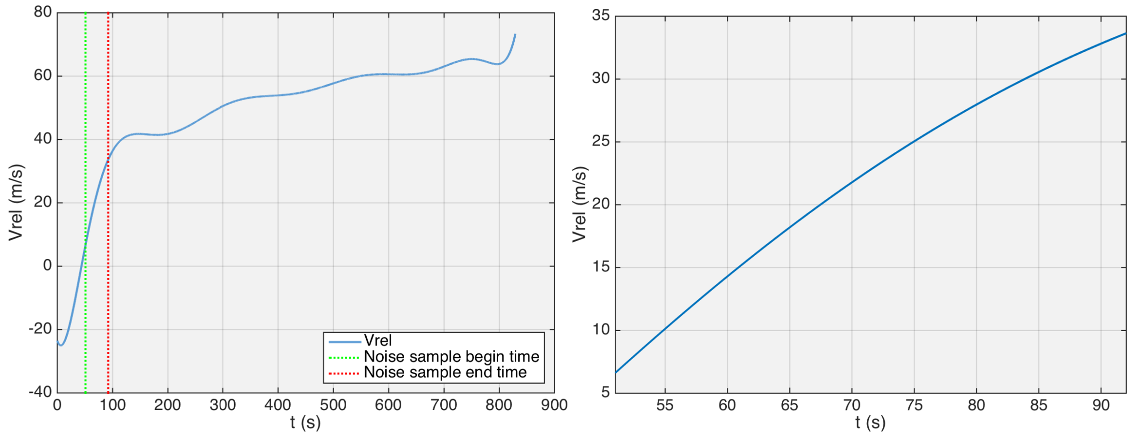

(a) Airbus A320

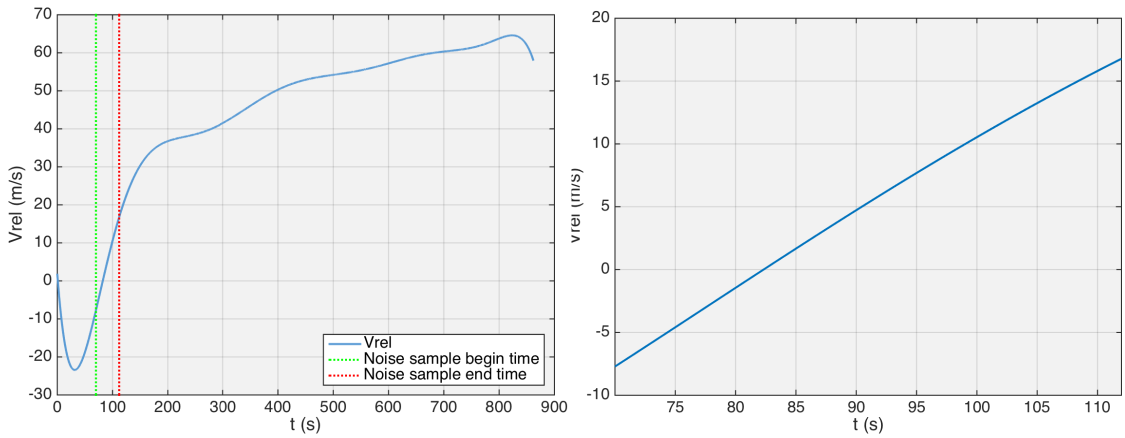

(b) Embraer 190

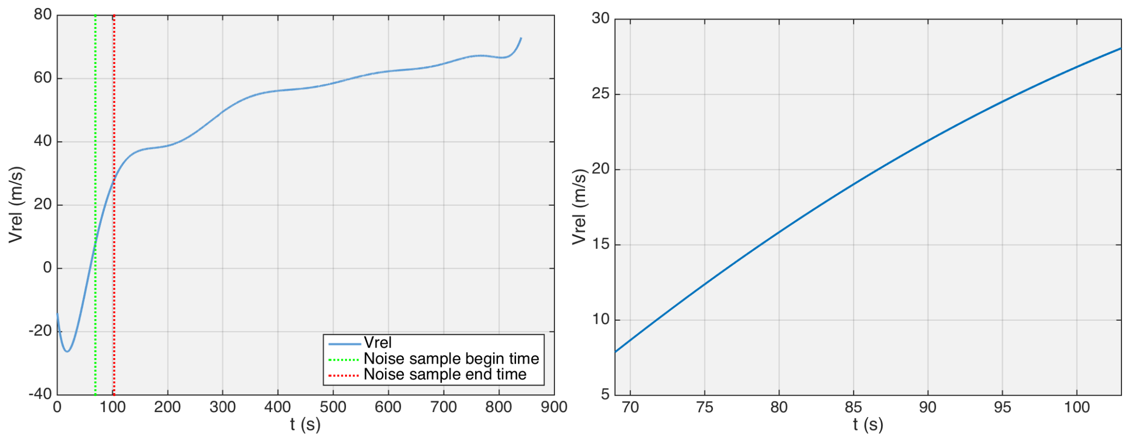

(c) Boeing B737-800

Figure 4.9: Adapted begin- and end times of relative velocity profiles

4.6 Noise Abatement Measures

Noise Abatement Measures intend to decrease noise levels observed on the ground as much as possible. Many measures have already been implemented, for example: Continuous Descent Approach (CDA), reduced flaps and idle reversed thrust.
NADP2 is the latest implemented NAM, while Noise Abatement Departure Procedure 1 (NADP1) used to be the standard procedure.

4.6.1 Noise Abatement Departure Procedure 2

NADP2 is a procedure 'quieter' compared to NADP1 and is most effective in reducing fuel consumption. In this case, 'quieter' means that summing up to difference in exposed noise levels over all areas in the vicinity of AAS, results in a negative value. Hence, less noise *after* the implementation of NADP2 is experienced, based on the outcome of the theoretical model used for this matter.
In addition, ICAO [20] expects that by implementing NADP2 as a standard departure procedure a noise and CO_2 reduction of 2-9 dB and 90-630 kg, respectively, can be realised depending on steepest climb and aircraft type. This would enable ICAO reducing noise levels and pollution as caused by aviation.

The former NADP1 is flown as follows [10]:

0 - 800 feet Altitude above Ground Level
: Adjust and maintain engine thrust in accordance with the noise abatement thrust schedule provided in the aircraft operating manual. Maintain a climb speed of $V_2 + 10$ to 20 knots with flaps and slats in the take-off configuration.

800 - 3000 feet Altitude above Ground Level
: While maintaining a positive rate of climb, accelerate and retract flaps/slats on schedule.

3000 feet - $\mathbf{h_{cruise}}$ Altitude above Ground Level
: Proceed to climb thrust, accelerate to Flaps Up speed and retract flaps/slats.

With h_{cruise} indicating the cruise height at which the cruise phase of the flight is initiated. h_{cruise} depends, among others, on company policy, weather, route and destination.

One of the biggest airlines of AAS, Koninklijke Luchtvaart Maatschappij (KLM), flew NADP2 as its standard departure procedure (in normal conditions) for the first time on 15th April 2014. While smaller airlines as Easyjet already saved millions of dollars on a yearly bases by flying NADP2, KLM finally managed to come to an agreement at the Alderstafel.
Since it is generally assumed that the majority of the fleet of civil transport aircraft will still consist of the present generation of modern transport aircraft within the next 10-15 years, airlines are seeking new ways in reducing costs, hence increasing profit [13].
Given the problem definition as stated earlier, it was NADP2 which initiated the demand of an improvement in distinctive capabilities. Given two airlines A and B flying the same procedure but with a known difference in acceleration height, it is expected that measuring the maximum noise level for aircraft of airline A should result in higher levels compared to airline B, because airline A flies over lower compared to airline B.

The NADP2 as recently implemented at AAS as being the airport its standard Noise Abatement Departure Procedure is flown as follows [10]:

0 - 800 feet Altitude above Ground Level
Climb to 800 ft Altitude above Ground Level (AGL) with take-off thrust at a speed of $V_2 + 10$ to 20 knots depending on the airline its policy.

800 - 3000 feet Altitude above Ground Level
Proceed to climb thrust, accelerate to Flaps Up speed and retract flaps/slats.

3000 feet - $\mathbf{h_{cruise}}$ Altitude above Ground Level
Continue at climb thrust and accelerate to normal climb speed.

A graphical comparison between NADP1 and NADP2 can be obtained in Figure 4.10.

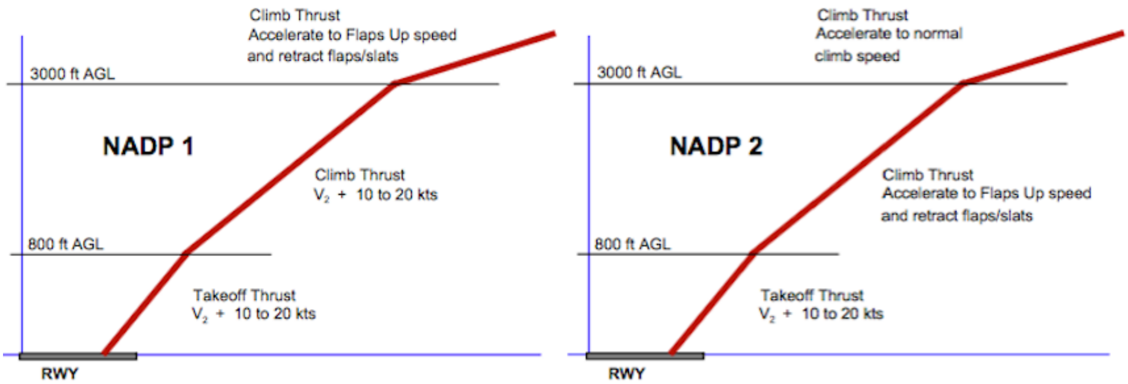

Figure 4.10: Comparison between NADP1 and NADP2. Retrieved from [10]

The aircraft configuration flying NADP2 is characterized by a thrust reduction with the initiation of the first flap/slat retraction or when the first zero flap/slat configuration is attained. Aircraft body angle (Angle of Attack (AoA) α) is decreased after 800 ft AGL and acceleration is increased towards the first flaps/slats retraction. Hence, the major difference between NADP1 and NADP2 is the height at which the acceleration phase takes place and the flaps are retracted.
The 800 ft limit of NADP2 is denoted as the acceleration height H_{ac}: the height at which the aircraft starts accelerating and stops gaining altitude. NADP2 as stated above contains the minimum heights at which it is allowed to proceed to the next step of the procedure. However, multiple variants exists in which generally H_{ac} is adapted.
Given the two airlines to be studied in this research, it is important to note that airline A in this case maintains an H_{ac} of 1000 feet, where airline B maintains an H_{ac} of 1500 feet. The difference of 500 feet, i.e. ± 150 meters, is expected to cause a difference in measured noise level. NADP2 as flown by airline A and B can be obtained in Figure 4.11, together with the height of airline A (H_A) and B (H_B) directly above the NOMOS station. H_A and H_B can vary slightly from flight to flight since the procedure is never flown exactly in the same manner. An example calculation with typical heights H_A and H_B will be given in section 5.4.

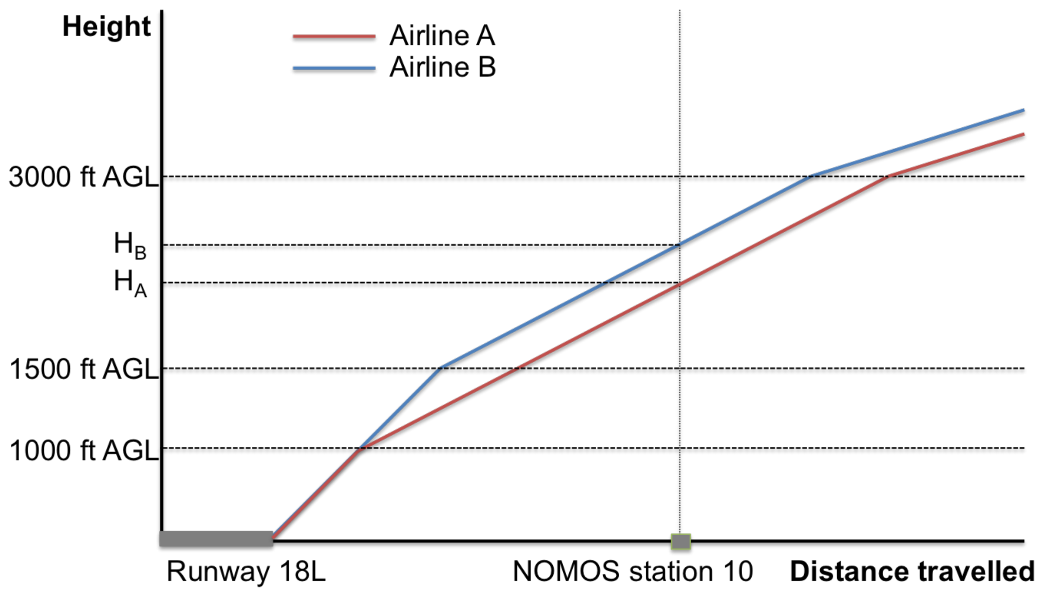

Figure 4.11: Comparison between NADP2 as flown by airline A and B

Chapter 5

Research Dataset

This chapter defines the dataset used during this MSc research. The choices made during the establishment of the dataset are clarified as well as the consequence of those choices with respect to the dataset size.
First, the dataset is defined and clarified in several steps. Second, one the dataset has been established, the problem definition is illustrated by two height profiles and last, the expected difference in measured noise level at the NOMOS station is calculated.

5.1 Defining the dataset

This section defines the dataset as used during this MSc research. Not all data available has been found to be useful and therefore this section clarifies the choices made to define the ultimate dataset to be used in further analysis.

5.1.1 Available resources

Since this is a MSc research in cooperation with Amsterdam Airport Schiphol, their data sources are completely available. Figure 5.1 shows the available resources and their contribution to the research.

NOMOS: Provides the full time series needed to estimate/determine $N1$ as well as noise measures such as Sound Pressure Level (SPL), OSPL, Overall A-weighted Sound Pressure Level (OASPL) and Maximum A-weighted noise Level ($L_{A_{max}}$).

Schiphol Information System: Provides the necessary information related to each flight. Time of departure/arrival, callsign, aircraft, engine type, number of passengers and Maximum Take-Off Weight (MTOW) are available among others. These parameters are used in the estimation/determination of $N1$.

KNMI: Provides weather information needed to correct noise spectrograms for the Doppler effect. Namely, the speed of sound c can be determined from the relative humidity h and the temperature T_{temp}, which can then be used to calculate the Doppler shift. These corrected spectrograms can then be used to estimate the engine setting $N1$ at the time the measurement was conducted.

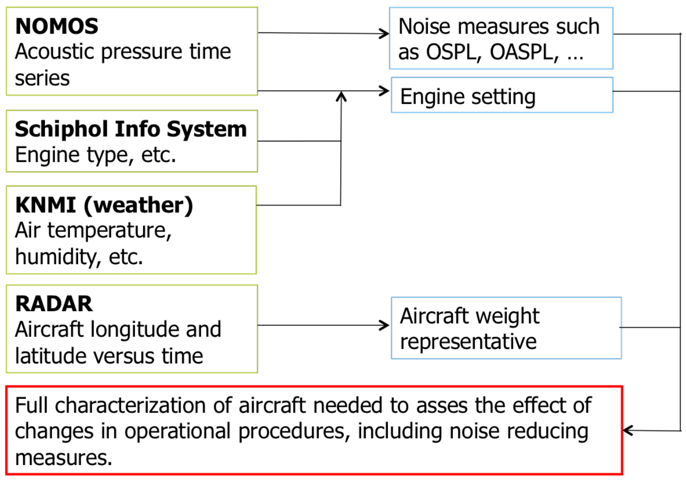

Figure 5.1: Available resources and their input

(TAR4) RADAR: Provides (LAT, LON) coordinates regarding the position of an aircraft over time. This information is used to correct noise spectrograms for the Doppler effect and provides the possibility to determine several characteristic speeds during take-off.

5.1.2 Measurement location

NOMOS stations are spread over different locations in the vicinity of AAS as shown in Figure 3.5. Not all locations are suited for this research due to the surrounding environment in which the NOMOS station is located and the amount of flights flying over each station.
For this MSc research NOMOS Station 10 (NMT10) is chosen as measurement location (see Figure 5.2) because full time series can directly be downloaded from this station, the position of this station is in the extension of runway 18L/36R (the 'Aalsmeerbaan'), the microphone is situated in a quiet environment thus very little background noise influencing the measurements and the station is located relatively close to the runway compared to other stations. The distance between the end of runway 18L/36R and NMT10 is approximately 3.1 kilometres.
Also, the difference in height can be obtained at this NOMOS station as shown in Figure 4.11. Other NOMOS stations are situated further away from the runway meaning that there is no difference in height any more between any airline flying NADP2.

Runway 18L/36R is situated in the extension of NMT10. NMT10 is positioned as such that it mainly measures noise from aircraft departed from this runway.
Runway 18L/36R can be used for landings (notation: runway 36R) and departures (notation: 18L). Due to regulatory restrictions runway 18L/36R can only be used in the southern direction. Now, a choice has to be made regarding the flight phase which is studied in this MSc research.
Since there are two operational *departure* procedures flown by two different airlines which are expected to cause a difference in measured L_{max} level, only departures from runway 18L/36R are considered. For the remainder of this research, runway 18L/36R will further be abbreviated as runway 18L.

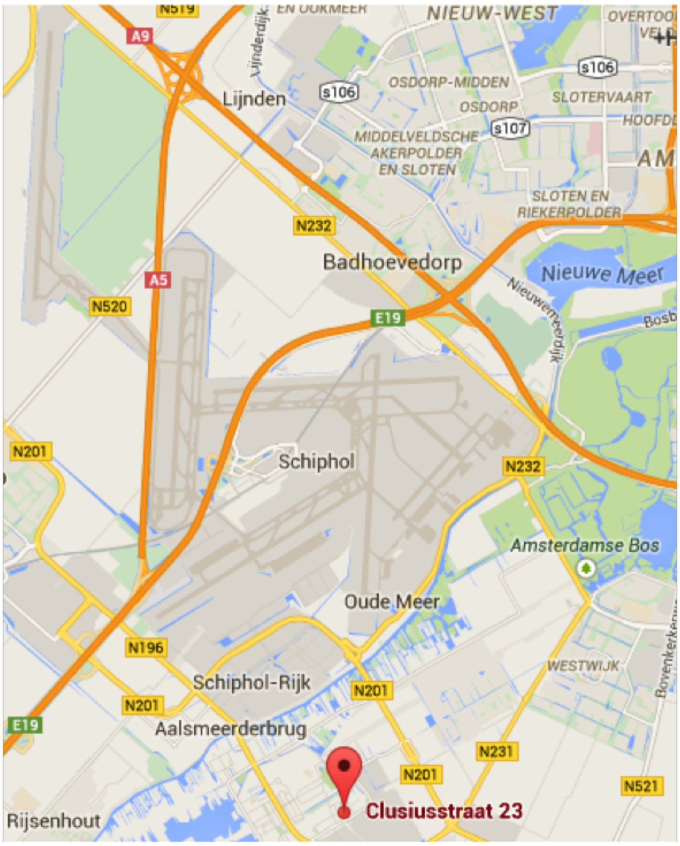

Figure 5.2: Location of NMT10 relative to runway 18L (the 'Aalsmeerbaan')

5.1.3 Routes from runway 18L

Seven different routes can be flown from runway 18L. The Aeronautical Information Publication (AIP) provides extensive informative charts regarding these routes which can be seen in Figure 5.3.

The routes prescribed by ATC actually differ slightly from practice since practical influences on aircraft cause the aircraft to deviate slightly from the 'ideal' routes. This is caused by for example wind, additional instructions from ATC or pilot steering deviations.
These seven routes as flown in practice can be obtained in Figure 5.4. Note that the possibility exists that the route flown by an aircraft is not available. Such unknown route is labelled as 'NULL'.

Nevertheless, Figure 5.3 together with Figure 5.4 show that two different combinations of routes can be distinguished, since NMT10 is located closely to the runway and multiple routes fly the same track at that position:

Route combination 1 (Route set 1): LOP2E/LEK2E/VAL2E/BER2E
Route combination 2 (Route set 2): ARN3E/LUN1E/AND2E

Each combination follows the same course in the vicinity of NMT10, hence these individual routes can be treated as one. Therefore, in the remainder of this MSc research

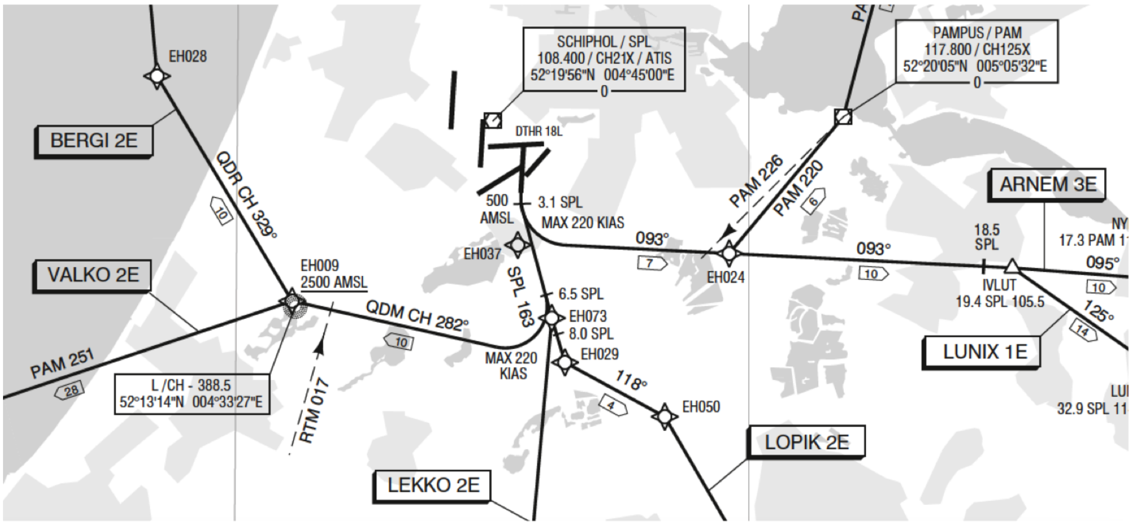

Figure 5.3: Departure routes (SIDs) from runway 18L. Retrieved from Ref. [1]

combinations of routes will be handled, in stead of individual routes. Route 'NULL' will not be used and these entries will be deleted from the dataset.

5.1.4 Measurement period

NMT10 is chosen as well suited measurement location for this MSc research. However, a choice has to be made regarding the period in which the measurements are collected/downloaded from NMT10.
Coincidentally, maintenance is committed in the period June 2014 up to and including September 2014 to the adjacent runway 06/24 (the 'Kaagbaan'). This means that runway 18L was used increasingly, hence more flights flew over NMT10. It was not possible to download the acoustic time series at NMT10 before the 20th of August 2014 due to technical difficulties. In the period 20th of August 2014 up to and including 31st of August 2014 runway 18L has been used intensively and hence all measurements performed by NMT10 in this period are used as data set for this MSc research.

5.1.5 Airlines

The aim of this research is to proof statistically the effect of two different variants of a departure procedure (NADP2), which is expected to cause a change in measured noise level. Initially, the aim of the research was to proof statistically that NADP2 is a quieter departure procedure compared to NADP1. However, no acoustic time series could be downloaded from any NOMOS station before the implementation of NADP2 as the standard departure procedure of AAS due to technical difficulties, meaning that the engine setting could not be determined for flights performing NADP1. However, the difference in measured noise level is expected to be caused by the difference in height between NADP1 and NADP2 at the measurement location. Therefore, two variants of NADP2 are studied from which it is known that there also exist a difference in height. Nevertheless, the difference in height between NADP1 and NADP2 is approximately 100 meters larger compared to the difference in height between the two variants of NADP2. The hypothesis is that

the difference in noise level between NADP1 and NADP2 would have only been larger, when the two variants of NADP2 show a difference in measured noise level.
Therefore, this research aims at statistically proving a difference in noise level between two variants of NADP1 and NADP2.

Thus, airlines have to be found which are known to fly NADP2 but with different variants. These airlines of course have to fly frequently enough to be able to collect an acceptable amount of data in the period previously mentioned.
Two airlines are found to fly NADP2 but with a different variant. The difference between these two variants is that one airline (called airline A in this thesis for confidential purposes) flies NADP2 with an acceleration height of 1000 feet, where the second airline (called airline B in this thesis for confidential purposes) flies NADP2 with an acceleration height of 1500 feet. Thus, airline A and B pass NMT10 at a different height, which is expected to cause a change in noise level. Unfortunately, no other airlines could be found from which the variant of NADP2 was known. Hence, two airlines encompassing 1048 measurements will be investigated during this research.

5.1.6 Aircraft

The dataset now contains multiple aircraft owned by either airline A or airline B. But, as will be clarified later on in this MSc research, comparisons must be made using one and the same aircraft type. Hence, the dataset must be checked for the presence of corresponding aircraft types. There is only *one* corresponding aircraft type between airline A and B: the Boeing 737-800, further abbreviated as the B738. Thus, only measurements from the B738 are used in further analysis. Hence, this narrows down the total dataset of 1048 measurements to 263 measurements.

5.2 Visualizing both airlines their height profile

As earlier mentioned, both airlines are known to fly the same departure procedure (namely NADP2) but operate it with a different acceleration height. The acceleration height h_{ac} is the height at which airlines continue their climb with the acceleration phase. With respect to NMT10, this difference in h_{ac} results in a lower flyover altitude for airline A compared to airline B (see Figure 5.5) and hence the flyovers of airline A are expected to cause higher noise levels compared to airline B.

The difference in height is not easily obtainable via Figure 5.5. Nevertheless, looking at the turn at approximately $(LON, LAT) \approx (4.55, 52.3)$ shows that airline A is lower compared to airline B, which also holds at the location closest to NMT10.

5.3 Alternative dataset

Once the dataset has been set to be used in this research, it is important to note that an alternative dataset has been used in chapter 7.
This alternative dataset, collected in 2010 for a former research, is used to study the validity of an aircraft mass representative for this research.
This alternative dataset contains aircraft related information as logged on the Flight

Management System (FMS) of the aircraft. For example, information regarding the left and right engine setting $N1$, aircraft mass m, landing gear up/down and flap position is available. However, generally the dataset as set in this chapter is used unless specifically appointed. Figure 5.6 shows a graphical representation of the two dataset on a timeline together with an overview of the available parameters in that particular dataset.

5.4 Expected difference in noise level

NADP2 is operated by both airlines with a difference in acceleration height, as well as a difference in height at the closest point with respect to NMT10.
On an average, the height of airline A and B closest to NMT10 equal 990 m and 1160 m, respectively. The difference in noise level is caused by atmospheric absorption and attenuation, described by $20\log(\frac{r_2}{r_1})$ and $\alpha\Delta r$,respectively. α is frequency dependent and expected to be maximum at 500 Hz. With the temperature equal to 10 °C and the relative humidity equal to 50%, α at 500 Hz equals 1.9 dB/km. Thus, the expected difference in noise level equals $20\log(\frac{1160}{990} + 1.9 \cdot (1160 - 990) = 1.7$ dB. Hence, the ultimate goal of this MSc research is to visualize a difference of 1.7 dB in noise level between airline A and B as caused by a difference in acceleration height.

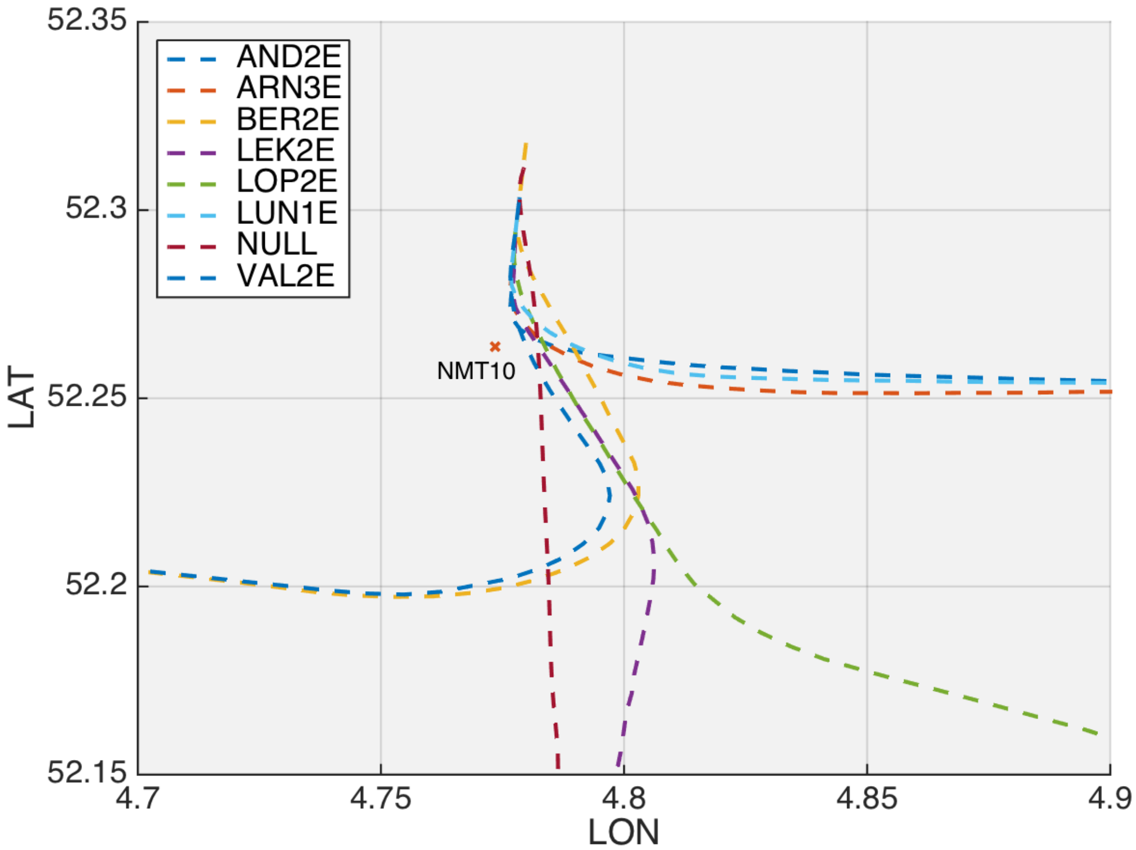

(a) Route development

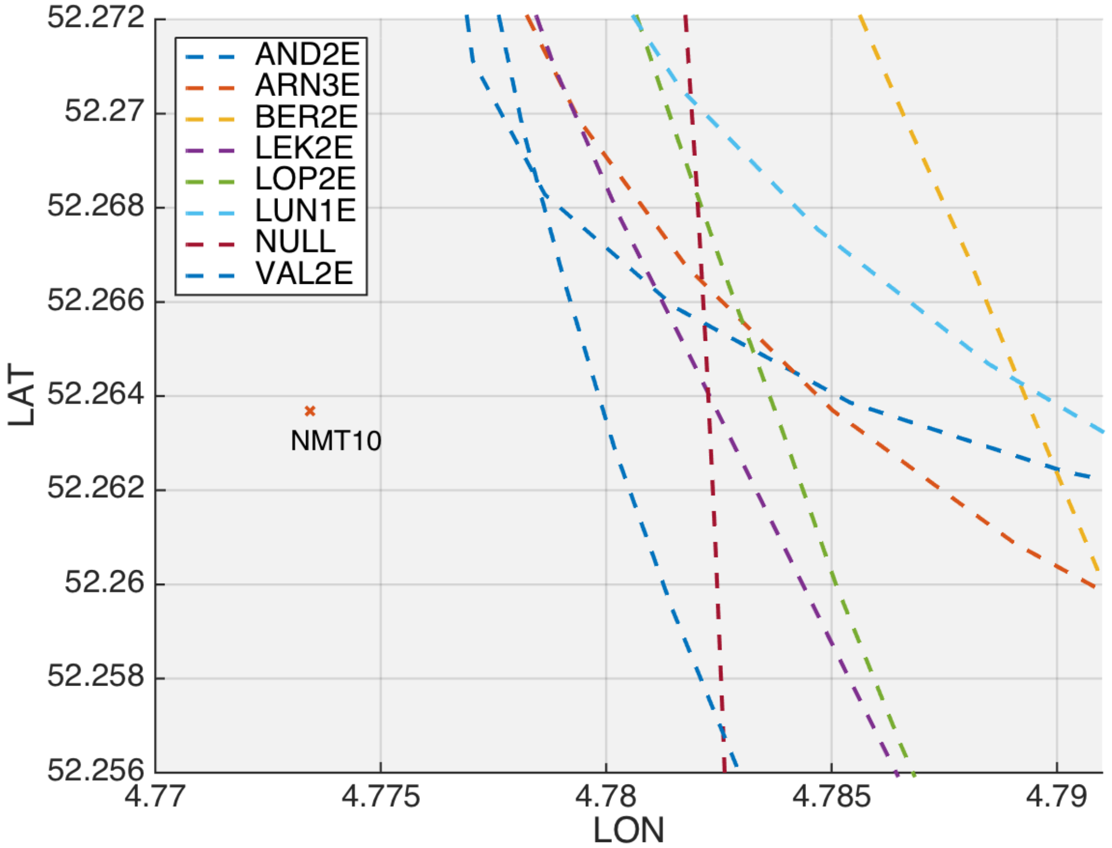

(b) Close-up of route development

Figure 5.4: Route development with respect to NMT10

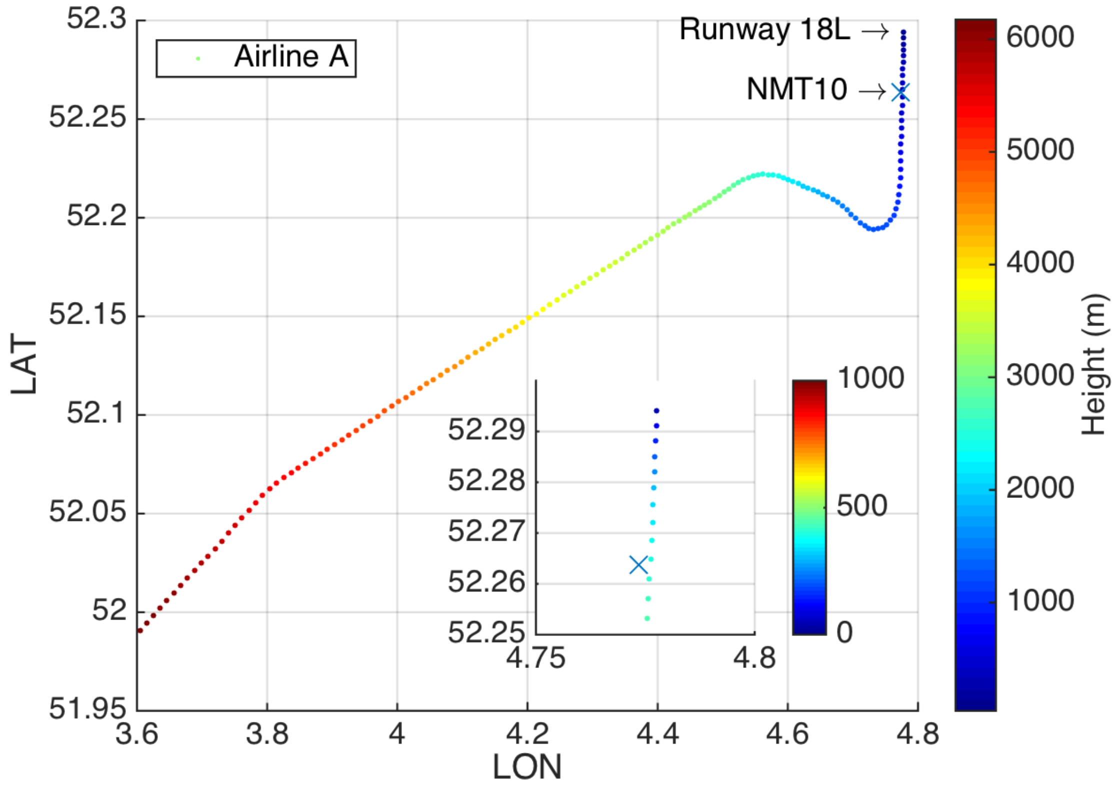

(a) Airline A

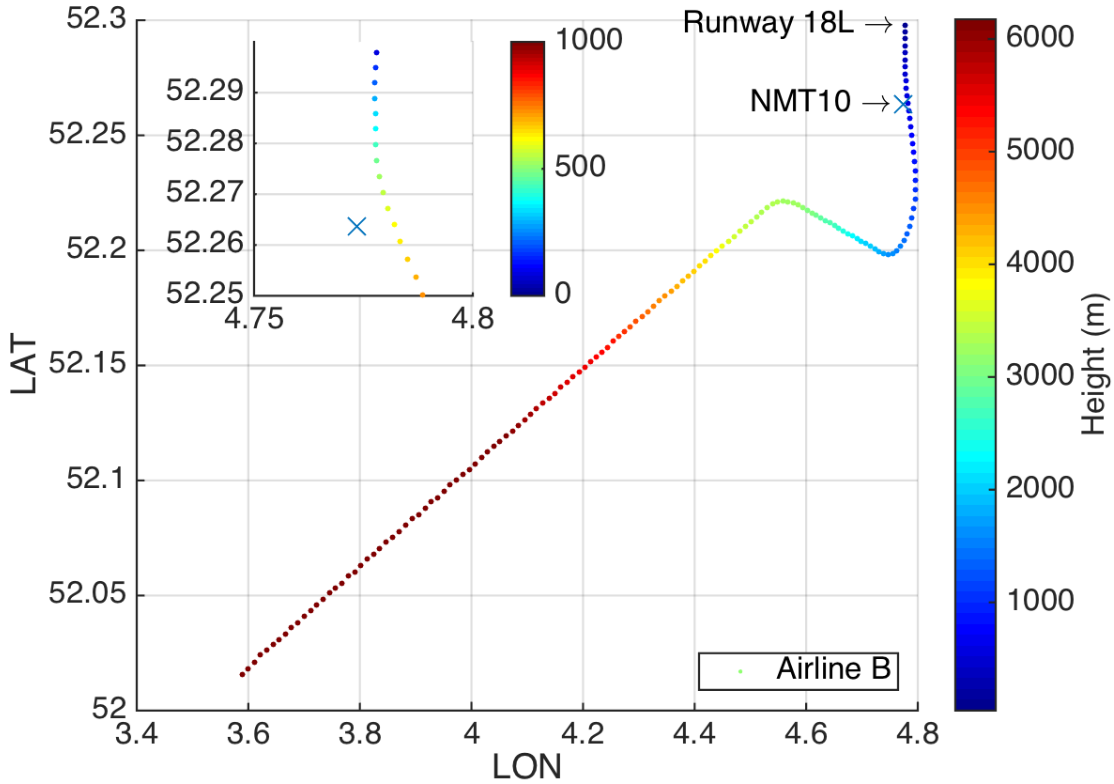

(b) Airline B

Figure 5.5: VAL2E route height profile for airline A and B

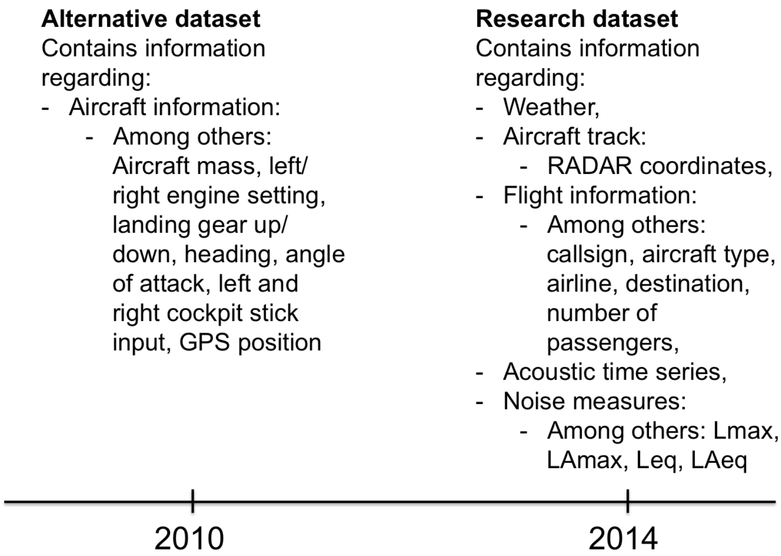

Figure 5.6: The alternative dataset and the research dataset

[Page intentionally left blank]

Chapter 6

Aircraft Engine Power Setting Determination Algorithm

In this study the aircraft engine power setting $N1$ is used as predictor for the noise measurement classification process and hence encompasses the determination of the actual engine power settings by using noise measurements; in particular determining the BPF from the spectrogram. This chapter provides information regarding the working principle of the aircraft engine power setting $N1$ determination algorithm, further denoted as the N1 Determination Algorithm (N1DA).

6.1 Reference measurements

For explanatory purposes this chapter uses three reference measurements from a Boeing 737-800, a Fokker 70 and an Avro RJ-100. The specifications of the reference measurements are listed in Table 6.1. Note that the time mentioned in Table 6.1 represents the local time at which NOMOS started measuring the noise event. Since this study only treats departures from runway 18L, the assigned Standard Instrument Departure (SID) is also mentioned because it provides information regarding the position of the aircraft relative to NMT10 as mentioned in subsection 5.1.3.

Table 6.1: Specifications of the reference measurements

Date	Time (LT)	Aircraft	Callsign	SID
25-08-2014	06:45:38	Boeing 737-800	TFL173	LUN1E
25-08-2014	07:00:47	Fokker 70	KLM1853	ARN3E
25-08-2014	07:02:31	Avro RJ-100	SWR737	LUN1E

Each measurement represents noise caused by the engines of each particular aircraft. The engine specifications of each aircraft are listed in Table 6.2.

With the number of blades and the blade rotational speed represented by b and Ω, respectively.

Table 6.2: Aircraft engine specifications for each example measurement

Aircraft	Engine	b	Ω (Hz)
Boeing B737-800	CFM56-7B26	24	5175
Fokker 70	TAY MK 620-15	22	8100
Avro RJ-100	LF507-1F,-1H	40	7602

6.2 Preprocessing the NOMOS acoustic data

The acoustic data from NOMOS needs to be preprocessed in order to be useful for this research. The visualization of the tonal component of the engines (the BPF) requires fundamental decisions considering the topics as discussed in section 4.4, which will be treated consecutively:

1. Program used for acoustic data analysis;
2. Handled resolution in time and frequency domain;
3. Chosen window function;
4. Chosen FFT properties;
5. Visualizing acoustic data.

A flowchart visualizing the approach of preprocessing acoustic data to a spectrogram is shown in Figure 6.1.

Figure 6.1: Flowchart representing the conversion of raw acoustic data to a spectrogram

6.2.1 Program used for acoustic data analysis

The acoustic data downloaded from NOMOS station 10 is encrypted in .ogg file format. .ogg files represent a bit-stream container format where the initial data is compressed and hence needs to be converted to a sampled data format in order to be useful for further analysis.

The program used for this research is MATLAB and so the acoustic data is loaded into MATLAB for further analysis. MATLAB reads the data and converts it to double-precision normalized samples. This results in the (time-amplitude)-plot as shown in Figure 6.2.

The amplitude increases until approximately 20 seconds and then decreases again, which is logical since the aircraft flew over the NOMOS station and NOMOS centers the noise event at its maximum Sound Intensity Level (SIL). Once the acoustic data has been loaded into MATLAB , the desired resolution in time and frequency domain has to be determined in order to window and transform the acoustic data to the frequency domain.

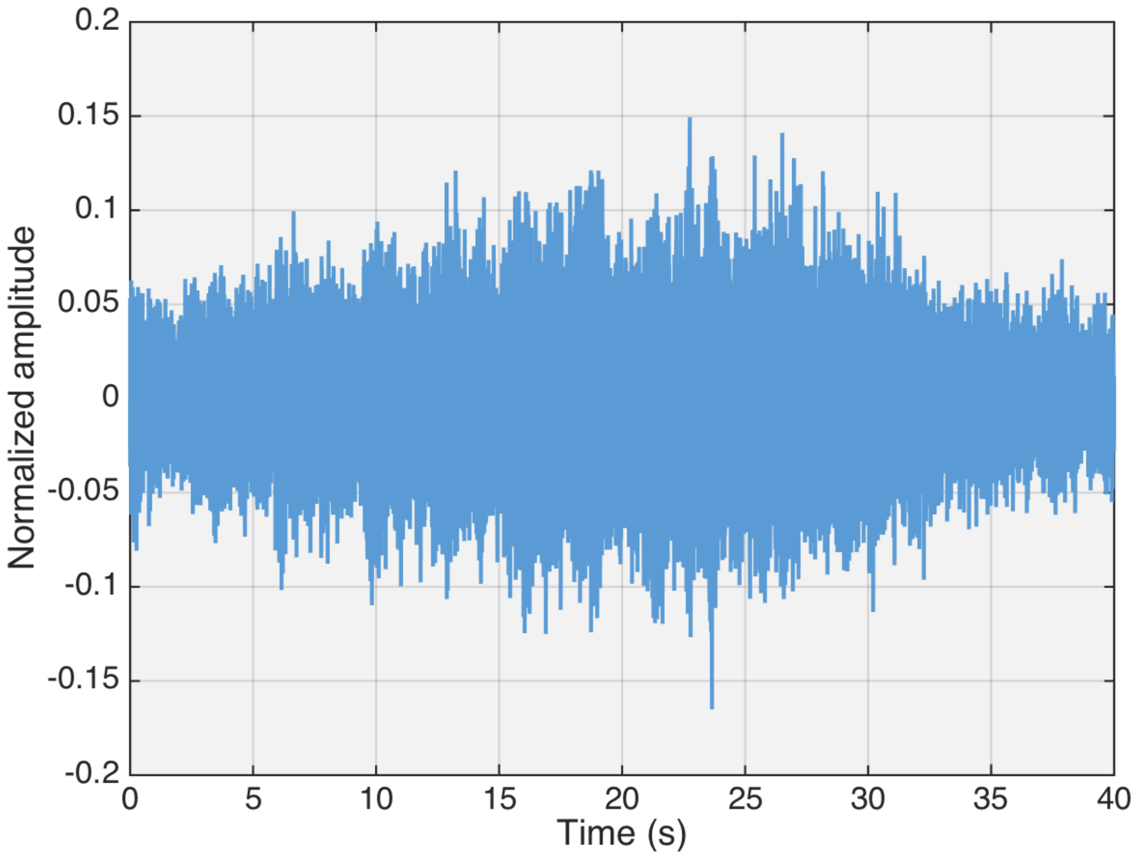

Figure 6.2: Time versus normalized amplitude example originated from raw data (.ogg-file) loaded into MATLAB

6.2.2 Handled resolution in time and frequency domain

For this research a time block T of 0.1 seconds is chosen, because it is found that $T = 0.1$ s provides enough resolution in the time domain to be able to visualize the BPF. Together with the given sample frequency F_s of 8000 Hz, the number of samples per block N_s becomes $N_s = T \cdot F_s = 0.1 \cdot 8000 = 800$ samples. Hence one bin of the spectrogram has a duration of 0.1 seconds and contains 800 samples.

6.2.3 Chosen window function

To visualize and distil the harmonics in the spectrogram resulting from engine noise, a *Hanning-window* has been chosen as the best suitable window function for this specific application. Figure 6.3 shows the raw-data versus the windowed data for the reference measurements.

6.2.4 Chosen Fast Fourier Transform properties

For the length of the FFT $NFFT$, 8 times the total length of the weights for windowing has been chosen to provide sufficient quality regarding frequency and amplitude information. A Hanning window function is chosen with its size obviously equal to the number of samples per block $N_s = 800$. The length of the FFT $NFFT$ therefore becomes $NFFT = 8 \cdot 800 = 6400$.

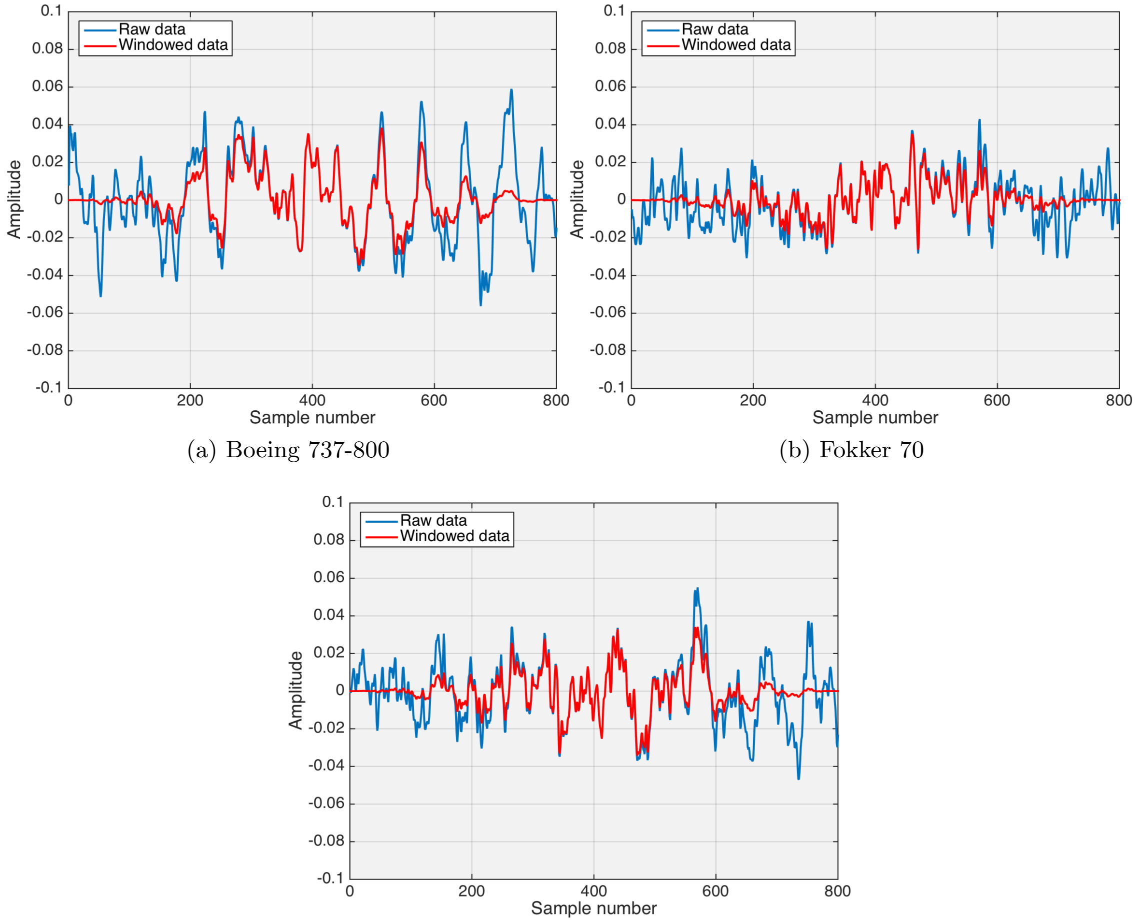

(a) Boeing 737-800

(b) Fokker 70

(c) Avro RJ-100

Figure 6.3: Hanning windowed amplitudes of reference measurements

6.2.5 Visualizing acoustic data

With the FFT carried out, frequency f over time t is known as well as the amplitude A of each frequency bin Δf. These three parameters are visualized by a spectrogram with t on the x-axis, f on the y-axis and A indicated by a color. The spectrograms for the reference measurements are shown in Figure 6.4.

6.3 Correcting acoustic data

As mentioned in section 4.5, the acoustic data needs to be corrected for the Doppler effect. This section explains the approach to correct the spectrograms for the Doppler effect. Using Equation 4.6 requires the relative velocity $\mathrm{d}r/\mathrm{d}t$ and the speed of sound c to be known so that the BPF subjected to the Doppler effect can be calculated and visualized in the spectrogram.

6.3.1 Determine $\mathrm{d}r/\mathrm{d}t$

The SR r is calculated by converting (LAT, LON) coordinates in the World Geodetic System 1984 (WGS84) to the Universal Transverse Mercator (UTM) coordinate system

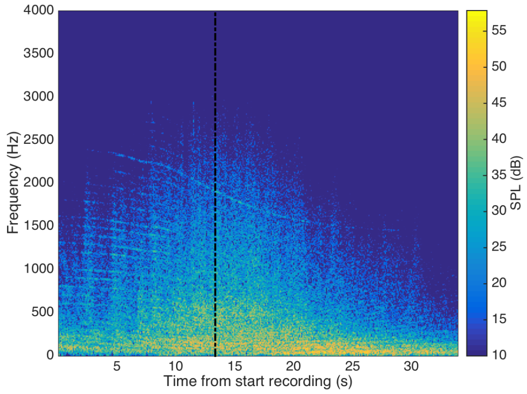

(a) Boeing 737-800

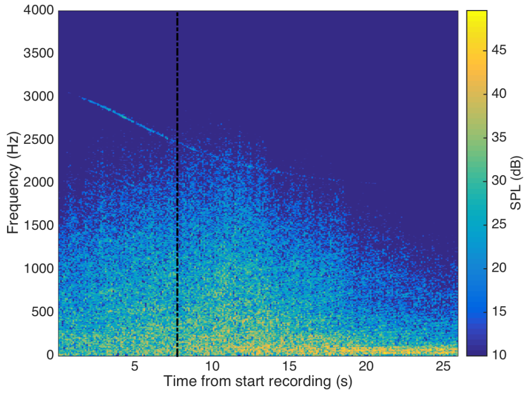

(b) Fokker 70

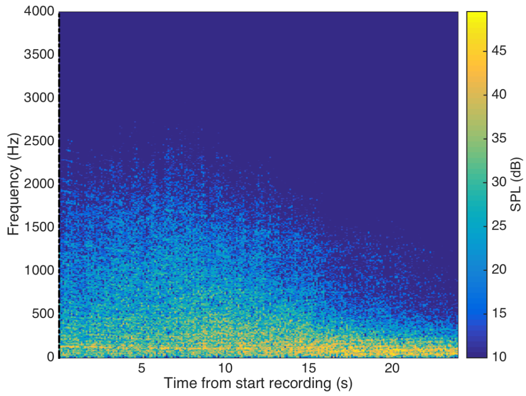

(c) Avro RJ-100

Figure 6.4: Spectrograms of the reference measurements

[29]. Calculating the time-derivative of r (Equation 4.8) results in a V_{rel} profile as indicated in Figure 4.8. Using the time-stamp of the noise sample and the time-stamps given by the RADAR track, results in the part of interest to correct the spectrogram for the Doppler effect. However, after correcting multiple spectrograms for the Doppler effect it seemed that apparently there exist a time-offset between the NOMOS noise sample time-stamp and the RADAR track. Since these two systems are not time-synchronized on a continuous basis, the assumption exist that the time-offset has to be constant.

Time-offset between NOMOS samples and RADAR tracks

The time-offset has been determined by manually choosing the time period in which the Doppler factors are calculated, resulting from the V_{rel} profile and Equation 4.6, for 10 different noise measurements. The calculated theoretical Doppler shifted BPF is then compared to the practical Doppler shifted BPF as visible in the spectrogram. The best fit between the theoretical Doppler shifted BPF and the practical Doppler shifted BPF as visible in the spectrogram results in a time-offset between the RADAR data and the NOMOS data. Registering the time-stamp of the noise sample and the begin-time of the

Table 6.3: Time-offsets between 10 different NOMOS samples and associated V_{rel} profiles

NOMOS time-stamp	RADAR begin-time	time-offset (s)
25-08-2014 06:45:38	25-08-2014 06:44:32	66
25-08-2014 06:48:46	25-08-2014 06:47:35	71
25-08-2014 06:51:35	25-08-2014 06:50:36	59
25-08-2014 07:00:47	25-08-2014 06:59:43	64
25-08-2014 07:02:31	25-08-2014 07:01:15	76
25-08-2014 07:03:44	25-08-2014 07:02:39	65
25-08-2014 07:04:56	25-08-2014 07:03:59	57
25-08-2014 07:06:35	25-08-2014 07:05:43	52
25-08-2014 07:08:03	25-08-2014 07:07:02	61
25-08-2014 07:09:30	25-08-2014 07:08:22	68
	Average =	64

best manual V_{rel} shift, results in 10 time-offsets. The results are shown in Table 6.3 and Figure 6.5.

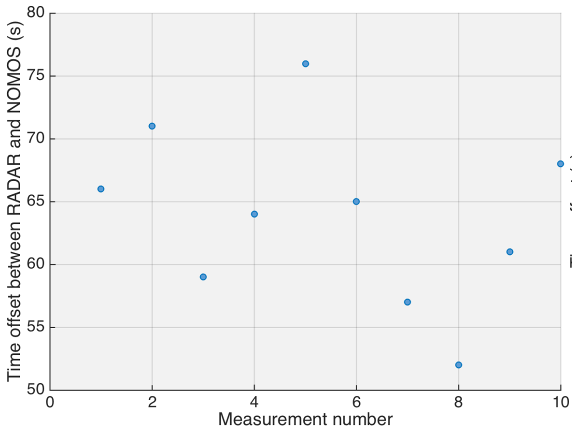

(a) Scatter plot

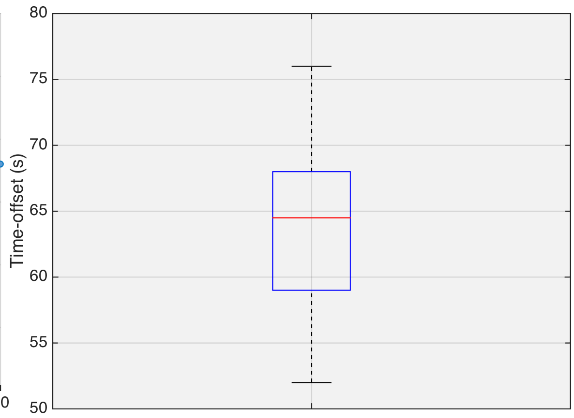

(b) Box plot

Figure 6.5: Scatter plot of time-offset between NOMOS and RADAR

More than 2000 noise-samples are treated and therefore it is highly undesirable to determine more than 2000 individual time-offsets manually. Hence, although the time-offset is not constant, according to Table 6.3 and Figure 6.5, a fixed time-offset of 64 seconds is assumed. Unfortunately, no conclusions could be drawn regarding the reason of such a large time-offset between the RADAR data and the NOMOS data.

The possibility exists that an error is made for certain spectrograms where the time-offset is not equal to 64 seconds. This causes an error in the theoretical Doppler shifted BPF and hence no qualitative good match can be found between the theoretical Doppler shifted BPF and the BPF visible in the spectrogram. However, the Peak Find Method (PFM) as explained in section 6.6 simply does not find a solution for $N1$ and rejects the spectrogram as "No solution can be found".

64 seconds are added to all RADAR tracks. This gives synchronised RADAR tracks and NOMOS measurements. Now, a V_{rel} profile can be constructed from a RADAR track, given the begin- and end time of the associated NOMOS measurement.

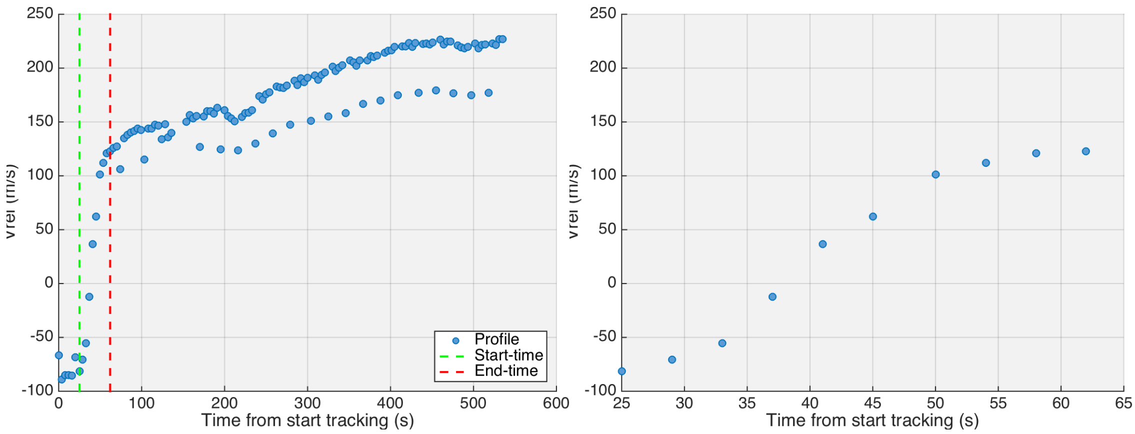

(a) Boeing 737-800

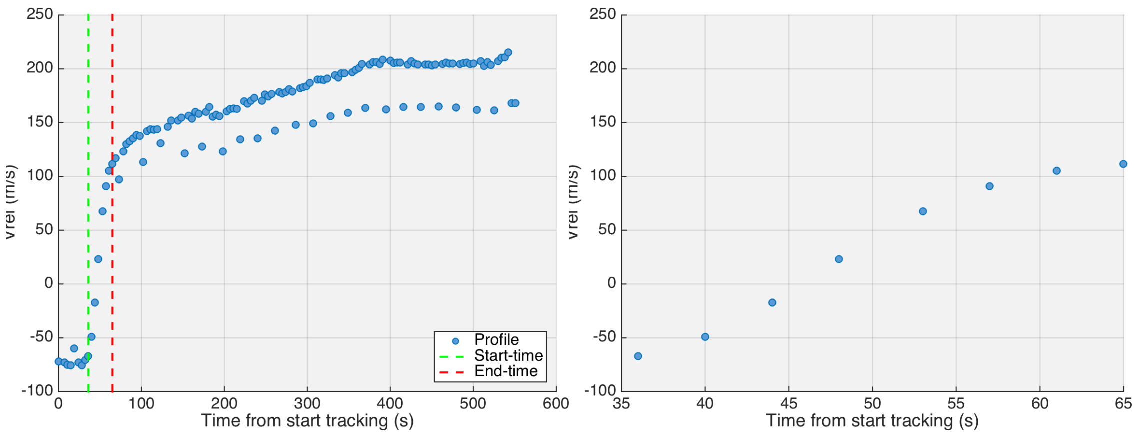

(b) Fokker 70 (c)

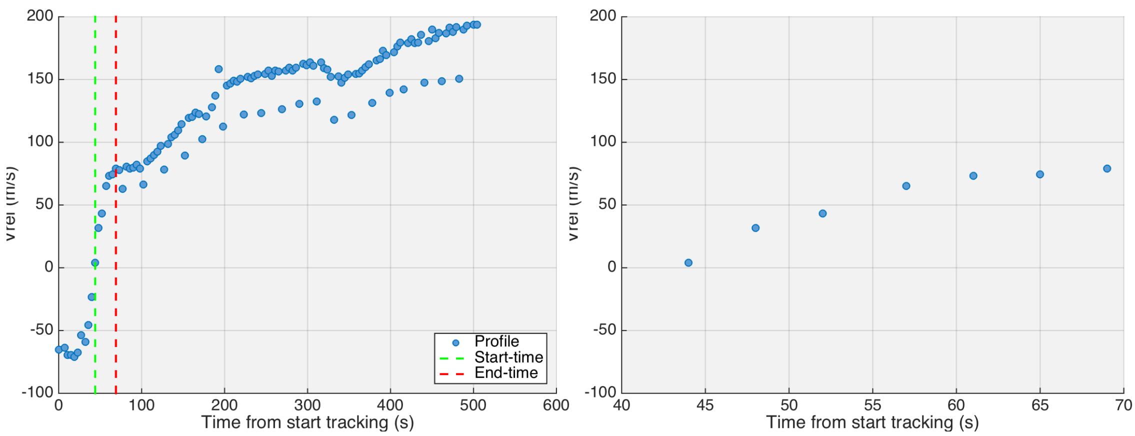

(c) Avro RJ-100

Figure 6.6: V_{rel} profile and cut-off

Table 6.4: Weather information at AAS. Retrieved from Ref. [21]

Date:	25 August 2014
Time period (LT):	06:00:00 h - 06:59:59 h
Temperature:	11.8 °C
Relative humidity:	88 %
Wind:	3.0 m/s
Gust_{max}:	12 m/s
Direction:	160 °
Air pressure:	1015.0 hPa

As already indicated, the outliers of Figure 6.6 are assumed to be caused by measurement errors since the position of an aircraft further away from the RADAR station cannot be determined accurately. Nevertheless, only the position of an aircraft in the first 100 seconds will be used so no outliers will then be present any more.

Calculating speed of sound c

The speed of sound can be culculated by using Equation 4.7 and filling in the meteorological conditions. Weather information from the Royal Dutch Metrology Institute on the day the reference measurements where taken (August 25$^{\text{th}}$ 2014) is summarized in Table 6.4.

Filling in Equation 4.7 with $c_0 = 340.29$ m/s results in:

$$\begin{aligned} c = 340.29 \cdot [1 + .88(9.66 \cdot 10^{-4} + 7.2 \cdot 10^{-5} \cdot 11.8 + \\ 1.8 \cdot 10^{-6} \cdot 11.8^2 + 7.2 \cdot 10^{-8} \cdot 11.8^3 + 6.5 \cdot 10^{-11} \cdot 11.8^4)] \\ = 340.94 \text{ m/s} \end{aligned}$$

The speed of sound c can now be used to calculate the Doppler factors for each time block ΔT in the spectrogram. These Doppler factors will then be used to calculate the theoretical BPF subjected to the Doppler effect. The theoretical BPF subjected to the Doppler effect should then have the same shape as the BPF as visible in the spectrogram, so that the theoretical BPF can be compared to the BPF as visible in the spectrogram.

6.3.2 Calculating the theoretical *BPF*

In order to determine the actual flown power setting, first the theoretical BPF has to be calculated for each engine type (see Table 6.5). The BPF has been calculated by using Equation 4.1 and a reference value for $N1$ which is equal to 55%. Example calculations are shown in Table 6.5. The aircraft- and associated engine type are retrieved from the Schiphol Information System, the number of blades b and the blade rotational speed at $N1 = 100\%$ are adapted from the internet (mostly from the website of the engine manufacturer) and $BPF_{N1=55\%}$ is calculated by using $BPF_{N1=55\%} = N1 \cdot BPF_{N1=100\%} = N1 \cdot \frac{b \cdot \Omega}{60} = 0.55 \cdot \frac{b \cdot \Omega}{60}$. Note that in this equation the fundamental frequency f_0 is treated, i.e. $k = 1$. However, it is possible that the first harmonic ($k = 1$ is not visible in the spectrogram, while harmonics for $k > 1$ might be visible. Therefore, the visible harmonic k is determined by investigating multiple spectrograms for all aircraft types in the dataset and hence 'predicting' which harmonic will most-likely be visible.

Table 6.5: BPF per aircraft and engine type

Aircraft	Engine	b	Ω (Hz)	$BPF_{N1=55\%}$ (Hz)
Boeing B737-800	CFM56-7B26	24	5175	1139
Fokker 70	TAY MK 620-15	22	8100	1634
Avro RJ-100	LF507-1F,-1H	40	7602	2787

6.3.3 Calculating the BPF subjected to the Doppler effect

Once, the time-offset $t_{b_{nomos}} - t_{b_{radar}} = +64$ seconds has been set, the relevant part of the V_{rel} profile can be distilled. Together with Equation 4.6 the Doppler factors for each measurement can be calculated, as to correct the BPF for each time-block T in the spectrogram. In this case, the spectrogram is not corrected for the Doppler effect, rather the theoretical BPF is calculated while not being corrected yet for the Doppler effect. This leaves a theoretical BPF which is subjected to the Doppler effect.

Since the main goal of the acoustic-data-processing-part is to determine the engine setting $N1$ at the time the noise measurement was collected, $N1$ is varied throughout the algorithm to find the actual engine setting.

Figure 6.7 shows the theoretical BPF subjected to the Doppler effect. This is done by using the associated RADAR track and calculating the Doppler factors associated to each time block T of the spectrogram. The 'raw BPF' shows the theoretical BPF points subjected to the Doppler effect. However, these points contain measurement errors caused by the RADAR station. Hence, a second order polynomial of the form $p(x) = p_1x^2 + p_2x + p_3$ is constructed to smooth the theoretical BPF, which is represented by the 'polynomial BPF'. Smoothing is applied to be able to compare a *realistic* theoretical BPF subjected to the associated Doppler effect.

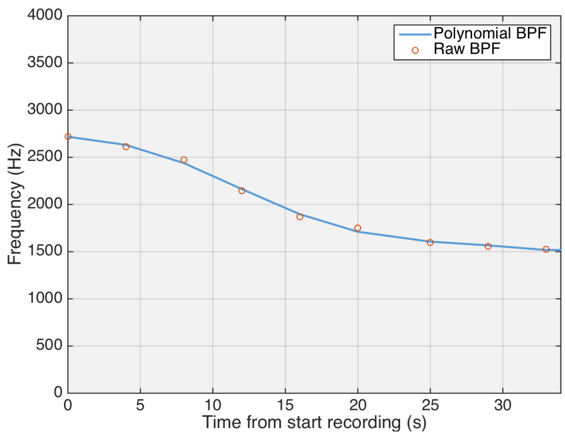

(a) Boeing 737-800

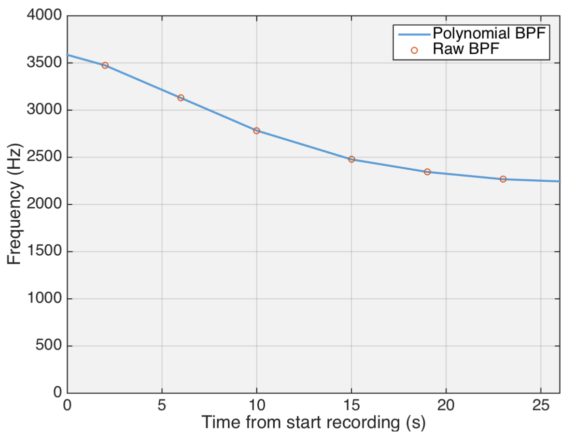

(b) Fokker 70

Figure 6.7: Theoretical BPF subjected to the associated Doppler effect

The theoretical BPF subjected to the Doppler effect for the Avro RJ-100 could not be calculated because the BPF ($N1 = 100\%$) for the aircraft engines of this measurement is equal to 5068 Hz. Since the maximum visible frequency bin is equal to 4000 Hz and $\frac{f'}{f} > 1$ $\forall\ \Delta T < t_{fo}$ with t_{fo} the time of fly-over, only a theoretical visualization of a harmonic can be achieved if: [1] $N1$ is low or [2] $\frac{f'}{f}$ is very low. Even in the second case, if $N1$ is too high, only for the first part of the spectrogram until $t > t_{fo}$ a theoretical approach can be made since $\frac{f'}{f} < 1$ for all $> t_{fo}$ and hence for $t > t_{fo}$ the BPF subjected to the Doppler effect is shifted upwards; outside the visible frequency region. This must be kept in mind when evaluating the $N1$-determination results for aircraft with the Honeywell LF507-1F and -1H engines.

6.4 Visualizing the theoretical BPF subjected to the Doppler effect

The theoretical BPF subjected to the Doppler effect can now be visualized in the actual spectrogram. The best fit to the measured BPF, visible in the spectrogram, is found by calculating the theoretical BPF subjected to the Doppler effect for $60 \leq N1 \leq 100$ and calculating the Root Mean Square Error (RMSE). $N1$ for which the RMSE is the lowest is chosen as the actual $N1$ for that particular measurement. The best fits for the reference measurements are shown in Figure 6.8.

The $N1$ values to obtain the best fitted theoretical BPF subjected to the Doppler effect, as shown in Figure 6.8, for the reference measurements are 92%, 84% and 38%, respectively. Note that indeed $N1$ is very small (and unrealistic) for spectrogram 6.8c because of a high characteristic BPF ($BPF(N1 = 100\%) = 5068\text{Hz}$) as earlier mentioned. Therefore, it can be concluded that NMT10 is not suitable for predicting $N1$ settings for $BPF_{N1=60\%} >$ 4000 Hz because the maximum frequency visible in the spectrograms for data derived from NMT10 equals $\frac{F_s}{2} = 4000$ Hz. $N1 = 60\%$ is assumed to be the minimum possible $N1$ setting as measured by NMT10 for aircraft departed from runway 18L.

6.5 Development of *N1* Determination Algorithm

The ultimate goal of this part of the study is to determine $N1$ automatically for multiple measurements performed by NOMOS. For this purpose an algorithm is developed: the *N1* Determination Algorithm, aptly named the *N1*DA. This section explains the approach towards an automated *N1*DA. Note that the measured BPF represents the BPF as visualized by the spectrogram, further denoted as BPF_{spec} and the theoretical BPF as calculated via theory BPF_{theory} (see subsection 6.3.3).

6.5.1 Distilling the measured BPF subjected to the Doppler effect

To compare BPF_{theory} with BPF_{spec} as visible in the spectrogram, first BPF_{spec} needs to be distilled. This is done by determining the maximum SPL value for each of the time block T within a predefined frequency domain $F_{lb} \leq \Delta F \leq F_{ub}$ with F_{lb}, F_{ub} representing the lower and upper frequency bound, respectively. Within the range between F_{lb} and F_{ub}, for each time block T, the frequency f at which the SPL is maximum is determined. BPF_{spec} as distilled from the spectrogram will further be denoted as $BPF_{spec,dist}$.

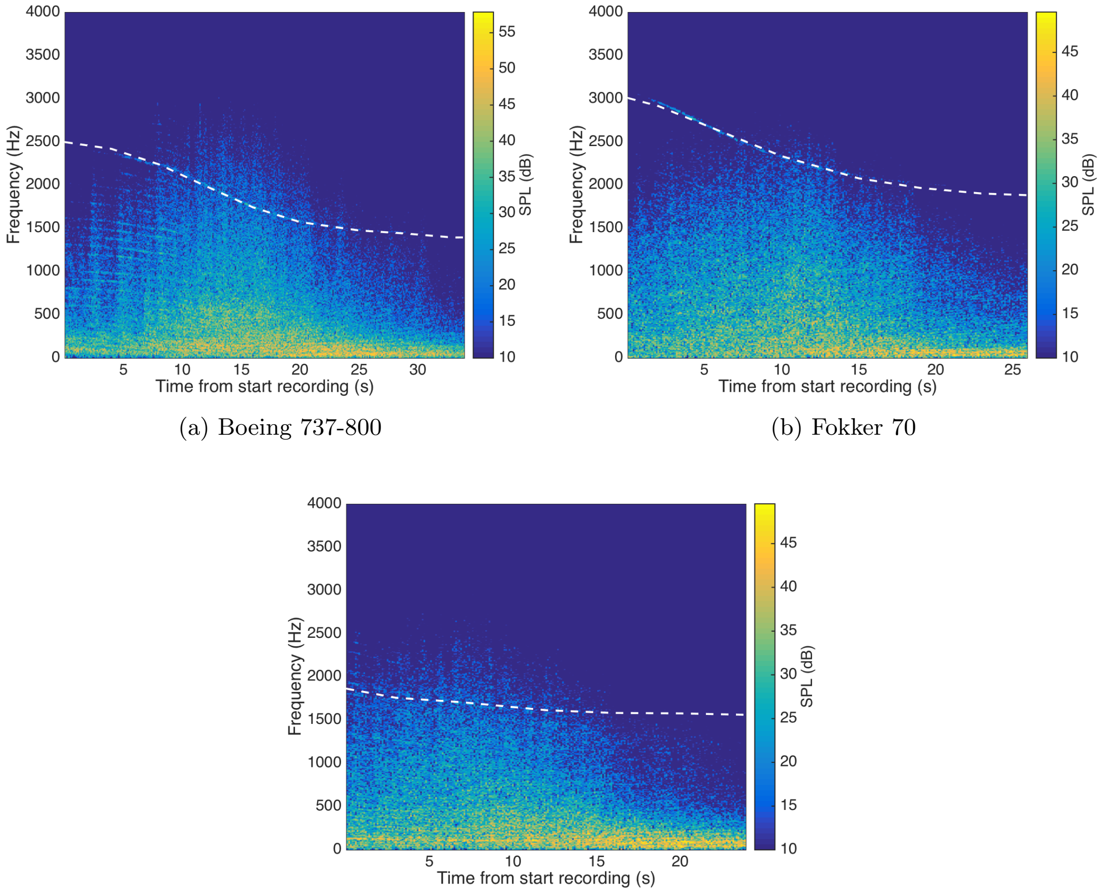

(a) Boeing 737-800

(b) Fokker 70

(c) Avro RJ-100

Figure 6.8: Spectrogram with best-fitted theoretical BPF subjected to the Doppler effect

An example of this process is shown in Figure 6.9. The dynamic upper- and lower boundary are visualized by dotted lines and the distilled maximum SPL for each time block T is visualized by the red dots. The dynamic frequency domain will be explained later in this section.

From Figure 6.9 can immediately be stated that the recognition of BPF_{spec} is poor. Most of the red dots are situated at the lower boundary, caused by broadband noise. Hence, this method has a major disadvantage of recognizing mostly broadband noise in stead of the measured BPF. The error of distinguishing the wrong frequencies, and thus frequencies which are not part of BPF_{spec}, can also be caused by the upper- and lower boundaries specified.

The frequency domain consists of a lower-bound and an upper-bound from which both cannot be too small or too large. Five cases are distinguished when having determined the upper- and lower-bound of the frequency search domain:

1. The frequency domain is exactly right: no buzz-saw or airframe noise present and BPF_{spec} is completely visible in the distillation;

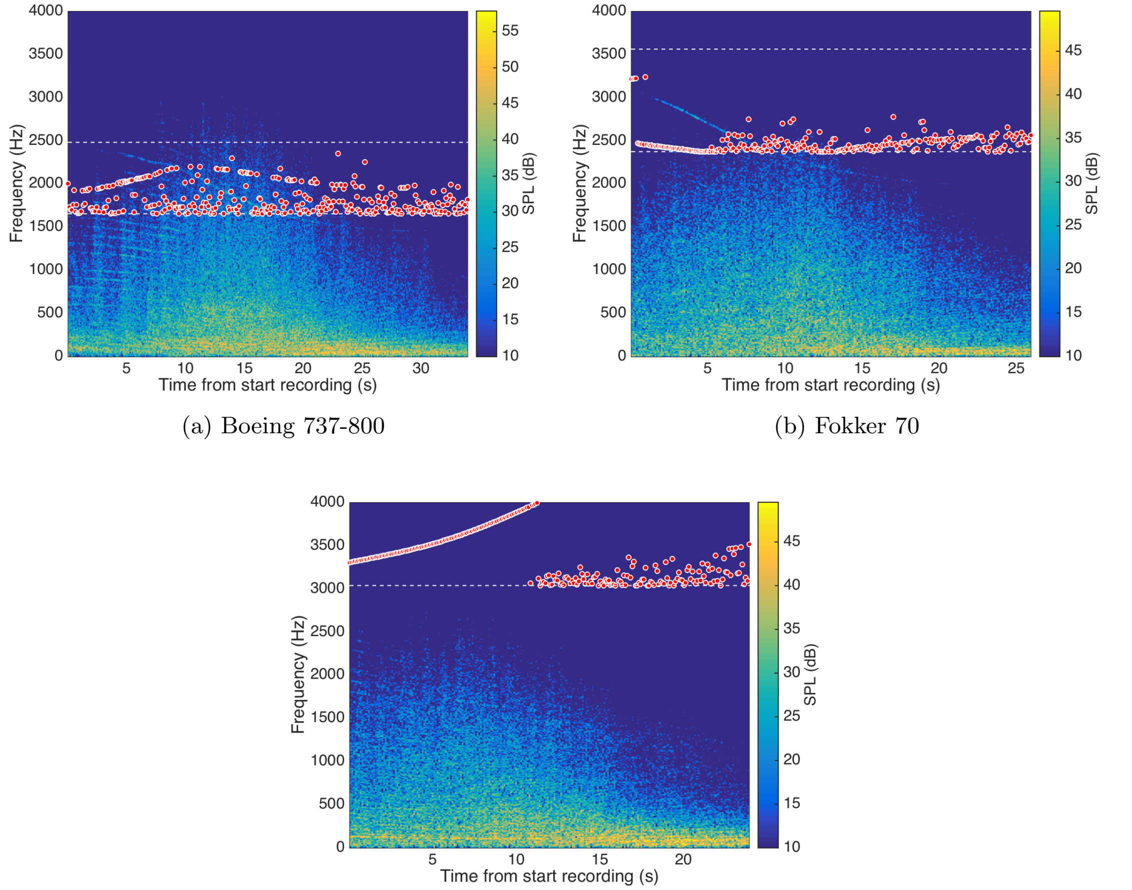

(a) Boeing 737-800

(b) Fokker 70

(c) Avro RJ-100

Figure 6.9: Spectrograms containing the identified maximum SPLs per time block T within the dynamic upper- and lower boundary

2. The lower-bound is too small: buzz-saw and/or airframe noise is included in the distillation;
3. The lower-bound is too large: a part of BPF_{spec} is not visible in the distillation;
4. The upper-bound is too small: a part of BPF_{spec} is not visible in the distillation;
5. The upper-bound is too large: SPL values originated from other components than the engine blades are shown in the distillation.

Of course the most desired case is represented by case 1, nevertheless it proved to be very difficult to predefine a static or a dynamic frequency domain which excludes cases 2 to 5 from appearing.

Static frequency domain

First, a static frequency domain has been investigated. The lower- and upper frequency boundary F_{lb} and F_{ub}, respectively, has been chosen as such that for all spectrograms the measured BPF will most-likely be enclosed. This resulted in F_{lb} = 1600 Hz and F_{ub} = 3000 Hz so that $\|\Delta F\|$ = 1400 Hz. $\|\Delta F\|$ appeared to be too large to determine

$N1$ accurately for all types of aircraft. BPF_{spec} is visible at different frequency ranges per aircraft type. When $\|\Delta F\|$ is too large, mostly frequencies near the lower boundary are identified. Hence, it is important to minimize $\|\Delta F\|$ to prevent the algorithm from identifying frequency which are not part of BPF_{spec}. From the static frequency domain can be concluded that the frequency domain, in which the search for f_0 is carried out, should be aircraft type and engine type dependent. The engine type should be given special attention since b and Ω largely determine $\|\Delta F\|$ in which there should be searched for BPF_{spec}.

Dynamic frequency domain

Second, a dynamic frequency domain has been investigated where BPF_{theory} of each engine is used and the expected visible harmonic k. For each aircraft-engine type multiple spectrograms were investigated which resulted in an expected visible-harmonic-number k as indicated in Table A.1. In this case it is therefore assumed that the k-th harmonic is visible in each spectrogram of each specific aircraft type.
These harmonic numbers where then used to calculate the lower- and upper bound as follows:

$$F_{lb} = k \cdot BPF_t(N_1 = 80\%)$$
$$F_{ub} = k \cdot BPF_t(N_1 = 120\%)$$

Then, the maximum SPLs per time block T in the spectrogram and the associated frequencies are determined within these bounds. The results for the reference measurement of the Boeing 737-800, together with the known best fitted BPF_{theory} and RMSE, are shown in Figure 6.10. Figure 6.10a shows the frequencies per time block T at which the maximum SPL is found and 6.10b shows the spectrogram with the frequencies per time block T highlighted at which the SPL reaches a maximum.

From figure 6.10b can be obtained that not only the desired harmonic k of BPF_{spec} is distilled, but also for example buzz-saw noise between 0 to ± 13 seconds is included. This in its turn is caused by, on the one hand, a too large frequency domain over which BPF_{spec} is divided and, on the other hand, poorly defined upper- and lower frequency bounds. Concluding: the frequency domain over which BPF_{spec} is divided is too large and should therefore be narrowed. This can be achieved by correcting the complete spectrogram for the Doppler effect, in stead of only BPF_{theory}, so that BPF_{spec} straightens over the entire time domain.

Spectrogram Doppler correction

In stead of correcting BPF_{theory} for the Doppler effect, the complete spectrogram is corrected from which the result can be obtained in Figure 6.11. The black dashed line indicates the time of flyover.

Correcting the complete spectrogram for the Doppler effect in stead of only the BPF makes it possible to define a much smaller frequency domain to search for maximum SPL values. Hence, the quality of the algorithm improves (if the defined searching frequency domain contains the BPF).

This approach has ultimately been used, together with the dynamic frequency domain where the upper- and lower frequency bound are defined as follows:

$$F_{lb,spec} = n_{xptd} \cdot BPF_t(N_1 = 60\%)$$
$$F_{ub,spec} = n_{xptd} \cdot BPF_t(N_1 = 100\%)$$

$N1$ is expected to have a value between 70% and 100%, but the range of 60% to 70% is also included to provide the algorithm the possibility to find lower values of $N1$. If multiple $N1$ determinations are below 70%, this means that there exists a fundamental mistake and so this working principle preserves space for improvement.

6.5.2 Finding the aircraft engine setting *N1*

$N1$ is found by calculating BPF_{theory} for different values of $N1$ and comparing BPF_{theory} with $BPF_{spec,dist}$. BPF_{theory} which minimizes Equation 6.1, represents the best fit and thus sets the value for $N1$.

$$RMSE(N1) = \sqrt{\frac{\sum_{i=1}^{n}(f_{i,p} - f_{i,t}(N1))^2}{n}} \tag{6.1}$$

With $f_{i,m}$ and $f_{i,t}$ representing element i of $BPF_{spec,dist}$ and BPF_{theory}, respectively. n is obviously equal to the number of time blocks in the spectrogram, thus the duration of the noise measurement divided by the duration of a time block T. So basically, the RMSE is a representation of the quality of the fit between BPF_{theory} and $BPF_{spec,dist}$.

6.6 Alternative *N1* Determination Algorithm: Peak Find Method

The Peak Find Method (PFM) uses the corrected spectrogram as shown in Figure 6.11 and calculates the median SPL per frequency bin ΔF, denoted as SPL_{median}. This results in Figure 6.12.

Figure 6.12b clearly indicates a peak between 2400 Hz and 2600 Hz, which shows that there is a significant difference in SPL within this frequency range compared to the surrounding frequency bins, hence this can be considered as an estimate for $BPF_{spec,dist}$. The only thing left to do is determining the exact frequency at which the maximum peak occurs.

The next step involves the calculation of the first derivative of SPL_{median}: dSPL_{median}. dSPL_{median} of Figure 6.12 is calculated and represented in Figure 6.13. Note that only negative derivatives are treated. Therefore, the upper limit of the y-axis of Figure 6.13 is set to zero.

This figure is used, together with the earlier mentioned dynamic frequency search domain, to find the minimum derivative, hence the highest decay in SPL. Thus the BPF as indicated in the spectrogram, which corresponds to a $N1$ satisfying $BPF_{dist} = N1 {\cdot} BPF_{theory}$ so that $N1 = \frac{BPF_{dist}}{BPF_{theory}}$.

Note that the spectrogram of measurement 5 does not show the measured BPF, as can be obtained from Figure 6.11 and hence the PFM does not find a match within the defined dynamic frequency search domain. Hence, this algorithm also provides the possibility of not finding minimum derivative which satisfies $60\% \leq N1 \leq 100\%$. Hence, in that case $N1$ cannot be determined for that specific noise measurement. This is an advantage since it adds confidence to those $N1$ determinations successfully carried out by the PFM.

6.7 Results: Comparison between both methods

This chapter introduced two methods to determine $N1$ from the acoustic spectrograms. Both methods are compared to each other, knowing beforehand that the best method is represented by the method which mostly determines $N1$ to have a value between 80% and 100%. According to internal information from one of the biggest airlines operating at AAS, $N1$ between 80% and 100% is commonly used when considering "normal" atmospheric conditions, i.e. among others: extreme windy conditions, extreme rainfall and snowfall.
A comparison of the results between both $N1$-determination methods is shown in Figure 6.14.

Ultimately, one would like to see the blue dots of figure 6.14a to coincide with the red dashed line, meaning that both algorithms produce exactly the same results. Unfortunately this is not the case at all, meaning that there is a fundamental difference between both methods. In fact, only 1 % of the outcome of the *N1*DA corresponds to the outcome of the PFM. The error E between both methods, i.e. $E = N1_{PFM} - N1_{N1DA}$, is shown in Figure 6.15. $N1_{PFM}$ and $N1_{N1DA}$ represent the $N1$ values as determined by the PFM and the *N1*DA, respectively. Note that the possibility exists that the PFM did not find a match. Therefore, the error is only calculated for measurements where both methods found a $N1$ value.

Figure 6.14b shows that the *N1*DA method never finds a $N1$ bigger than 80%, which is caused by the fact that during the maximum SPL value distillation (as explained in subsection 6.5.1) many SPL values originating from buzz-saw noise are distilled. This forces the method to find $N1$ matches which are structurally depreciated compared to the actual $N1$ values. For example, the spectrograms of the Boeing 737-800 include many buzz-saw noise harmonics, resulting in a wrong $N1$ determination by the *N1*DA method. Figure 6.16 shows a boxplot which indicates that the PFM typically determines higher $N1$ values compared to the *N1*DA method.

The PFM qualitatively performs better and does not necessarily need to find a value for $N1$. Hence, the results are more reliable. Therefore, the PFM is used for the remainder of this study.

The results for the $N1$ determination of both methods and the example measurements 1, 4 and 5 as treated in this chapter are listed in Table 6.6. The aircraft configuration, listed in Table 6.2, is used to determine $N1 = \frac{BPF_{dist}}{BPF_{theor}}$. Table 6.6 contains the $N1$ setting as found by the *N1*DA and PFM, indicated by $N1_{N1DA}$ and $N1_{PFM}$, respectively. $N1_{manual}$ is determined manually by correcting the spectrogram for the Doppler effect and determining the frequency at which the BPF is visible. This fundamental frequency

f_0 is then used in combination with the BPF for $N1 = 100\%$ and the expected harmonic k to calculate $N1$, resulting in $N1_{manual}$.

Table 6.6: *N1* of reference measurements

Measured aircraft	$\mathbf{N1_{N1DA}}$ (%)	$\mathbf{N1_{PFM}}$ (%)	$\mathbf{N1_{manual}}$ (%)
Boeing 737-800	67	[-]	92
Fokker 70	68	88	84
AvroRJ-100	66	[-]	38

This table indicates that the PFM was not able to determine $N1$ for the spectrograms of measurement 1 and 5. Though, the *N1*DA method did find a match for $N1$, simply because it *always* does by the way it is programmed. Comparing both methods for the Fokker 70 measurement results in a significant difference of 20%. The determination of the *N1*DA method of 68% is very low and most likely caused by the broadband noise present in the lower and middle of the spectrogram. Nevertheless, the determination of 88% is explainable because the resolution of the available RADAR data is too low, resulting in a lower resolution when the spectrogram is corrected for the Doppler effect.
However, a $N1$ with only 4% difference, compared to the best-fitted $N1$ of 84%, is satisfactory.
$N1_{manual}$ for the Avro RJ-100 is very low (only 38%) and hence not likely to be any harmonic of the BPF. Such low $N1$ values are very unusual during flight, especially during the climb phase which is the phase of the flight the measurement was conducted. Hence, this determined $N1$ is not compared since the $N1$ setting as flown is very likely to be much higher compared to this determined $N1$ value. Also, the fundamental frequency f_0 is hardly visible in the spectrogram of the Avro RJ-100, as can be seen in figure 6.8c.

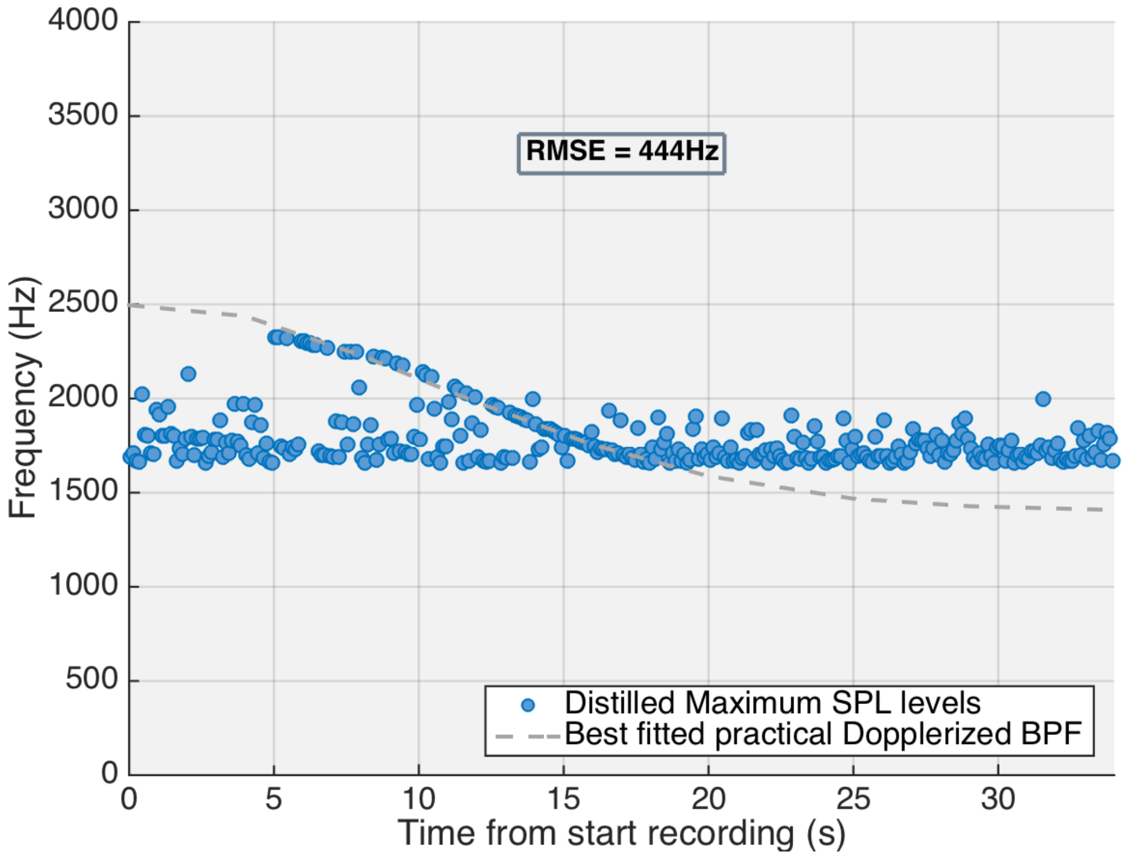

(a) Distilled SPL_{max} per frequency bin with best fit of the theoretical BPF subjected to the Doppler effect

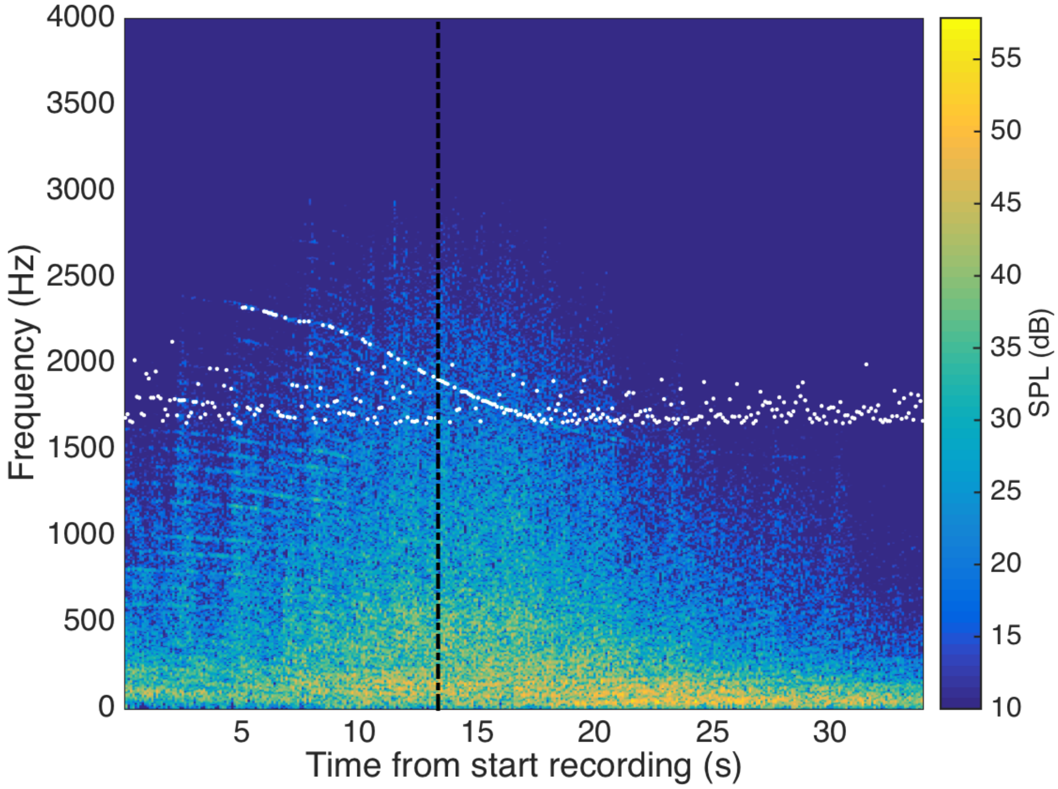

(b) Distilled SPL_{max} per frequency in spectrogram

Figure 6.10: SPL_{max} distillation results for the Boeing 737-800 reference measurement

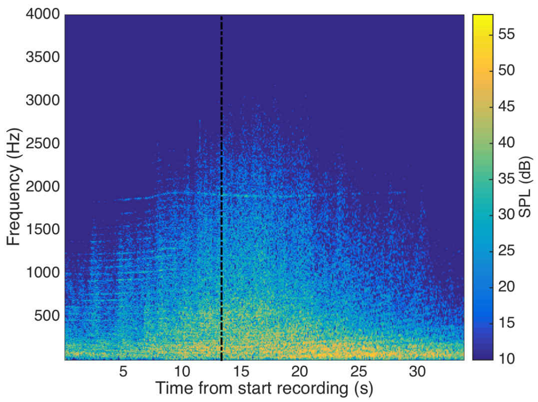

(a) Boeing 737-800

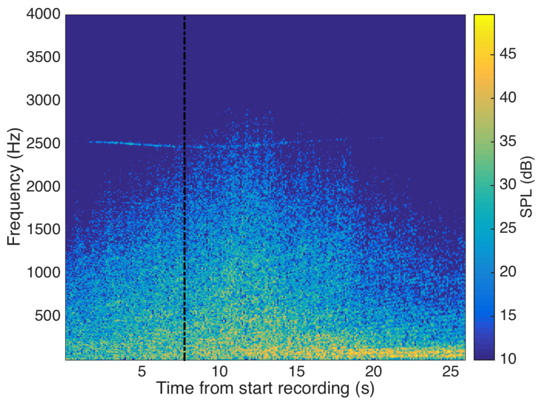

(b) Fokker 70

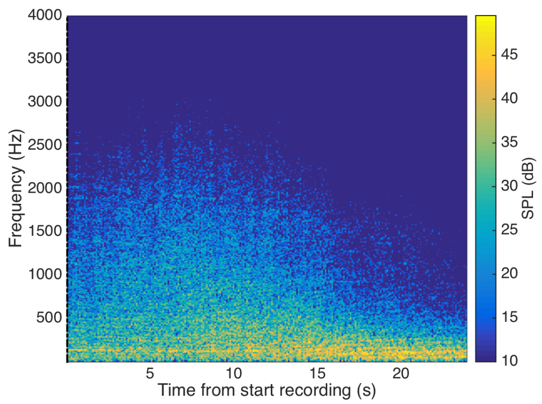

(c) Avro RJ-100

Figure 6.11: Doppler corrected spectrograms

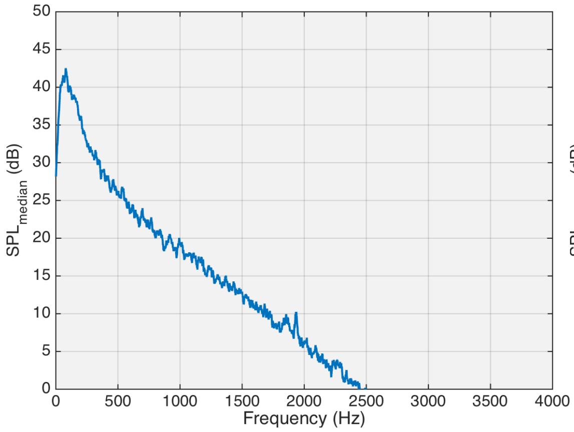

(a) Boeing 737-800

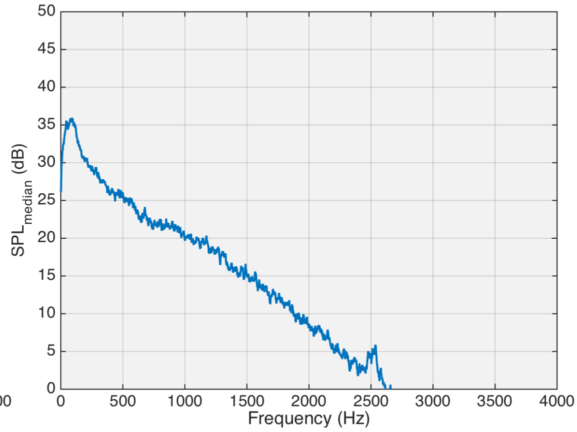

(b) Fokker 70

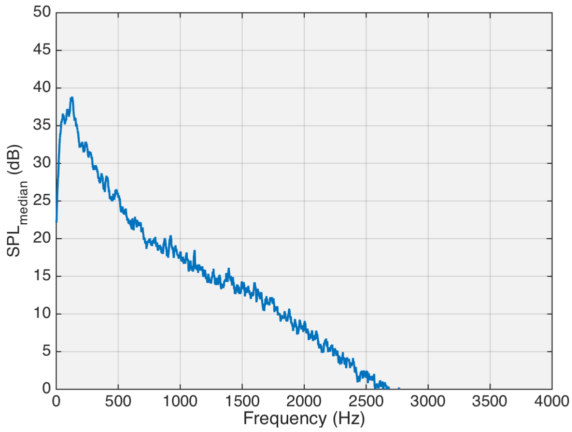

(c) Avro RJ-100

Figure 6.12: SPL_{median} per frequency bin ΔF

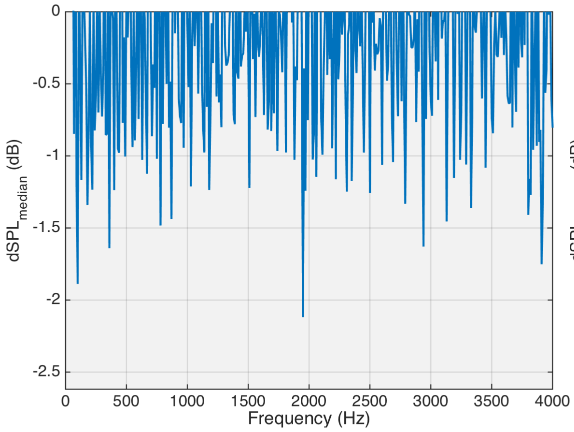

(a) Boeing 737-800

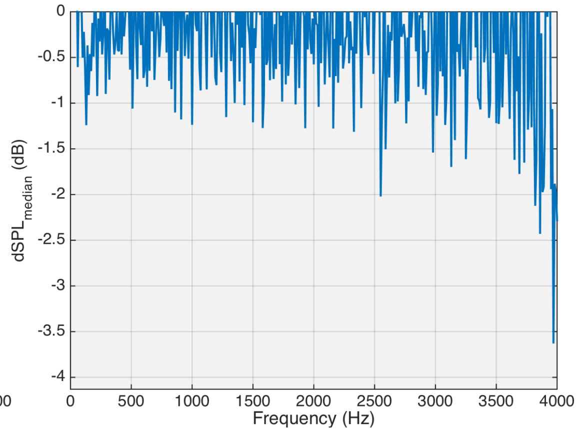

(b) Fokker 70

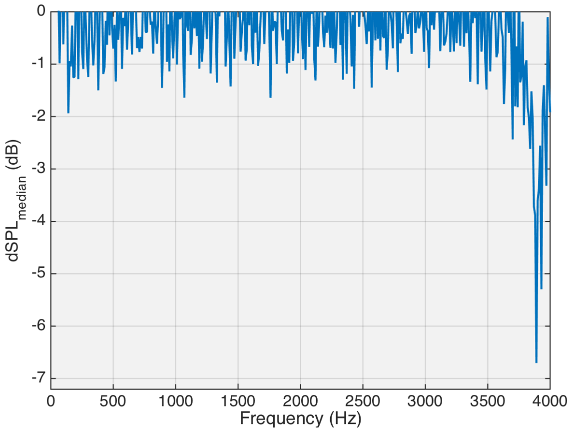

(c) Avro RJ-100

Figure 6.13: dSPL_{median} per frequency bin ΔF

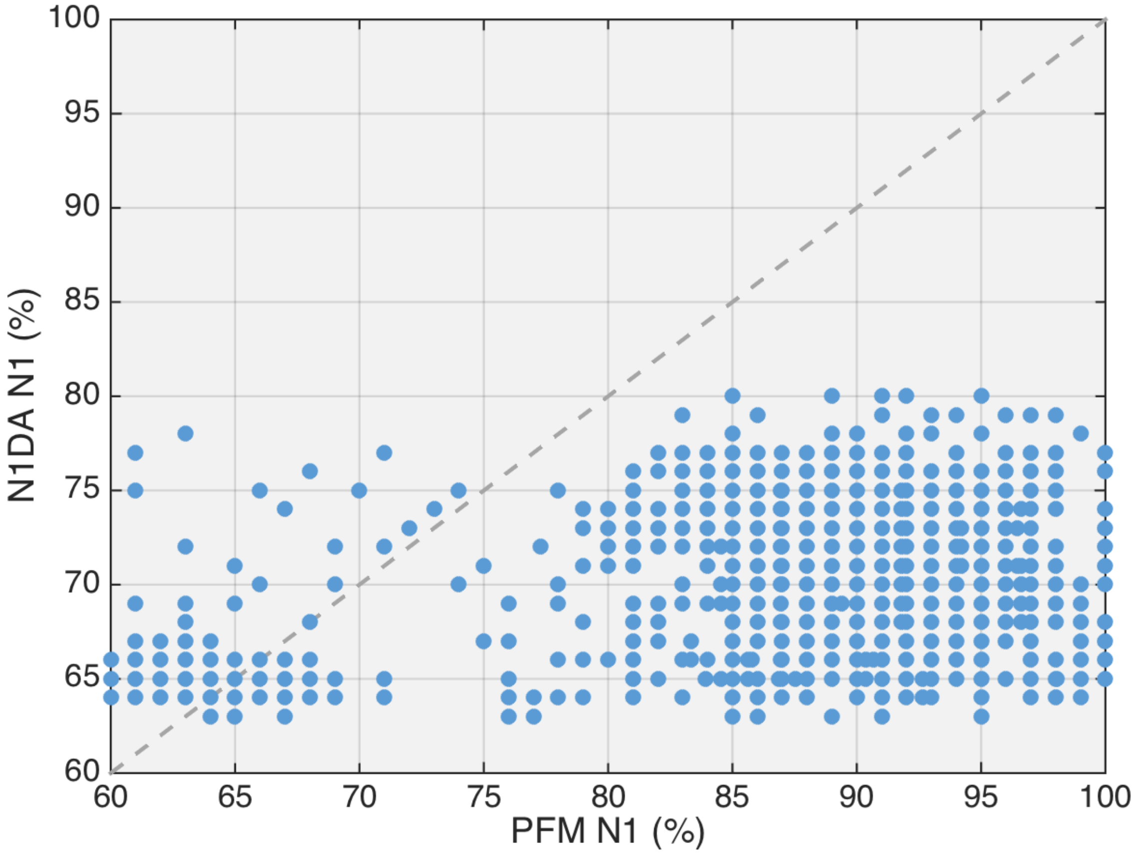

(a) $N1_{PFM}$ vs. $N1_{N1DA}$

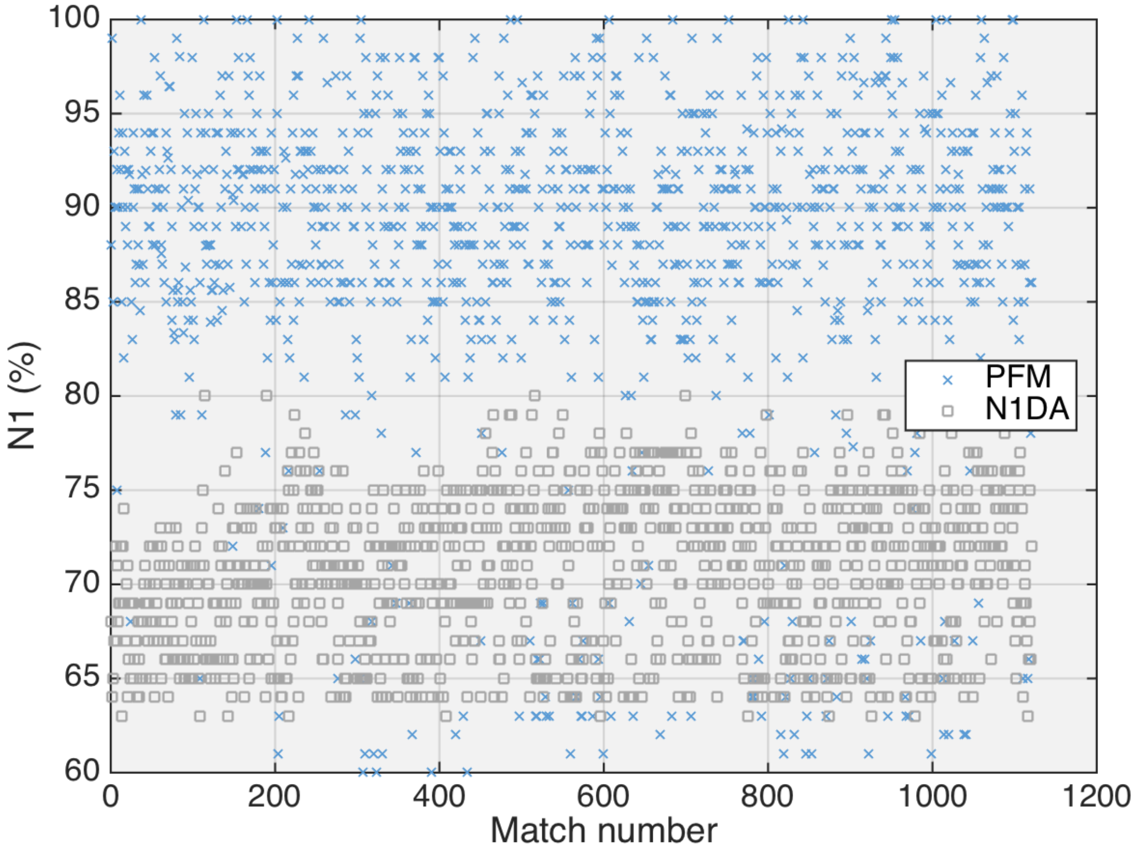

(b) Determined $N1$ per method

Figure 6.14: Comparison of results between both $N1$-determination methods

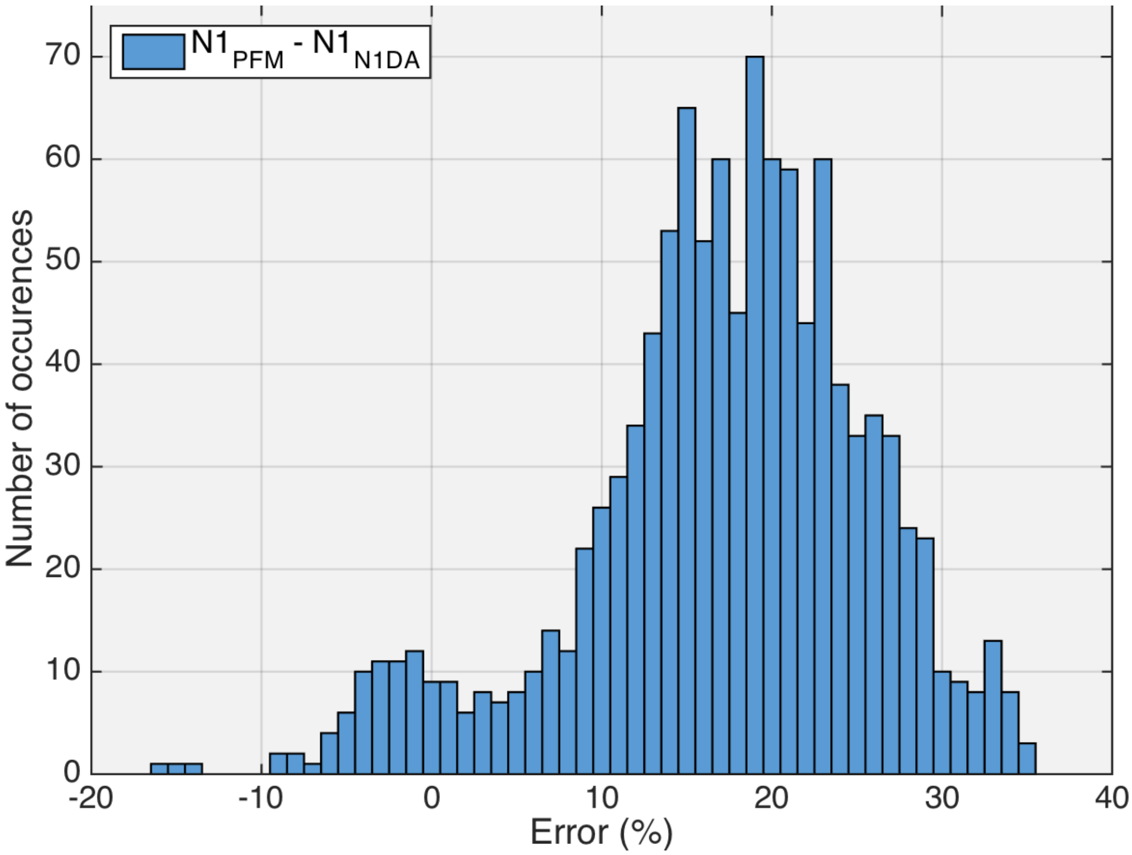

Figure 6.15: Error E between both $N1$-determination methods

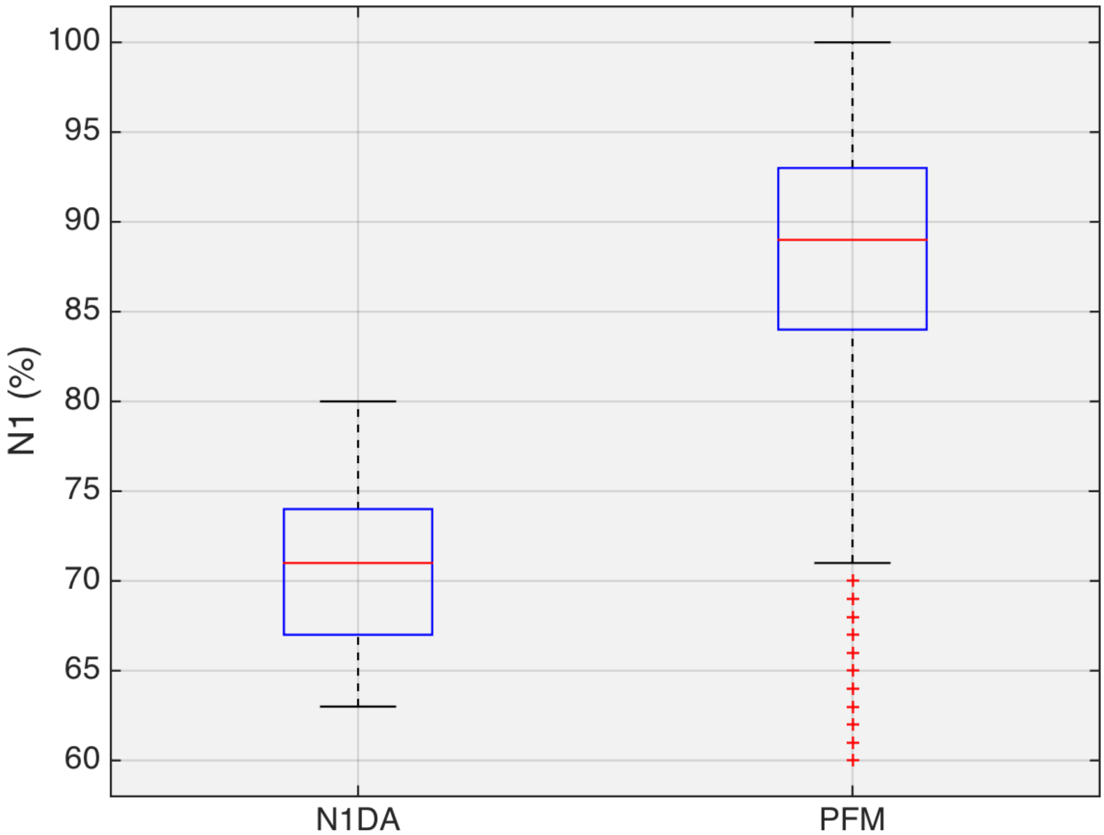

Figure 6.16: Variation and mean of both $N1$-determination methods

[Page intentionally left blank]

Chapter 7

Aircraft Mass Determination Algorithm

The hypothesis is that aircraft mass masks the effect of the implementation of a change in operational procedure to the total noise level. Aircraft mass is not readily available since it is recognized as being highly classified information and the goal of this chapter is to develop an algorithm able to determine actual aircraft mass m.
This chapter first defines an alternative dataset used as experimental dataset for the development of the Mass Determination Algorithm (MDA). Second, a theoretical background is given concerning the approach to estimate aircraft mass from basic aircraft performance equations. And last, a parameter is defined as aircraft mass representative during the classification process.

7.1 Alternative dataset

This graduation project uses a dataset collected between the 25th of August and the 30th of August 2014. Nevertheless, AAS possesses a dataset from former research containing FMS data from flights flown between May and July 2010. This research was performed in cooperation with a well-known airline of AAS which will further be abbreviated as 'Airline A'. The advantage of this dataset is that it contains actual aircraft performance related information including aircraft mass at multiple stages in flight. In this way, the relation between aircraft mass at take-off m_{to} and other aircraft performance parameters can be investigated.
Among others, the alternative dataset contains information regarding: date, time, destination, gross weight, logging interval, Long-Lat coordinates, height, ground speed, true airspeed, selected/indicated flap deflection roll rate, flight path angle, angle of attack, selected/indicated N1, total amount of fuel (kg) and gear deflection (true/false).

7.2 Theoretical background

From basic aircraft dynamics the following equation holds:

$$W = L = C_{L_{max}} \frac{1}{2} \rho V_{min}^2 S \tag{7.1}$$

Where V_{min} represents the minimum speed at which the total lift L exactly matches the weight W of the aircraft. This situation occurs at a particular moment during take-off and by using this equation the mass at take-off ($W = m \cdot g \rightarrow W_{to} = m_{to} \cdot g$ can be determined.

But, since the aircraft already has a height of approximately 800 meters when NMT10 starts sampling, one does not want to know the aircraft mass at take-off but the actual aircraft mass at the time of sampling. Nevertheless, Roberson (Senior Safety Pilot) and Johns (Flight Operations Engineer) [26] state that for the 717-200, 737-800 Winglets, 777-200 Extended Range, 747-400 and the 747-400 Freighter less than 1% of the total Take-Off Gross Weight (TOGW) is used during take-off. Since NMT10 is located approximately 3.1 kilometres from the end of runway 18L (the 'Aalsmeerbaan'), it is assumed that aircraft mass has not been significantly decreased during take-off. And thus it is assumed that $m = m_{to}$ at NMT10.

Going back to Equation 7.1, immediately some difficulties arise since $C_{L_{max}}$ is a parameter which fluctuates enormously during take-off, ρ is a parameter which cannot be determined exactly at the runway but rather in the neighbourhood of the runway, V_{min} is unknown and wing surface S is strongly depended upon the deflection of the flaps.

7.2.1 Air density

The air density at the runway continuously changes. Since there is no data available directly at the runway, but rather in the neighbourhood of the runway, the fluctuations in air density are investigated. Figure 7.1 shows the air density as logged by a station of the Koninklijk Nederlands Meteorologisch Instituut/Royal Netherlands Meteorological Institute (KNMI) nearby AAS. From this figure can be obtained that the air density is far from constant and hence must be known accurately to be able to accurately determine m_{to}.

7.2.2 Flaps deflection

As already indicated, the alternative dataset contains aircraft configuration and performance information as logged by the FMS and also contains the deflection of the flaps during different stages of flight. The wing area S strongly depends upon the flap deflection.

Nine possible flap deflection modes can be chosen by the pilot in the cockpit, namely mode 1, 2, 5, 10,15, 25,30 and 40. Since drag is very high at flap position 30 and 40 it is rarely used during take-off.

The flap deflection for each specific flight of the alternative dataset is plotted in Figure 7.2.

Figure 7.2 shows that for the 286 flights included in the alternative dataset only in one case an other flap deflection than flap deflection 5 is chosen at AAS for airline A. Therefore, it

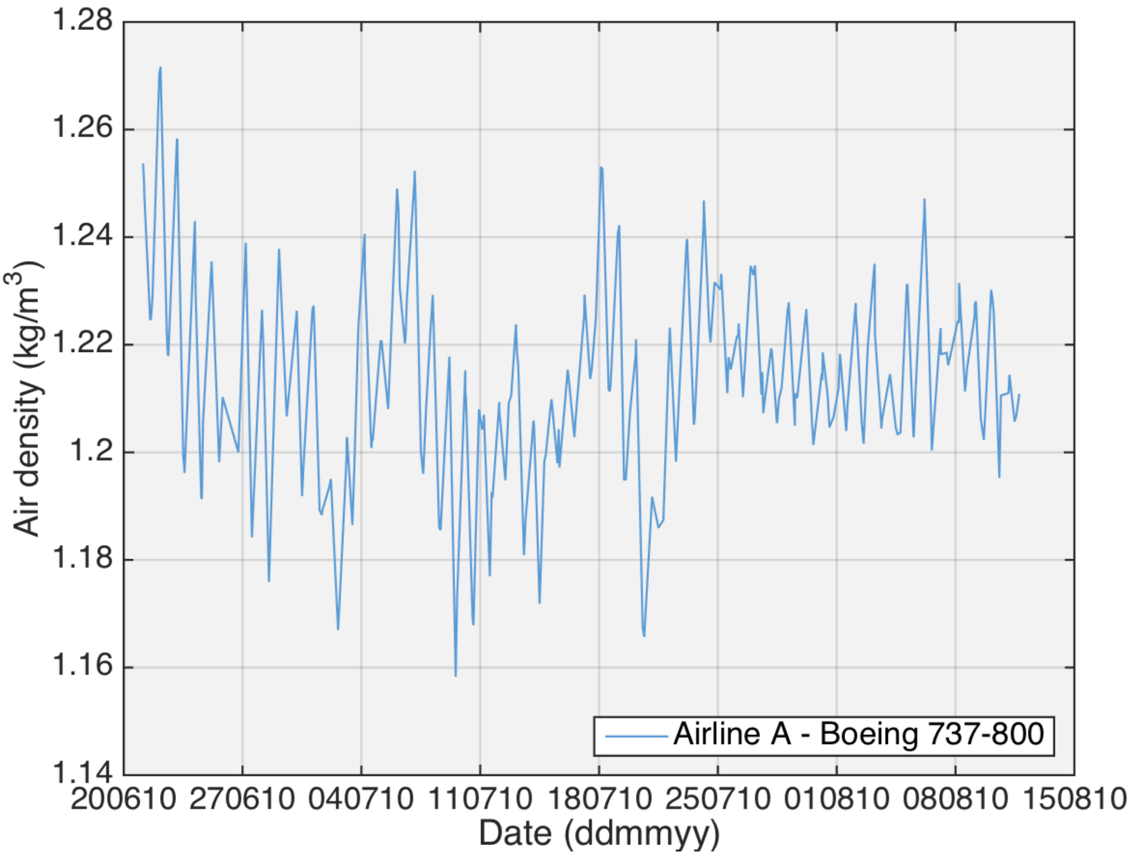

Figure 7.1: Alternative dataset: Air density over time

is assumed that all pilots of the Boeing 737-800 of airline A use flap deflection 5 at take-off from AAS, i.e. assuring constant S for all flights with the Boeing 737-800 for airline A.

From personal contact between AAS and airline B followed that airline B also uses flap deflection 5 at AAS as standard flap deflection mode during standard meteorological conditions, i.e. no snow, no rain and no extreme wind conditions. Thus, also constant S is assumed for all flights with the Boeing 737-800 for airline B.

7.2.3 Minimum speed V_{min}

The minimum speed V_{min} cannot readily be determined from RADAR data, but the lift-off speed V_{lof} can since V_{lof} is the speed at which height $h > 0$ for the first time. So, a relation between V_{min} and V_{lof} must be found. Although there is not an exact relation between V_{min} and V_{lof}, there exists a relation between the rotational speed V_{rot} and V_{min}. Note that V_{rot} is the speed at which the pilot starts to rotate the aircraft, i.e. starts to pull the stick and lift the aircraft off the ground during take-off.
In basic aircraft performance calculations, V_{rot} is related to V_{min} as:

$$V_{rot} \approx 1.2 \cdot V_{min} \rightarrow V_{min} \approx \frac{V_{rot}}{1.2} \tag{7.2}$$

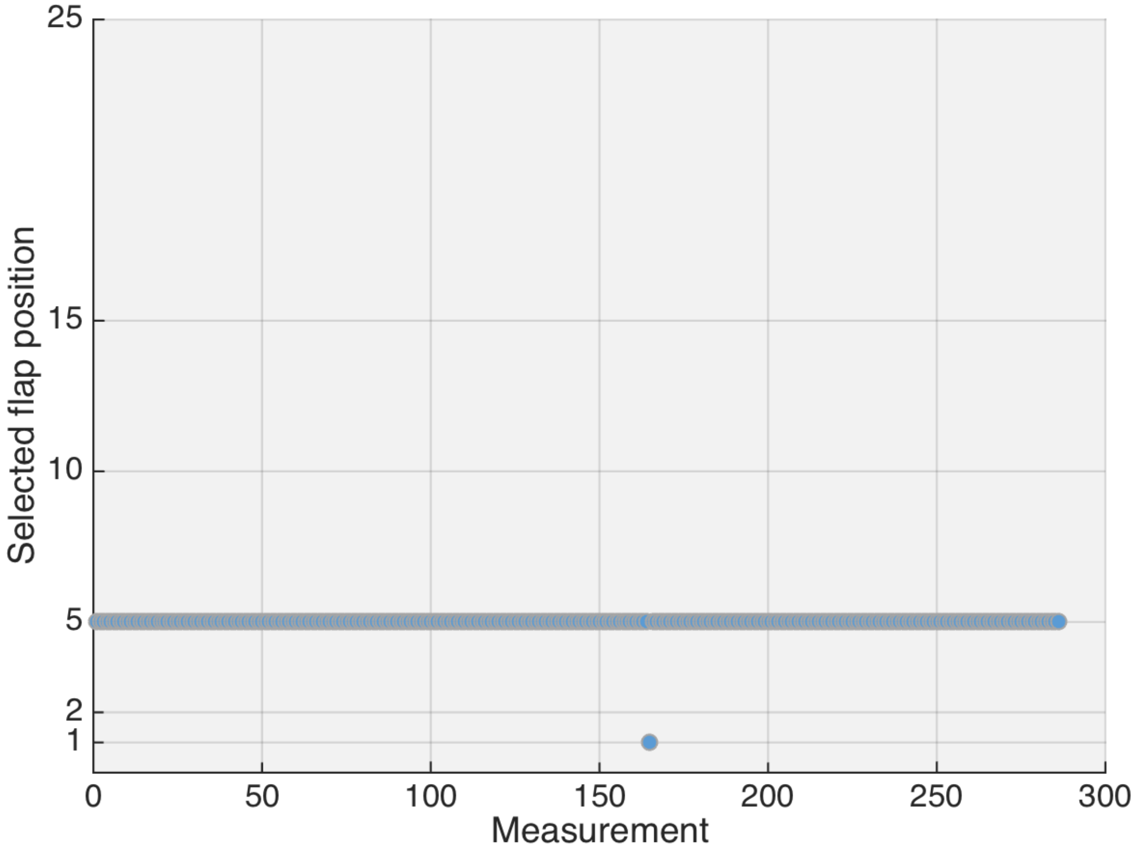

Figure 7.2: Alternative dataset: pilot choice for the flap position during take-off for all flights

Filling in Equation 7.2 in Equation 7.1 gives:

$$W \approx L \approx C_{L_{max}} \frac{1}{2} \rho (\frac{V_{rot}}{1.2})^2 S \tag{7.3}$$

Using $W = m_{to} \cdot g$, with m_{to} representing the mass at take-off, gives:

$$m_{to} g \approx L \approx C_{L_{max}} \frac{1}{2} \rho \left(\frac{V_{rot}}{1.2} \right)^2 S \tag{7.4}$$

Nevertheless, the relation between V_{lof} and V_{rot} depends on the actual aircraft mass at take-off m_{to}. V_{lof} can be determined from the available RADAR track data, since V_{lof} is represented as the speed where the aircraft first gains height. Hence, a relation between V_{rot} and V_{lof} has to be found.
V_{lof} is determined by adding a speed V_{diff} to V_{lof}, depending on the actual aircraft mass at take-off m_{to}. Hence, a relation for V_{rot} can be found:

$$V_{diff} = V_{lof} - V_{rot} \rightarrow V_{rot} = V_{lof} - V_{diff} \tag{7.5}$$

According to the Boeing 737 technical site [9] the relation between V_{rot} and V_{lof} for a Boeing 737-500 is as shown in Figure 7.3.

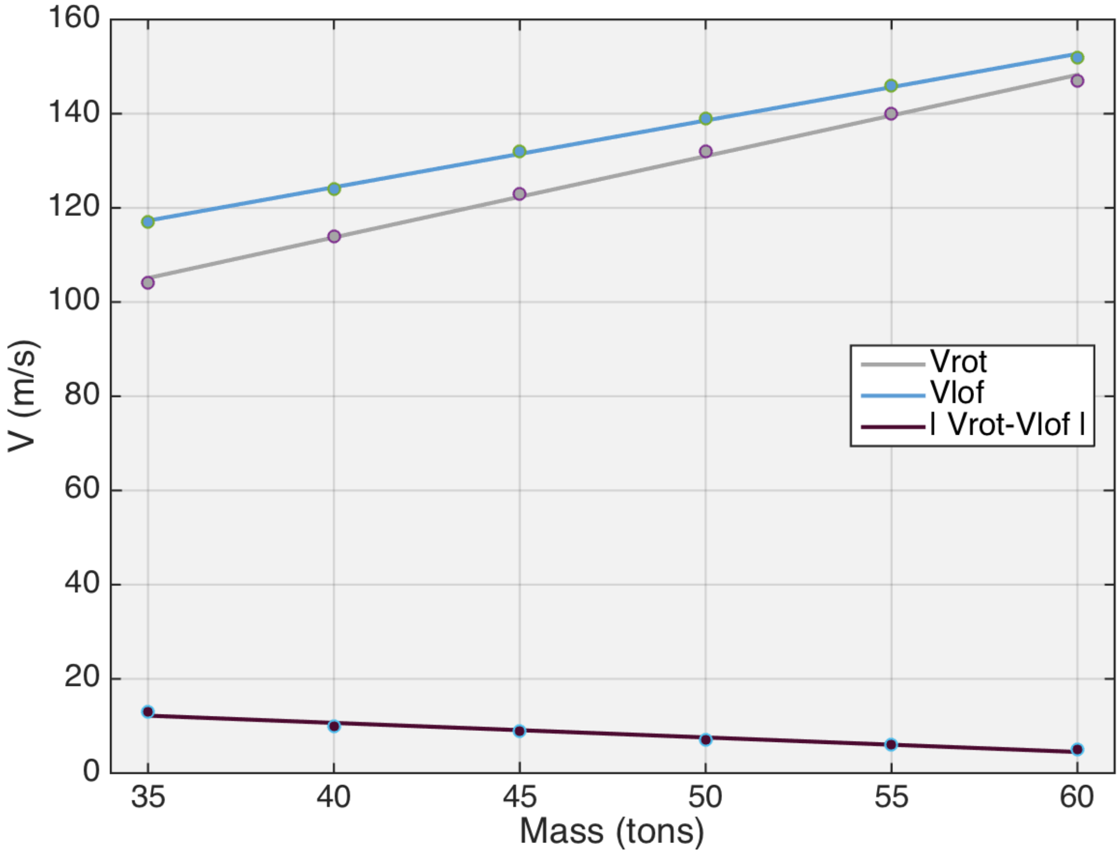

Figure 7.3: Relation between V_{rot} and V_{lof} for the Boeing 737-500. Retrieved from [9]

Note that this holds with the assumption of flap 5, pressure altitude less than 5000 ft, outside air temperature less than 35 °C, zero runway slope, zero wind and a dry runway.

V_{rot} is a function of aircraft mass at take-off m_{to} and thus Equation 7.4 becomes:

$$m_{to}g \approx L \approx C_{L_{max}} \frac{1}{2} \rho \left(\frac{V_{lof} - V_{diff}}{1.2} \right)^2 S \tag{7.6}$$

As shown in Figure 7.3, V_{diff} is assumed to be related linearly to m_{to}, which gives:

$$V_{diff} = C_1 m_{to} + C_2 \tag{7.7}$$

With C_1 and C_2 being constants. Filling in Equation 7.7 in Equation 7.6 gives:

$$m_{to}g \approx L \approx C_{L_{max}} \frac{1}{2} \rho \left(\frac{V_{lof} - (C_1 m_{to} + C_2)}{1.2} \right)^2 S \tag{7.8}$$

This equation is used for measurements sorted on the same aircraft type. It is assumed that all aircraft of the same aircraft type have the same wing profile, so that $C_{L_{max}}$ and

S become constants.
Rewriting Equation 7.8 results in:

$$m_{to} \approx C_3\rho \left(V_{lof} - C_1 m_{to} - C_2\right)^2 \tag{7.9}$$

With:

$$C_3 = \frac{C_{L_{max}} 1/2S}{1.2^2 g} \tag{7.10}$$

Expanding the term $(V_{lof} - C_1 m_{to} - C_2)^2$ results in:

$$\begin{aligned}(V_{lof} - C_1 m_{to} - C_2)^2 = V_{lof}^2 - 2V_{lof}C_1 m_{to} - 2V_{lof}C_2 + \\ (C_1 m_{to})^2 + 2C_1C_2 m_{to} + C_2^2\end{aligned} \tag{7.11}$$

Filling in Equation 7.11 in Equation 7.9 gives:

$$m_{to} \approx C_3\rho \left(V_{lof}^2 - 2V_{lof}C_1 m_{to} - 2V_{lof}C_2 + (C_1 m_{to})^2 + 2C_1C_2 m_{to} + C_2^2\right) \tag{7.12}$$

Hence:

$$\begin{aligned}m_{to} - 2C_1C_2C_3\rho m_{to} + 2C_1C_3\rho V_{lof} m_{to} - C_3\rho(C_1 m_{to})^2 \approx C_3\rho\left(V_{lof}^2 - 2V_{lof}C_2 + C_2^2\right) \rightarrow \\ (-C_3\rho C_1^2)m_{to}^2 + (1 - 2C_1C_2C_3\rho + 2C_1C_3\rho V_{lof})m_{to} - C_3\rho\left(V_{lof}^2 - 2V_{lof}C_2 + C_2^2\right) \approx 0\end{aligned} \tag{7.13}$$

The "ABC method" in this case implies:

$$m_{to} \approx \frac{-B \pm \sqrt{B^2 - 4AC}}{2A} \tag{7.14}$$

With the condition that m_{to} can never be lower than zero kilograms and $A = -C_3\rho C_1^2, B = 1 - 2C_1C_2C_3\rho + 2C_1C_3\rho V_{lof}$ and $C = -C_3\rho(V_{lof}^2 - 2V_{lof}C_2 + C_2^2)$, Equation 7.14 results in:

$$\begin{aligned}m_{to} \approx -(1 - 2C_1C_2C_3\rho + 2C_1C_3\rho V_{lof}) \pm \\ \sqrt{(1 - 2C_1C_2C_3\rho + 2C_1C_3\rho V_{lof})^2 - 4(C_3\rho C_1^2)(C_3\rho(V_{lof}^2 - 2V_{lof}C_2 + C_2^2))} \cdot \\ \frac{1}{2(-C_3\rho C_1^2)}\end{aligned} \tag{7.15}$$

Assuming the lift-off speed V_{lof} is mostly dominated by the aircraft mass m, it follows:

$$m_{to} = f(V_{lof}) \tag{7.16}$$

When dealing with the Boeing 737-500, typical values for the constants C_1, C_2, C_2^2 and C_3 are $1/3125, 25, 625$ and 8, respectively. However, this research only incorporates measurements of the Boeing 737-800 and unfortunately no data is available with respect to the constants. Nevertheless, the speed V is represented quadratically in Equation 7.1, therefore V_{lof}^2 is assumed to be the most dominant factor when determining m.
V_{lof}^2 *can* be determined from the available RADAR data.
Next, the variability of m_{to} against V_{lof} is studied by using the alternative dataset as described in section 7.1.

7.3 $\mathbf{m_{to}}$ versus $\mathbf{V_{lof}}$

It appeared that it is very difficult to estimate m_{to} from V_{lof} since there are many parameters dependent upon m_{to}. Nevertheless, to investigate the variability of m_{to} against V_{lof} the actual aircraft masses at take-off from the alternative dataset are plotted in Figure 7.4. Since one is interested in the lift-off speed not containing any wind effects, V_{lof}^2 of Figure 7.4 is corrected for these wind effects, also referred to as the true lift-off speed. The true airspeed is one of the parameters available in the alternative dataset.
Figure 7.4 shows that for each specific aircraft mass multiple V_{lof} exist and it is therefore very difficult to find a relation between V_{lof} and m_{to}. Because of this difficult relation between V_{lof} and m_{to}, thereafter a simple second order polynomial fit has been investigated although it was known beforehand that not all data points can be fitted using this approach. The result of a second order polynomial fit of the form $p(x) = p_1x^2 + p_2x + p_3$ is shown in Figure 7.4. The correlation r between the second order Least Squares Polynomial Fit (LSPF) and m_{to} equals 0.385 with a very low probability value of $p = 1.6 \cdot 10^{-11}$. The red line as shown in Figure 7.4 indicates the mass function represented in Equation 7.15.

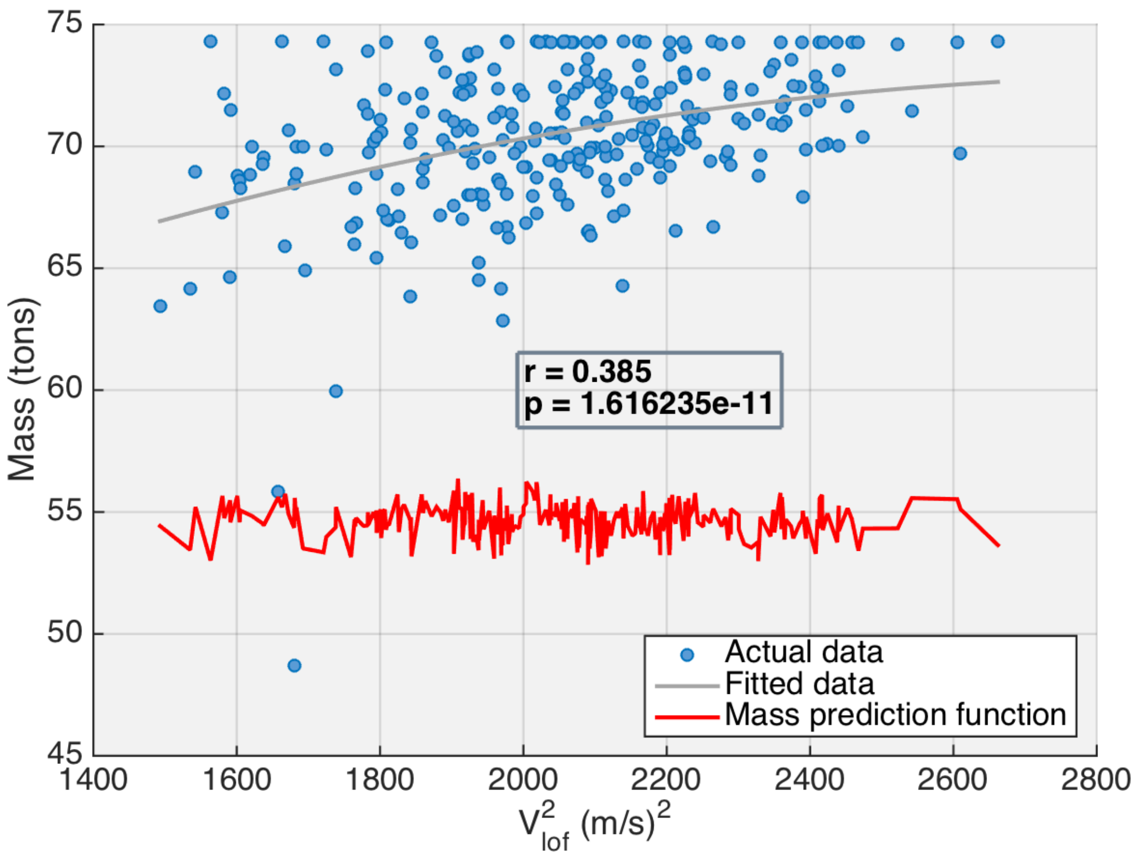

Figure 7.4: Alternative dataset: polynomial fit to V_{lof} versus m_{to}

From Equation 7.15 can be concluded that the mass prediction function, as represented in Equation 7.15, has low predictive capabilities with respect to the actual aircraft mass at take-off m_{to}. Hence, the simplifications and assumptions made to obtain Equation 7.15 are too generic to approach the m_{to} from the alternative dataset.

7.3.1 V_{lof} versus L_{max}

The hypothesis of this research is that aircraft mass m is a good predictor for the variability in L_{max}, i.e. it is expected that the variation of m masks the contribution of a change in operational procedure to L_{max}. The goal of this chapter was to determine m at take-off (m_{to}) from aircraft performance equations but it appeared immediately that the determination of m_{to} is very difficult and not straight forward. Since V_{lof} takes actual aircraft mass into consideration it was expected that V_{lof} is a good representative for m so that V_{lof} can be used as a representative predictor. Nevertheless, as Figure 7.4 already indicated, multiple possible aircraft masses at take-off exist for single V_{lof} speeds. Unfortunately due to a lack of time the relation between V_{lof} and m_{to} could not be properly investigated and for the remainder of this research V_{lof}^2 will be used as a predictor for L_{max}.

7.4 Determining V_{lof}^2 from the research dataset

Is has been chosen to use the predictor V_{lof}^2 as aircraft mass representative. V_{lof} is determined by calculating the ground speed from (LAT, LON) coordinates and determining the speed where the height of the aircraft first increases. An important condition is that the ground speed of the aircraft should be higher than 30 m/s, hereby preserving any wrong ground speed determinations caused by a bumpy terrain. However, the speed determined now is the airspeed which is subjected to wind conditions. Namely, strong head winds significantly decrease V_{lof}^2. The speed as available in the *alternative dataset* is corrected for any wind conditions, hence the true airspeed is available. Nevertheless, the speed calculated in the research dataset is the airspeed which is *not* corrected for any wind conditions. Therefore, the airspeed that follows from the RADAR track available in the research dataset, needs to be corrected for the present wind conditions to obtain the true airspeed, thus to cancel out the effect of any wind conditions.
This correction of the airspeed of the research dataset is carried out by using the wind direction and the wind speed available from meteorological data (KNMI) together with the direction of the departing aircraft, so that the direction of the velocity vector of the departing aircraft can be determined. An example of this process is shown in Figure 7.5.

Block 1 of Figure 7.5 shows the situation with a runway and a wind vector V_{wind} in the direction of the runway. V_{wind} can be divided into a horizontal- and a vertical component: $V_{wind,h}$ and $V_{wind,v}$, respectively.
Block 2 of Figure 7.5 shows the situation with an aircraft departing from the runway. This aircraft has a ground speed $V_{aircraft}$ and is subjected to the vertical velocity component of the wind $V_{wind,v}$.
Block 3 of Figure 7.5 shows the true airspeed V_{true} where the vertical velocity component of the wind $V_{wind,v}$ has been subtracted from the ground speed of the aircraft $V_{aircraft}$.

Concluding, for each measurement available in the research dataset first V_{lof} is determined by searching for the speed, higher than 30 m/s, where the aircraft first gains height and second this speed is corrected for any wind condition influencing this lift-off speed.

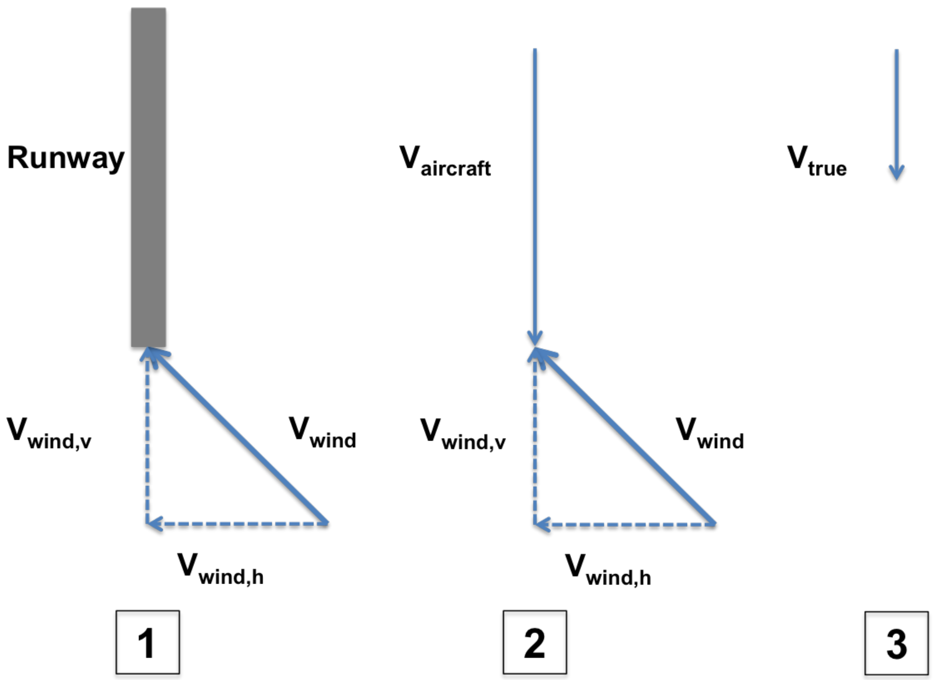

Figure 7.5: Correcting airspeed for wind conditions to obtain the true airspeed

[Page intentionally left blank]

Chapter 8

Research Results

This chapter shows all results with respect to this MSc research, using the theories and predictors as found in the previous chapters. Ultimately, the contribution of $N1$ and V_{lof}^2 is subtracted from the L_{max} levels as to visualize the effect of a difference in flown operational procedure by two different airlines A and B.
First an explanation is given about the filtering of the dataset for each comparison. Second and third, the results for $N1$ and V_{lof}^2 are set out individually. Fourth, fifth, sixth, seventh and eight the results for the predictors versus L_{max} are stated. Ninth, an Multivariate Linear Regression Analysis is performed on the predictors versus L_{max}. Tenth, an overview is given on possible parameters influencing the results and last an alternative approach as aircraft mass representative versus L_{max} is explained.

8.1 General

This chapter shows the results of this MSc research. As mentioned before, the total dataset has been narrowed down from 2073 measurements to 263 measurements for comparison purposes. This new dataset of 263 measurements will however be narrowed down even more because a distinction is made between measurements for which $N1$ and/or V_{lof} could be determined. Measurements for which one or both parameters could not be determined, will be eliminated from the new dataset since no further comparisons can be made for these measurements. The settings for each individual comparison will be indicated in the next sections.

8.2 N1 determination

As mentioned in chapter 6, the PFM method is used to determine $N1$ for all spectrograms. The PFM, together with the assumption of a fixed time-offset, performs really well, even if the BPF is hardly visible in the spectrogram. Figure 8.1a shows a spectrogram corrected for the Doppler effect with many buzz-saw noise harmonics. Nevertheless, the PFM finds a good match for the BPF, as can be obtained in Figure 8.1. Also, Figure 8.1 shows that the *N1*DA performs really bad, caused by the buzz-saw noise harmonics.

A histogram containing all results for the PFM is shown in Figure 8.2. The settings for this plot are stated in Table 8.1.

Table 8.1: Settings for the $N1$ plot (Figure 8.2)

Parameter	Setting
Aircraft:	Boeing 737-800
Airline:	A or B
Route:	Route option 1 and 2
ADS-B available:	Does not matter
$N1$ determined:	Yes

The median $N1$ of airline A equals 93%, while the median $N1$ of airline B equals 90%. A higher median for airline A seems logical because airline A is still climbing when the measurement is conducted, while airline B has continued to the acceleration phase hence decreased $N1$, since lower $N1$ settings are used in the acceleration phase of the NADP2 procedure.
However, a Two-Sample t-Test (TStT) showed that this results is not statistically significant. With a set significance level of 5%, the p value from the TStT equals 0.1689, thus the significance level is exceeded and hence this result is not statistically significant.

8.3 $\mathbf{V_{lof}^2}$ determination

As mentioned in the previous chapter due to a lack of time V_{lof}^2 is used as predictor in the classification process. The determined lift-off speeds, corrected for the present wind condition, have been made clear by means of a histogram represented in Figure 8.3. Note that both airline A and B are represented by a color. Since airline B does not fly as frequent as airline A at AAS there could only 32 lift-off speeds be identified for airline B and 190 for airline A. Table 8.2 states the settings used for Figure 8.3.

Table 8.2: Settings for the V_{lof} plot (Figure 8.3)

Parameter	Setting
Aircraft:	Boeing 737-800
Airline:	A or B
Route:	Route option 1 and 2
ADS-B available:	Yes
$N1$ determined:	Does not matter

The results as shown in Figure 8.3 lie within the expected bandwidth. These aircraft are reasonably assumed to possess different masses and thus apply different lift-off speeds.
The medians of airline A and B are 85.9 m/s and 82.8 m/s, respectively. This means that in general, assuming that all aircraft are flown in the same configuration, the aircraft of airline A are heavier than those of aircraft B, if the assumption is valid that the lift-off speed is mostly dominated by the actual take-off weight.
Again, a TStT is performed which showed that the set significance level of 5% is *not* exceeded with a p value of 0.0294 and a confidence interval between 0.2065 and 3.9069. Hence, the difference between the lift-off speeds of airline A and airline B are statistically significant.

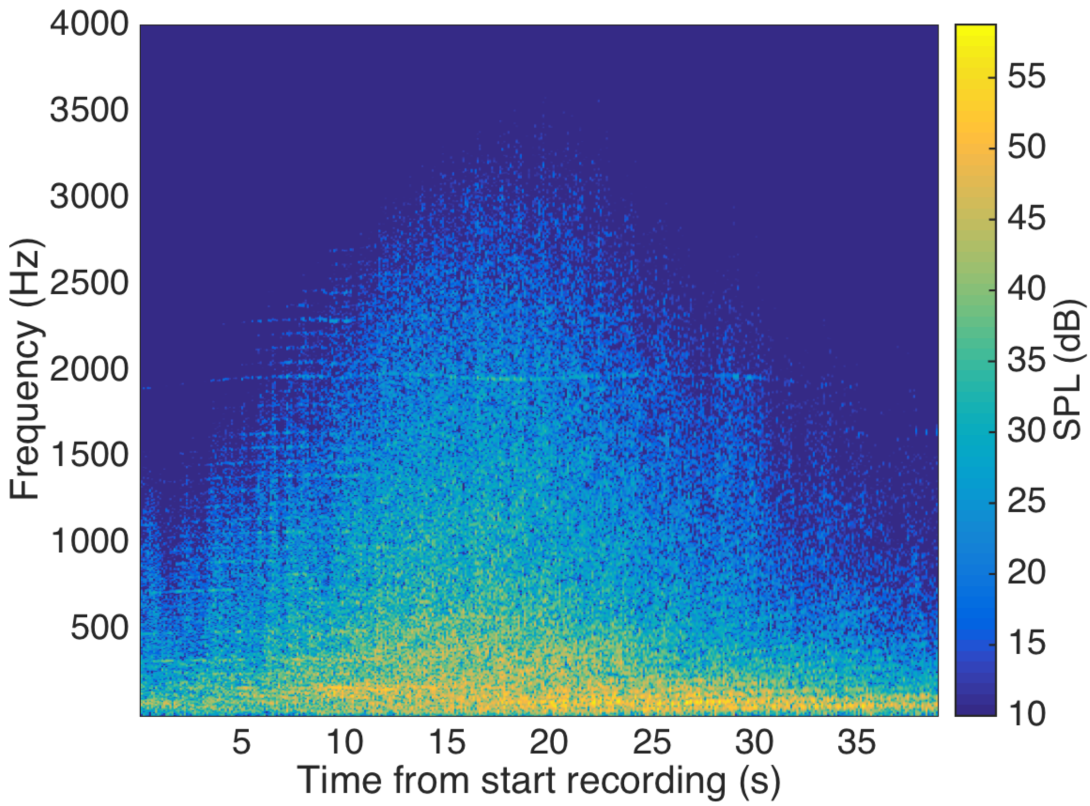

(a) Original spectrogram

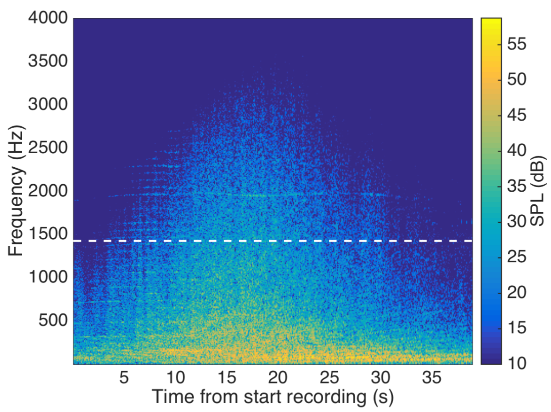

(b) Result N1DA

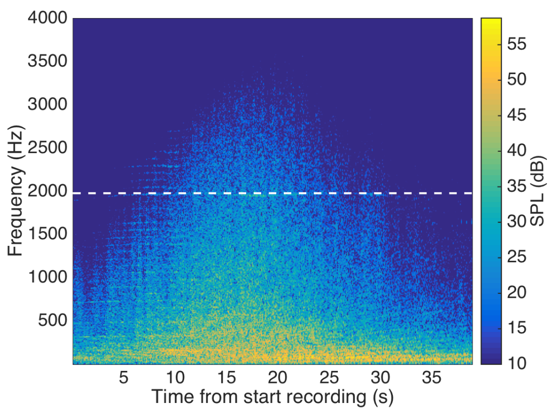

(c) Result PFM

Figure 8.1: Comparison of N1 determinations between N1DA and PFM

8.4 $\mathbf{L_{max}}$ determination

Two parameters are used as predictors ($N1$ and V_{lof}^2) to minimize the variance in L_{max}. Therefore, it is important to know the way in which L_{max} is determined.
In this research, NOMOS offers the possibility to download L_{max} from each noise even directly from each NOMOS station. Thus, for the sake of simplicity and to save time,

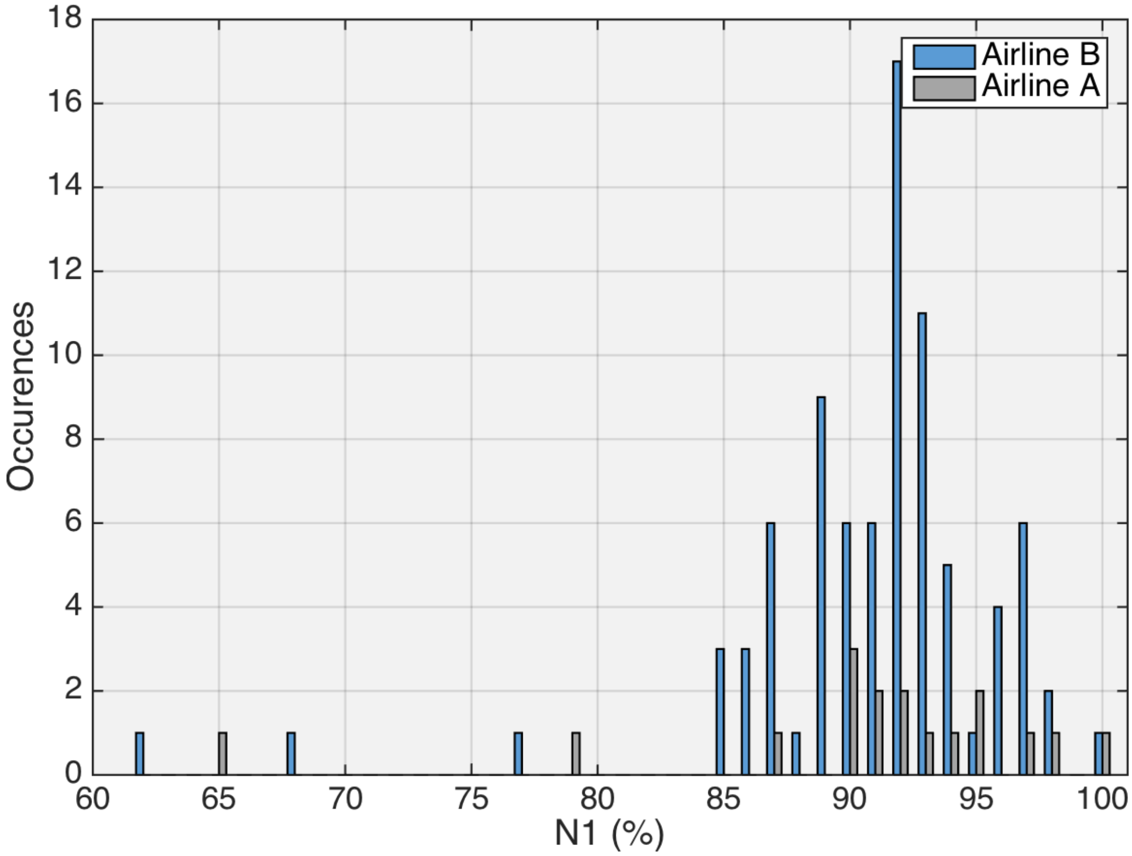

Figure 8.2: Results: histogram of $N1$ for airline A and B

each noise sample together with the associated L_{max} have been downloaded directly from NMT10.
Figure 8.4 shows L_{max} values for all measurements which comply with Table 8.3.

Table 8.3: Settings for the L_{max} plot (Figure 8.4)

Parameter	Setting
Aircraft:	Boeing 737-800
Airline:	A or B
Route:	Route option 1 (figure 8.4a)
	Route option 2 (figure 8.4b)
ADS-B available:	Does not matter
$N1$ determined:	Does not matter

8.5 N1 versus $\mathbf{L_{max}}$

To study the correlation between $N1$ and L_{max} first a visualization has been made. Ultimately, one is interested in the linearity between these two parameters and the hypothesis is that L_{max} increases with an increase in $N1$. The results are shown in Figure 8.5 with the associated settings indicated in Table 8.4.

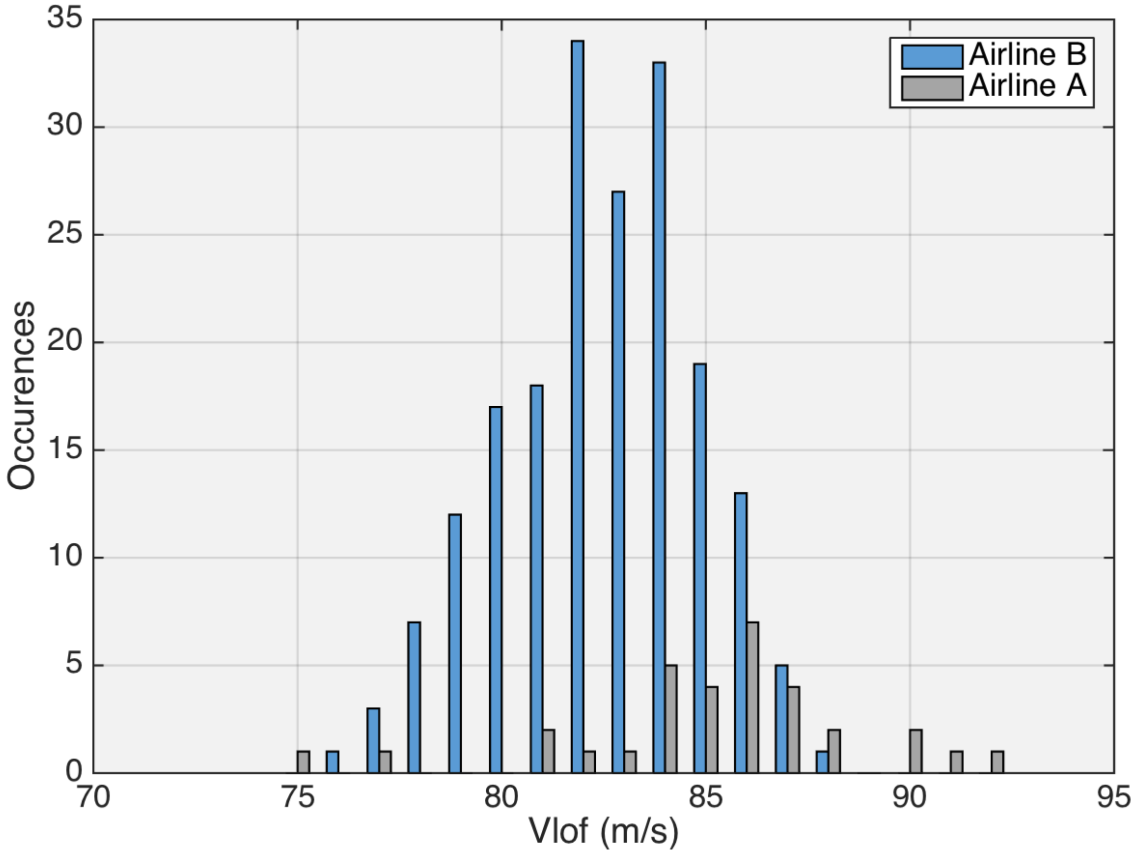

Figure 8.3: Results: histogram of V_{lof} for airline A and B

Table 8.4: Settings for the $N1$ versus L_{max} plot (Figure 8.5)

Parameter	Setting
Aircraft:	Boeing 737-800
Airline:	A or B
Route:	Route option 1 (figure 8.5a)
	Route option 2 (figure 8.5b)
ADS-B available:	Does not matter
$N1$ determined:	Yes

8.5.1 Routes from 18L to the south and west

Figure 8.5a shows that there is a very low correlation ($r = 0.054$) between $N1$ and L_{max} with a relatively high p value ($p = 0.712$). Since all aircraft flying southern routes fly directly over NMT10 it is expected that there should be certain linearity between these two parameters, although not visible in the plot. A low r and a high p is expected to be caused by the limited number of measurements and that there is still a lot more information present in the noise measurements which is expected to mask this before-mentioned linear relation.

8.5.2 Routes from runway 18L to the east

All aircraft flying eastern routes are captured in route option 2. The determined $N1$ settings versus the measured L_{max} values are plotted in figure 8.5b.

r is very low ($r = 0.041$) and p is relatively high ($p = 0.773$). r has even decreased by using an other route option, although not significant. p values less than 0.05 are treated as statistically significant.
The decrease in r could be caused be the fact that these aircraft, with eastern routes, are in the middle of a turn the moment NMT10 starts sampling. Therefore, the noise measurements of flights flying routes to the eastern might be disturbed because of this turn. Hence, the expected linear relation between $N1$ and L_{max} is not visible nor supported by the correlation coefficients r and the probability value p.

8.6 $\mathbf{V^2_{lof}}$ versus $\mathbf{L_{max}}$

The same approach, as carried out with $N1$ versus L_{max}, has been used to study linearity between V_{lof} and L_{max}. For V_{lof} a quadratic exponent is expected since V is quadratic expressed in the equation $W = m \cdot g = L = C_{L_{max}} \frac{1}{2} \rho V^2 S$ and so V^2_{lof} is shown on the x-axis of Figure 8.6.
Beforehand, the hypothesis was that aircraft mass m would be a good predictor to explain the variability in L_{max}. Since it was very difficult to determine m, V^2_{lof} was chosen as m representative.
The results for both route-combinations will be explained accordingly. The settings used for Figure 8.6 are indicated in Table 8.5.

Table 8.5: Settings for the V_{lof} versus L_{max} plot (Figure 8.6)

Parameter	Setting
Aircraft:	Boeing 737-800
Airline:	A or B
Route:	Route option 1 (figure 8.6a)
	Route option 2 (figure 8.6b)
ADS-B available:	Yes
$N1$ determined:	Does not matter

8.6.1 Routes from runway 18L to the south and the west

At first sight figure 8.6a suggests that there is a correlation between V^2_{lof} and L_{max} because of the relatively high correlation factor ($r = 0.304$) and low probability value ($p = 2.477 \cdot 10^-3$). This is actually caused by the data point slightly above the legend which causes r to increase. A manual correction for this data points decreases r to 0.269 with $p = 8.1 \cdot 10^{-3}$.
A residual analysis cancelling out these kind of outliers would improve the quality of the correlation analysis.

8.6.2 Routes from runway 18L to the east

Again, a very low r ($r = 0.030$) with a low p ($p = 0.738$) as well for the routes flying directly over NMT10.

The situation now occurs that two possibilities arise to explain the low correlation: [1] m is not a good predictor to explain the variability in L_{max} and [2] V^2_{lof} is not a good representative for m, meaning that no further conclusions can be drawn about the quality of m as a predictor. Therefore, V^2_{lof} in relation with m should be further investigated to be able to draw valid conclusions.

8.7 N1 versus V^2_{lof}

If there exist high correlation between $N1$ and V^2_{lof}, it makes no sense to use them both as a predictor in the classification process since both predictors than actually add the same information. To investigate this, $N1$ versus V^2_{lof} is plotted in Figure 8.7 with the settings indicated in Table 8.6.

Table 8.6: Settings for the $N1$ versus V_{lof} plot (Figure 8.7)

Parameter	Setting
Aircraft:	Boeing 737-800
Airline:	A or B
Route:	Route option 1 (figure 8.7a)
	Route option 2 (figure 8.7b)
ADS-B available:	Yes
$N1$ determined:	Yes

8.7.1 Routes from runway 18L to the south and the west

Figure 8.7a shows that there is no correlation between $N1$ and V^2_{lof}.
At the time of flyover, all aircraft are climbing and so climb thrust is maintained. It is was therefore not expected that V^2_{lof} as a mass representative is interconnected with $N1$ at that moment in flight.

8.7.2 Routes from runway 18L to the east

Figure 8.7b states that although there is a little correlation between $N1$ and V^2_{lof}, there also exist a relatively high p value which indicates that the reliability of r is low.

8.8 N1 versus V^2_{lof} versus L_{max}

All predictors have been discussed and thus the linearity between V^2_{lof} & $N1$ with respect to L_{max} can be investigated. Since the individual results between V^2_{lof} and $N1$ with respect to L_{max} were unfortunately not promising, it is expected that there will be no visible linear relationship in the $N1$ versus V^2_{lof} versus L_{max} plot.
Figure 8.8 shows $N1$ on the x-axis, V^2_{lof} on the y-axis and L_{max} indicated by a color. Also, airline A and B are indicated by means of a square and a hexagram, respectively. Ultimately, one would like to see a positive slope in this figure with its color dark blue in the lower left corner, increasing to yellow in the upper right corner. The data points of airline A would lie on the upper right corner and the data points of airline B in the lower left corner, since the flown procedure of airline A is expected to be flown with higher

$N1$ settings than the procedure of airline B. Also, it is expected in advance that NMT10 measures higher L_{max} levels for the procedure of airline A, compared to the procedure of airline B, caused by a difference in height above NMT10 of approximately 300 meters. The settings for Figure 8.8 are stated in Table 8.7.

Table 8.7: Settings for the $N1$ versus V_{lof} versus L_{max} plot (Figure 8.8)

Parameter	Setting
Aircraft:	Boeing 737-800
Airline:	A or B
Route:	Route option 1 (figure 8.8a)
	Route option 2 (figure 8.8b)
ADS-B available:	Yes
$N1$ determined:	Yes

8.8.1 Routes from runway 18L to the south and the west

Figure 8.8a unfortunately does no show any linear relationship. This is explainable by the fact that the individual correlations of $N1$ and V_{lof}^2 with respect to L_{max} where small. The flown route of each individual measurement is expected not to play a significant role, i.e. does not significantly contribute to the desired/expected linear relationship.
Nevertheless, airline A systematically produces higher L_{max} levels compared to airline B, which is in line with the expectation because airline A flies over with a lower height compared to airline B.

8.8.2 Routes from runway 18L to the east

The same explanation can be given for figure 8.8b: unfortunately, due to small correlations between the individual predictors and L_{max}, no relation can be found whatsoever. Likewise, in this case airline A does not produce higher L_{max} levels than airline B which actually was the case for route from runway 18L to the south and west. This could mean that there actually is no significant effect of route with respect to airline and L_{max} level, or that the shown results of figure 8.8a are established by means of coincidence. This will be further investigated by making use of a MLRA model.

8.9 Multivariate Linear Regression Analysis

A Multivariate Linear Regression Analysis (MLRA) is carried out to investigate the linear relation numerically. The goal is to construct a model which approaches the produced L_{max} levels and subtract these from the measured L_{max} levels. This should then result in a model in which the direct effect of $N1$ and V_{lof}^2 with respect to L_{max} is subtracted, hence the contribution of a difference in flown procedure should become visible. Since noise levels are substracted, the possibility exists that this results in negative noise levels. To prevent this from occurring, the L_{max} level for a reference situation is calculated and added to all modelled noise levels.
Thus:

$$L_{max,modelled} = C_0 + C_1 N1 + C_2 V_{lof} + C_3 V_{lof}^2 \tag{8.1}$$

$$L_{max,ref} = C_0 + C_1 N1_{ref} + C_2 V_{lof,ref} + C_3 V^2_{lof,ref} \tag{8.2}$$

$$L_{max,corr} = L_{max,measured} - L_{max,modelled} + L_{max,ref} \tag{8.3}$$

Where $L_{max,modelled}$ is the L_{max} as modelled with the MLRA, C_0, C_1, C_2 and C_3 are constants, $L_{max,ref}$ is the reference L_{max} for a given reference situation, $N1_{ref}$ is the reference $N1$, $V_{lof,ref}$ is the reference V_{lof} and $L_{max,corr}$ is the corrected L_{max} for $N1$ and V_{lof}. The reference situation is set to the median value for $N1$ and V_{lof} where the dataset fulfils the settings as stated in Table 8.7. Again, the two route options are treated separately which results in two different datasets, containing $N1, V_{lof}$ and L_{max}. These two datasets are used to construct two separate MLRA models. Table 8.8 and Table 8.9 state the results from a MLRA carried out using MATLAB for route option 1 and 2, respectively.
The coefficient of determination R^2, indicates the proportionate amount of variation in the response variable L_{max} explained by the independent variables $N1$ and V_{lof} in the linear regression model. The larger the R^2 is, the more variability is explained by the linear regression model. However, R^2 tends to increase as additional predictors are included in the model. Thus, one can artificially get higher R^2 by increasing the number of predictors in the model. To penalize this effect, R^2_{adj} is used and stated in Table 8.8.

MLRA model characteristics for routes from runway 18L to the south and the west

The characteristics of the MLRA model for routes from runway 18L to the south and the west are shown in Table 8.8.

Table 8.8: Results from the Multivariate Linear Regression Analysis using MATLAB (incorporating routes from runway 18L to the south and the west)

C_0	C_1	C_2	C_3	R^2_{adj}	$N1_{ref}$	$V_{lof,ref}$	$L_{max,ref}$
407.35	7.6849	-8.4281	0.052353	0.0773	91.8%	83.3 m/s	76 dB

R^2_{adj} shows that only ±8% of the total variability in L_{max} is explained by the MLRA model. Also, C_2 is negative and equal to -8.4281 which means that L_{max}, as caused by the aircraft mass representative V_{rot}, decreases with increasing V_{rot}. This is against all expectations and could be caused by the fact that the dataset is too small.
The MLRA model is constructed by using a dataset containing measurements which satisfy the conditions: [1] $N1$ is determined and has a value between 60% and 100%, [2] V_{lof} is determined and, of course, [3] L_{max} is available. However, this only leaves 41 measurements for this specific route option. Probably, this is insufficient to be able to construct a representative MLRA model.

MLRA model characteristics for routes from runway 18L to the east

The characteristics of the MLRA model for routes from runway 18L to the east are shown in Table 8.9.

Table 8.9: Results from the Multivariate Linear Regression Analysis using MATLAB (incorporating routes from runway 18L to the east)

C_0	C_1	C_2	C_3	R^2_{adj}	$N1_{ref}$	$V_{lof,ref}$	$L_{max,ref}$
119.88	2.6056	-1.0677	0.0056	0.055	92.0%	83.3 m/s	72 dB

In this case, 41 measurements where available to construct the MLRA model and only $\pm 6\%$ of the total variability in L_{max} is explained, according to R^2_{adj}. Again, C_2 has a negative value equal to -1.0677. To be able to ascertain the results as obtained in Table 8.9 the dataset should be enlarged and the construction of the MLRA model should be repeated.
Despite the unexpected characteristics as stated in Table 8.8 and Table 8.9, the MLRA models will still be used due to a lack of more measurements.

The results related to $L_{max,corr}$ for both route options are visualized by means of box plots (see Figure 8.9), where airline A* and B* indicate the L_{max} levels after correction for the contribution of $N1$ and V_{lof}, according to Equation 8.3. The settings used for these plots are exactly the same as earlier stated in Table 8.7.

8.9.1 Routes from runway 18L to the south and the west

Comparing the results for airline A is becomes clearly visible that with the additional of two additional predictors, the bandwidth has increased in stead of decreased. Correcting the L_{max} values for airline A and B both resulted in lower levels which was expected to occur because the effect on L_{max} as contributed by $N1$ and V^2_{lof} is distilled, hence the L_{max} levels should decrease.
Making a comparison between both airlines in the old and in the new situation shows that in the L_{max} levels overlap in the new situation where that was not the case in the old situation (before correction for $N1$ and V^2_{lof}. One actually added, in stead of removed, inaccuracies/scatter.
Although the L_{max} levels for airline B slightly decreased after correcting for $N1$ and V^2_{lof}, the total bandwidth increased. Also, the Two-Sample t-Test (TStT) shows no significant improvement between the situation before correction and the situation after correction.
The p value before correction equals 0.0105 with confidence bounds between 0.5049 and 3.5706 and the p value after correction equals 0.0847, with confidence bounds between -0.1858 and 2.7811. Hence, variance is added to the data in stead of removed.

8.9.2 Routes from runway 18L to the east

Figure 8.9b actually illustrates the initial problem: variances are large and the bandwidth of both airlines before correction are fully overlapping. Though, the removal of the contribution of $N1$ and V^2_{lof} do not remove the overlap as to be able to compare both sets of L_{max} levels. Also, the TStT shows no significant improvement between the situation before correction and the situation after correction.
The p value before correction equals 0.7498 with confidence bounds between -1.0574 and 1.4566 and the p value after correction equals 0.3658, with confidence bounds between -0.6630 and 1.7583. Hence, no conclusions can be drawn about the impact on L_{max} due

to a difference in flown operational procedure.

Possibly worse $N1$ estimates have been added which returns worse results. Also, the addition of V_{lof}^2 as a m representative could not be valid. It is therefore first important to check the validity of V_{lof}^2 as a m representative before any other conclusions can be drawn.

This research was carried out to decrease variance and to show the direct effect of a difference in operational procedure flown by two airlines by means of a visual representation as well as numerical substantiation. It can be concluded that the addition of $N1$ and V_{lof}^2 did not decrease variance and actually increased variance and even worsened the visual representation.

8.10 Result overview

The results for $N1$ with respect to L_{max} and V_{lof} with respect to L_{max} where unfortunately very disappointing. No clear relation could be obtained from the individual plots, nor did the MLRA provide any proof of a possible improvement in results. The ultimate goal was to correct the measured L_{max} levels to decrease variability and hence be able to visualize the direct effect as caused by a difference in flown procedure. Nevertheless, the MLRA resulted in an even wider spread (increase in variance) for both airline A and B and hence the expected difference in L_{max} could not be visualized.

8.10.1 Impact of weather on results

Since the measured L_{max} is dependent upon meteorological conditions, possibly the weather (temperature and humidity) plays an important role. Hence, the local temperature and humidity are studied and visualized in Figure 8.10 for all individual measurements.

Figure 8.10 shows a continuous change in temperature and humidity which argues to correct the measured L_{max} for these additional predictors. However, this is solely meant as a recommendation for future research. Note, for example, the continuous ascending part of the humidity line between 26082014 and 27082014: this is caused by the fact that there are no measurements in between this interval resulting in more or less a 'connection line' between the two data points just before 26082014 and just after 27082014, respectively.

8.10.2 $\mathbf{L_{max}}$ residual analysis

To obtain an overview of the results for $N1, V_{lof}^2$ versus L_{max}, first all rows are sorted. $N1$ and V_{lof}^2 occur in ascending order with its associated L_{max} level. Then, the median of the L_{max} levels is calculated and this median is subtracted from the measured L_{max} levels. This results in the plot as shown in Figure 8.11. Note that this plot contains the south and western routes solely.
From this figure can be obtained that the residuals show no clear relation with ascending $N1, V_{lof}^2$. Therefore, it can be concluded that at least one predictor is poorly determined or that actually no true relation between $N1$ and V_{lof}^2 with respect to L_{max} exists.

8.11 Alternative approach: distance to destination versus L_{max}

Since no clear conclusions can be drawn with respect to the representative capabilities of V_{lof}^2 and m, the distance from AAS to its final destination has been studied as an alternative aircraft mass m representative.
Fuel can take up to 25% of the total aircraft mass [16] and the destination determines how much fuel has to be carried. It is thus expected that the destination of a flight could be a good representative for m and hence a good predictor for L_{max}. Figure 8.12 contains the results for both route options with the settings of this plot equal to those as indicated in Table 8.7.
Since this is comparison is made just to get a basic idea whether or not the distance to travel is a good m representative, it is important to note that the so-called 'great-circle distance' is taken as the distance to travel. Of course, in general this is never the case since aircraft fly from way point to way point and do not travel direct routes to their destination. In the case of promising results, this gives input to future scientific research.

8.11.1 Routes from runway 18L to the south and the west

Unfortunately, figure 8.12a shows a negative correlation between distance to destination D and L_{max} ($r = -0.166$) which means there exists a downward in stead of an upward correlation. This could be the case if the aircraft as plotted contain different amounts of fuel due to, for example, economic purposes (the fuel price could be significantly lower at different airports [30]). Hence, aircraft travelling a longer distance do not necessarily have to be heavier compared to aircraft travelling shorter distances.
Also, the probability value p indicates that there is a significant chance that the observed r is obtained by random ($p = 0.298$), hence no further conclusions can be drawn with regards to r.

8.11.2 Routes from runway 18L to the east

Figure 8.12b shows a significant correlation ($r = 0.512$) and a good (low) p value ($p = 0.001$) when considering all data points (r and p as stated in figure 8.12b for the data points associated to a distance-to-destination between 0 and 5000 kilometres). Hence, in this case their exists a linear relation between D and L_{max}. However, the correlation analysis is influenced by the two most-right data points, which advocates an extensive residual analysis to correct for outliers hence improving the statistical quality of the correlation analysis.
Assuming the two most-right data points are outliers, the correlation coefficient r becomes 0.536 with a p value of 0.001 (r and p as stated in figure 8.12b for the data points associated to a distance-to-destination between 0 and 2000 kilometres). So, by simply removing the (assumed) outliers, the correlation between the data points improves. Assuming the two most-right data points are not outliers, one of the explanations might be that aircraft travelling to the east carry exactly the amount of fuel needed, hence a good comparison can be made with regards to D and L_{max}. One of the arguments supporting this statement is that the fuel prices in the eastern division of Europe is cheaper compared to destinations in the south and west of Europe [30]. However, this is true for most (and not all) of the eastern airports compared to the south and western airports.

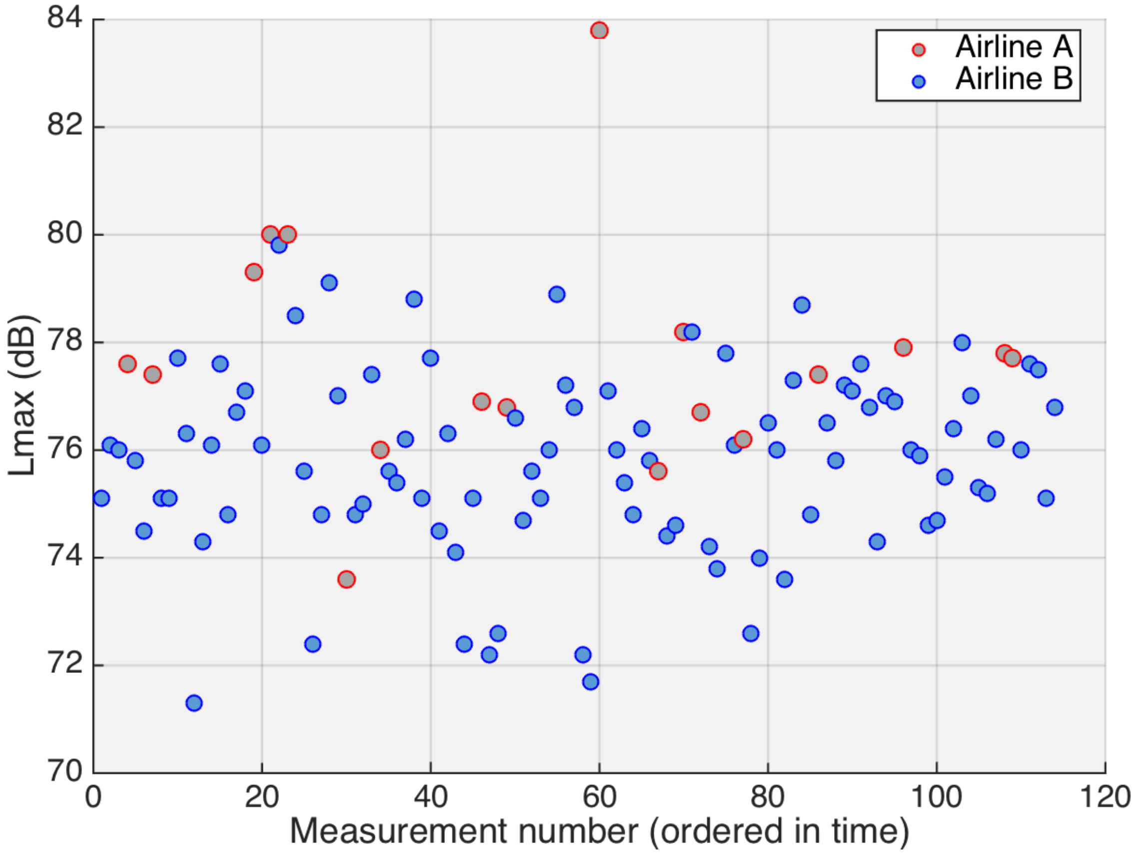

(a) Southern and western routes

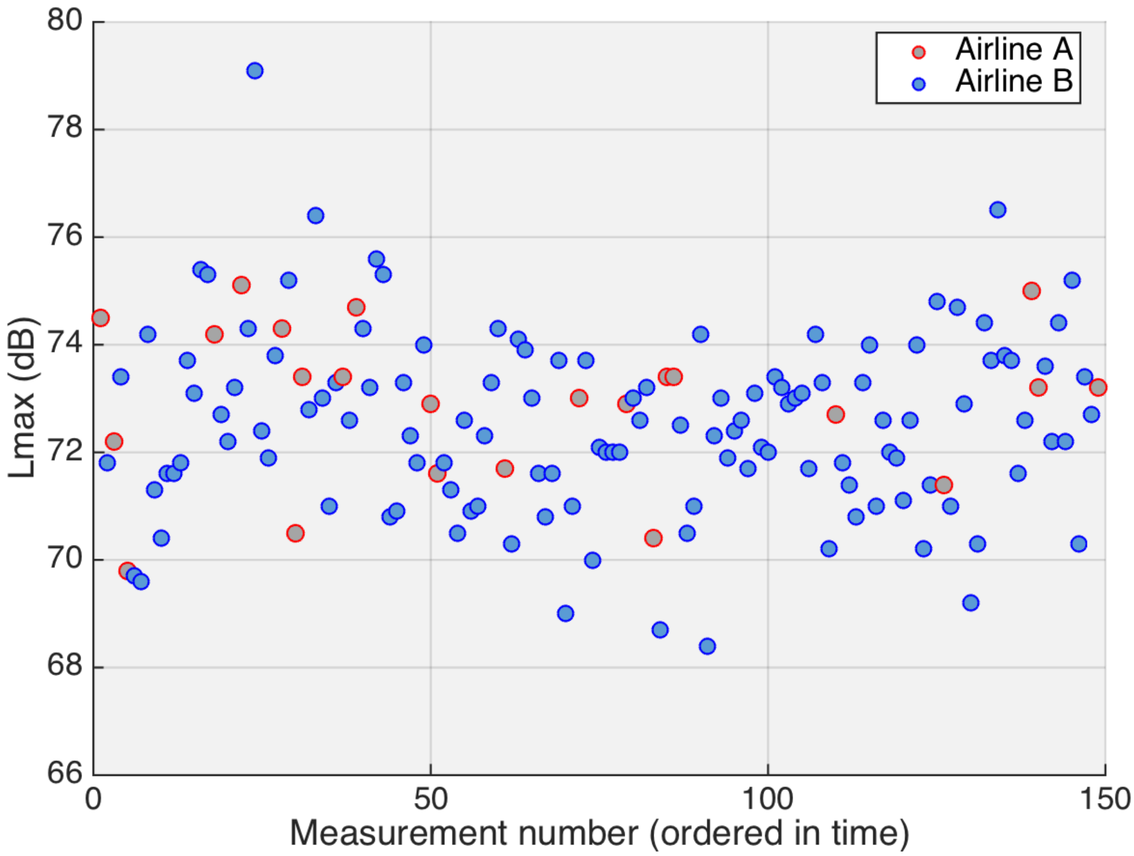

(b) Eastern routes

Figure 8.4: L_{max} values for all measurements

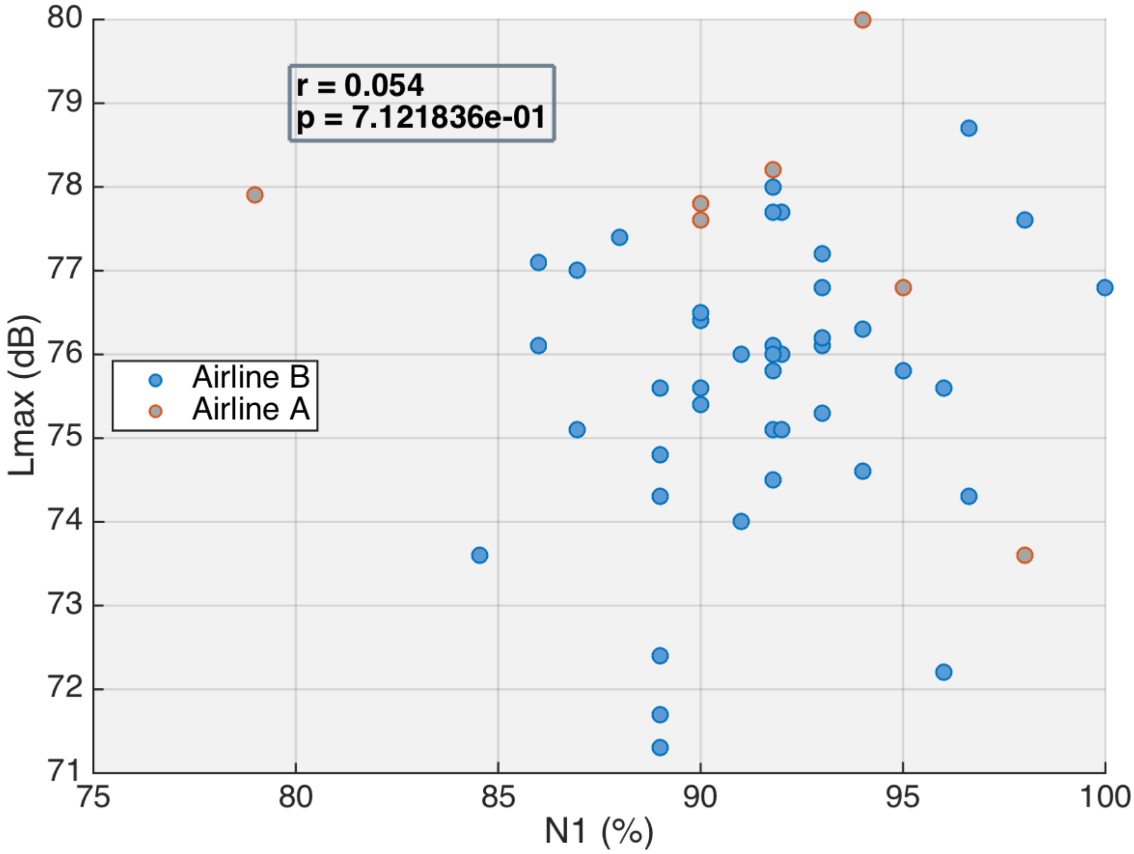

(a) Southern and western routes

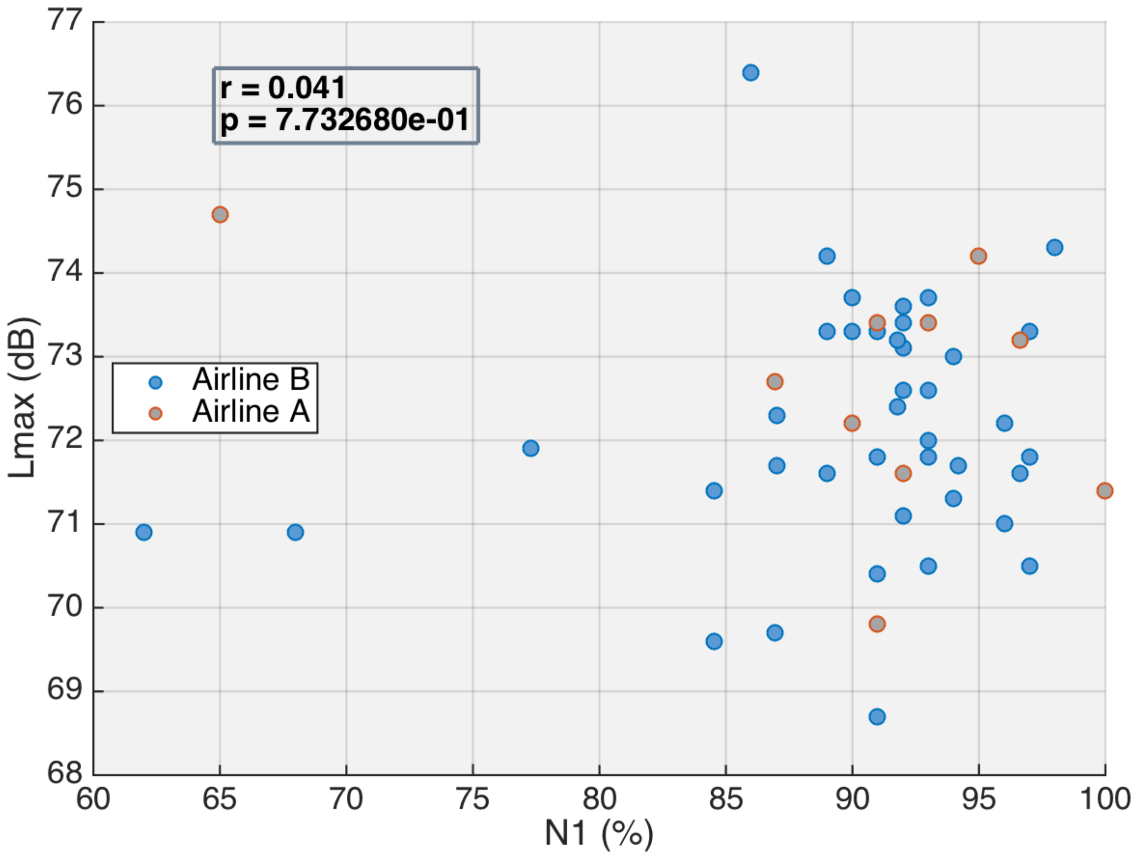

(b) Eastern routes

Figure 8.5: Determined $N1$ settings versus L_{max} values

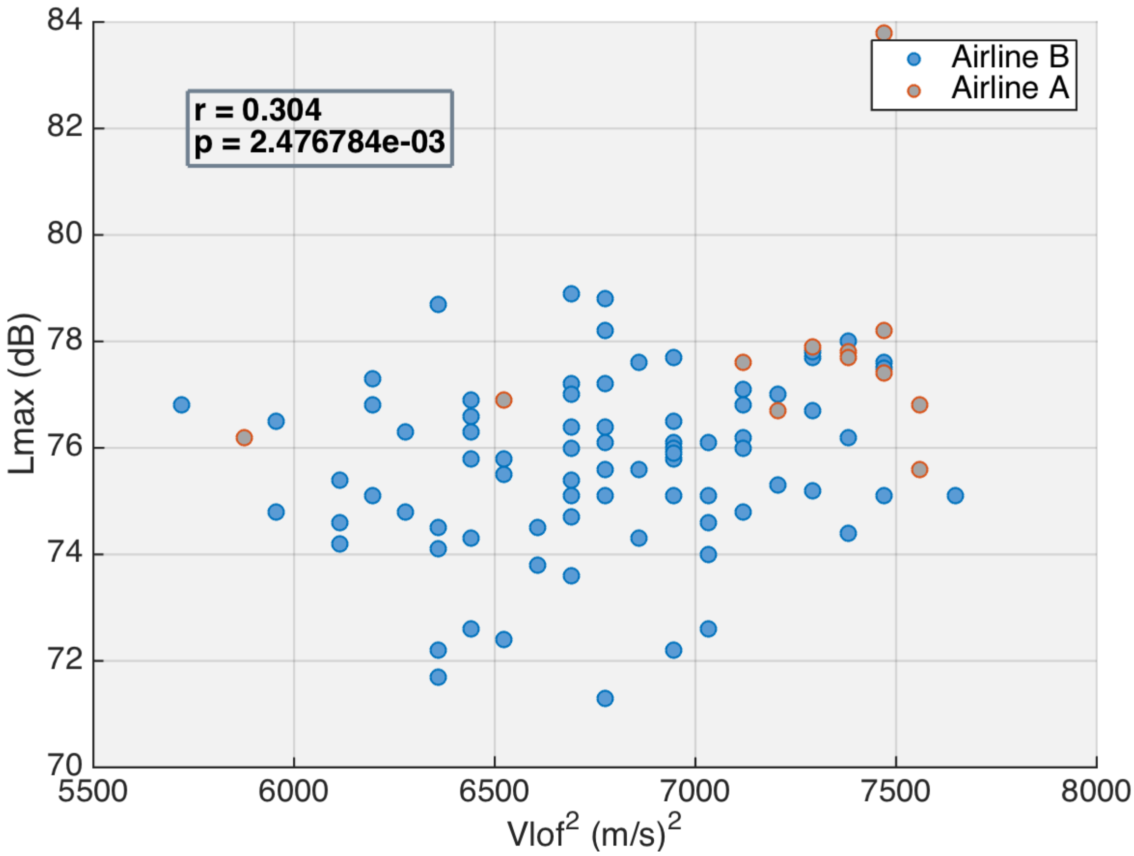

(a) Southern and western routes

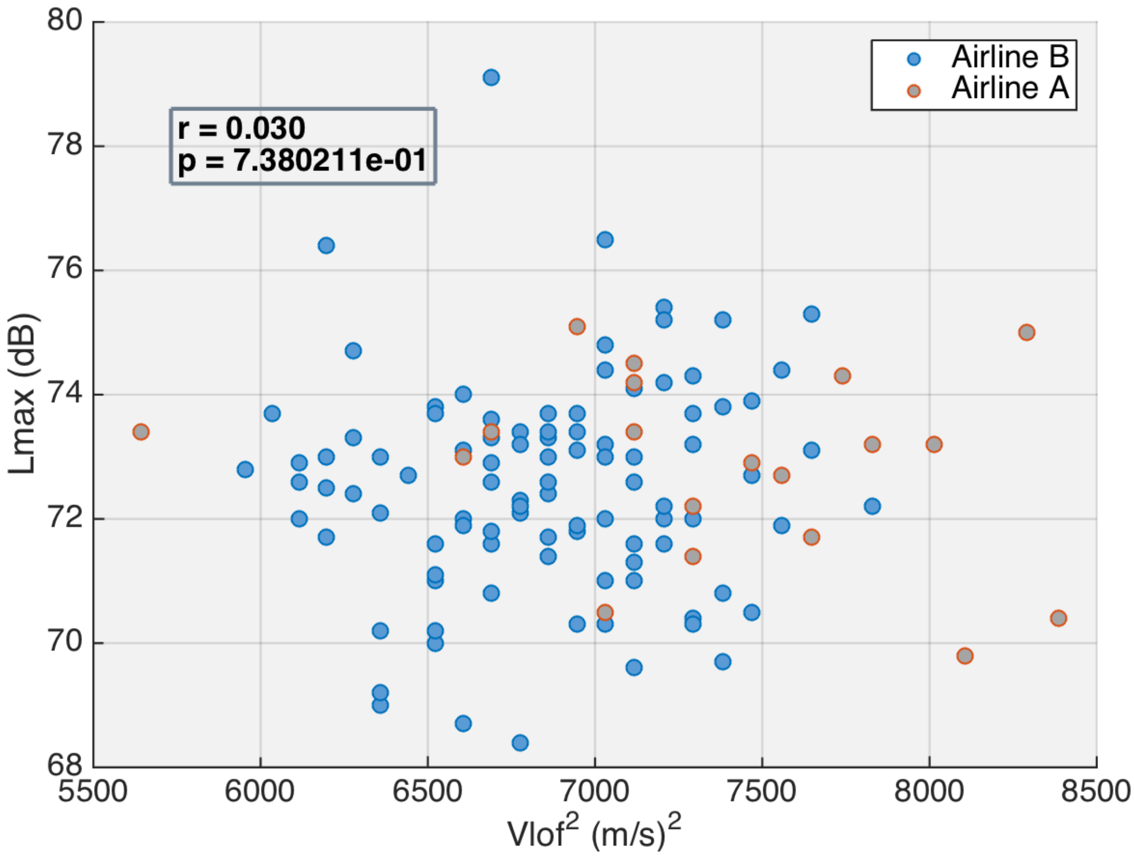

(b) Eastern routes

Figure 8.6: Determined V_{lof}s versus L_{max} values

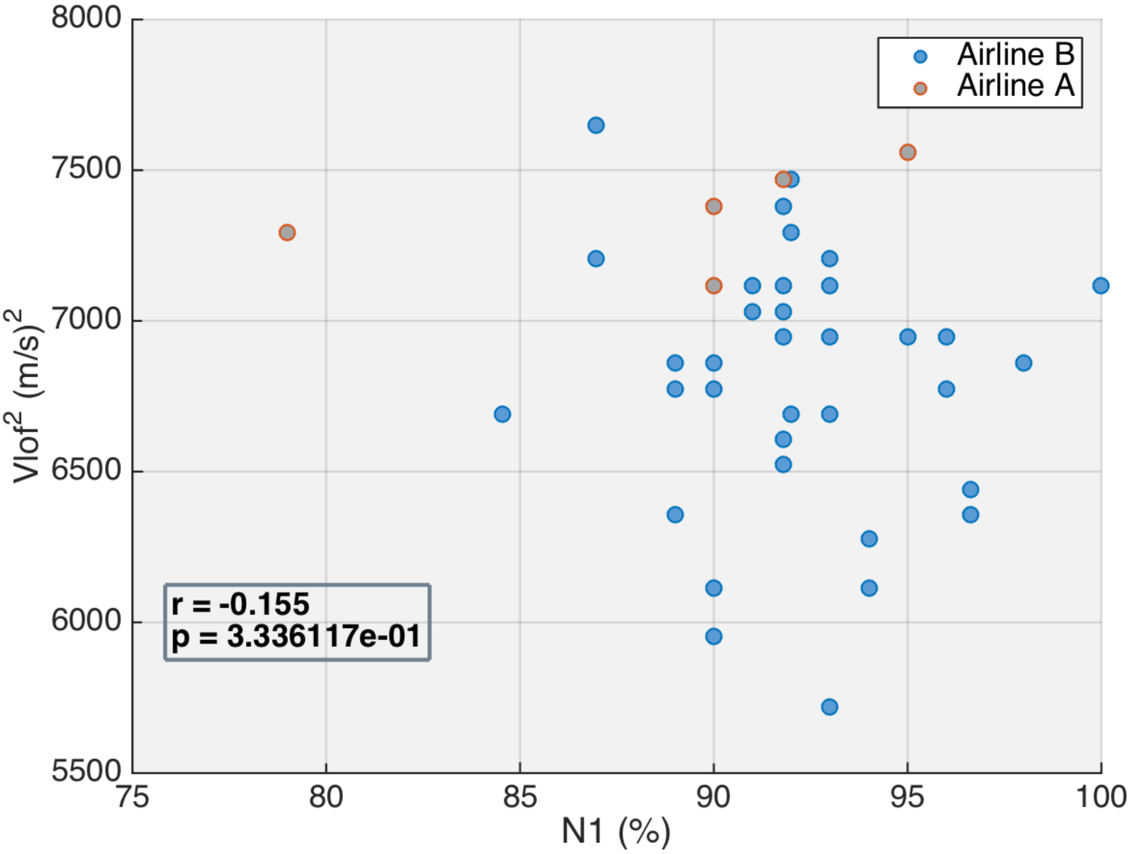

(a) Southern and western routes

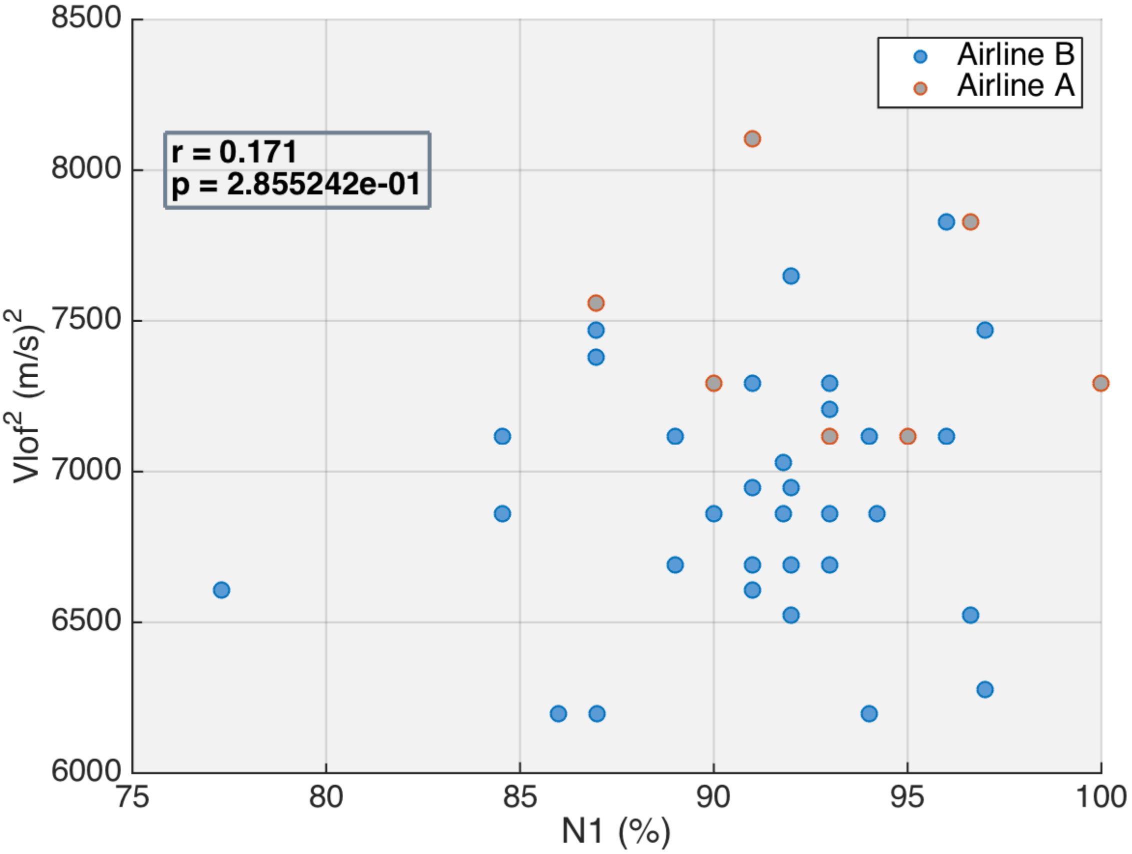

(b) Eastern routes

Figure 8.7: Determined $N1$ settings versus V_{lof}^2s

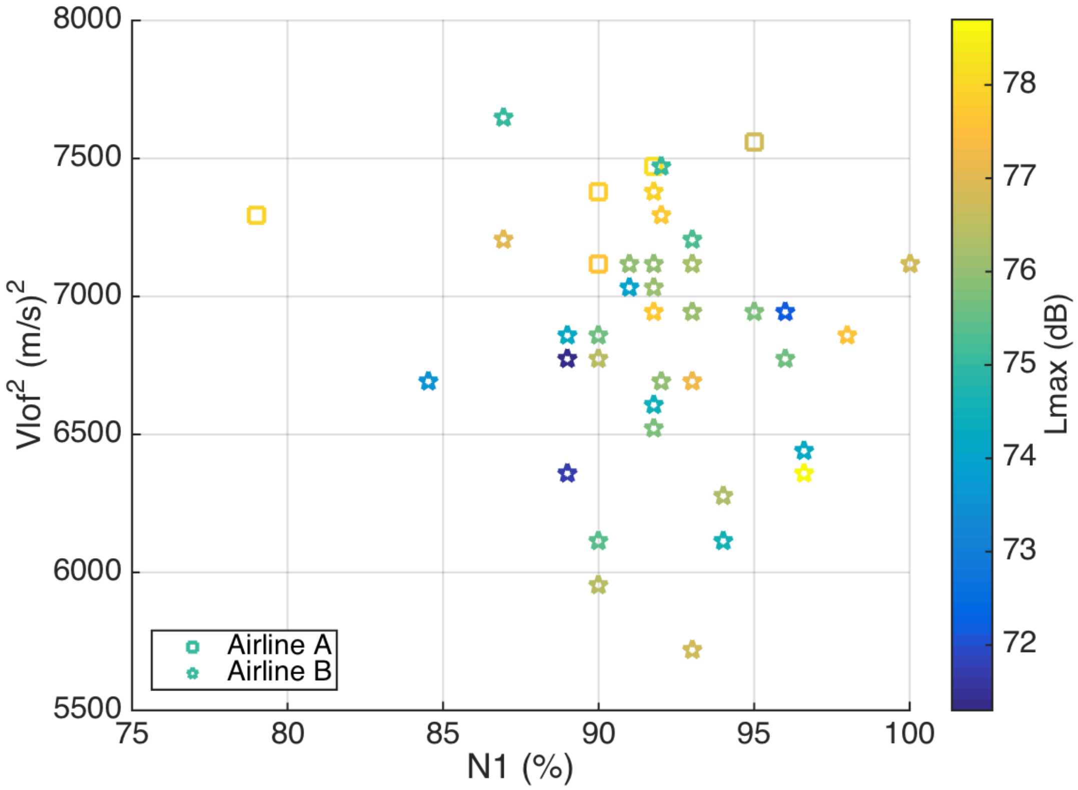

(a) Southern and western routes

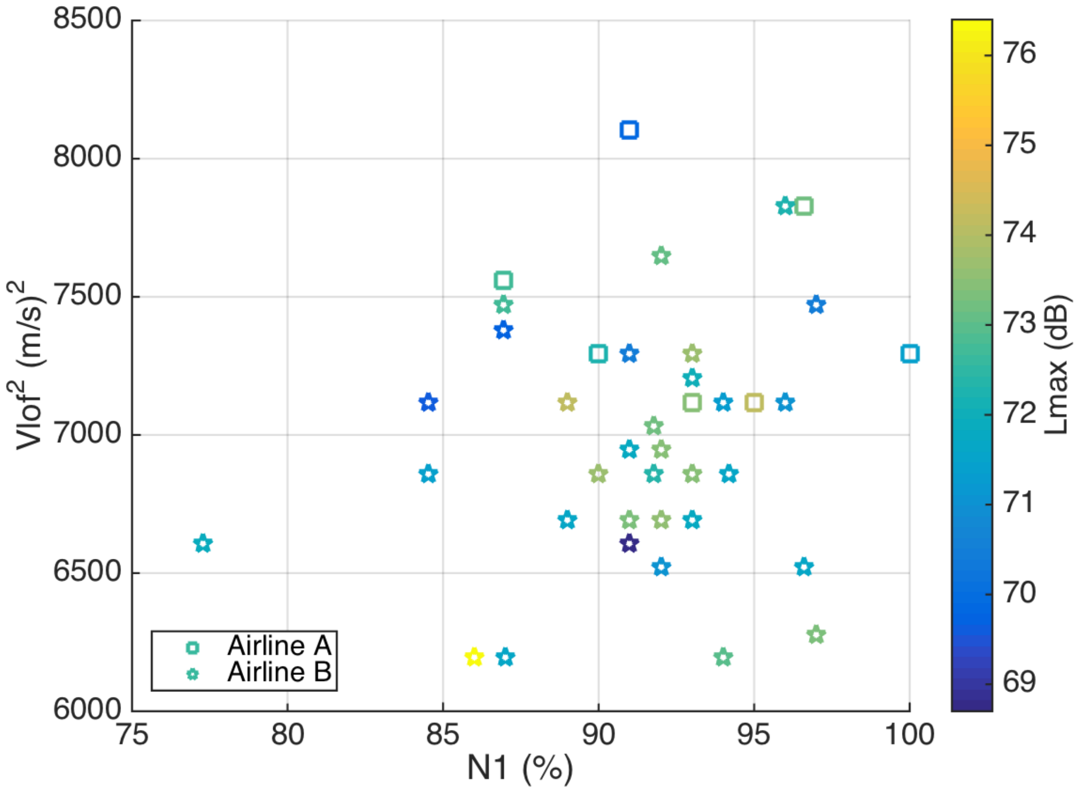

(b) Eastern routes

Figure 8.8: Determined $N1$ settings versus V_{lof} versus L_{max}

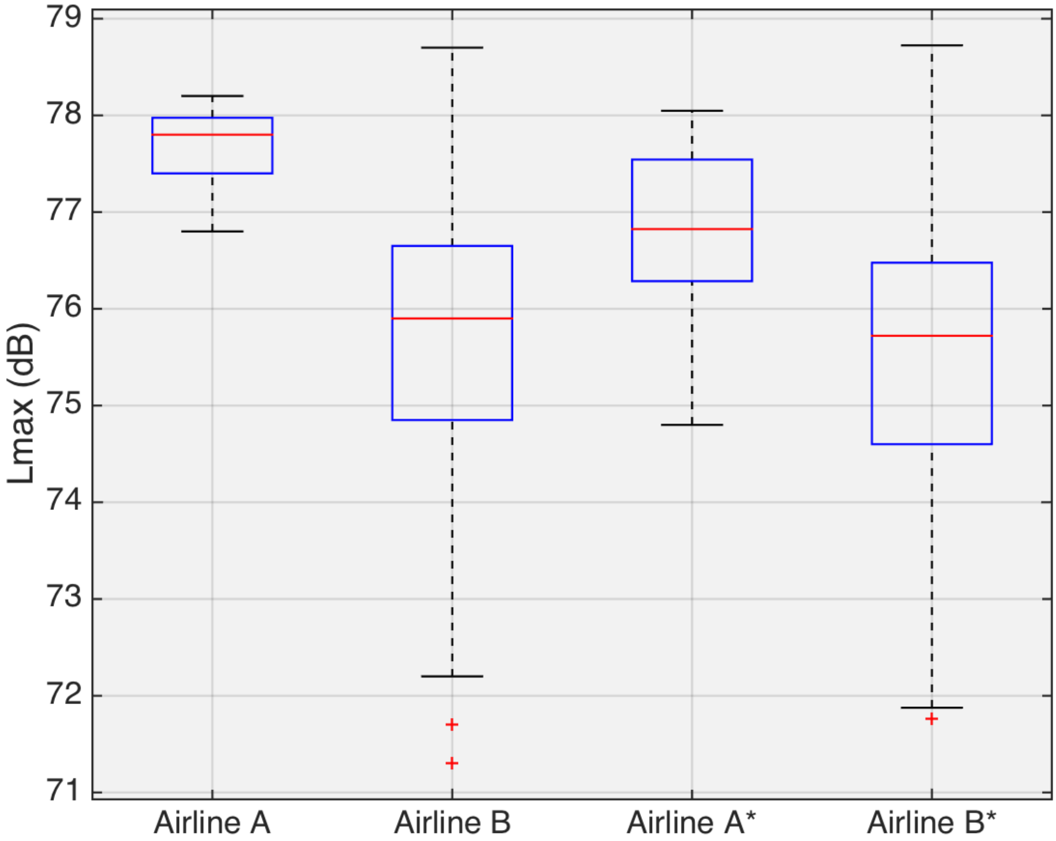

(a) Southern and western routes

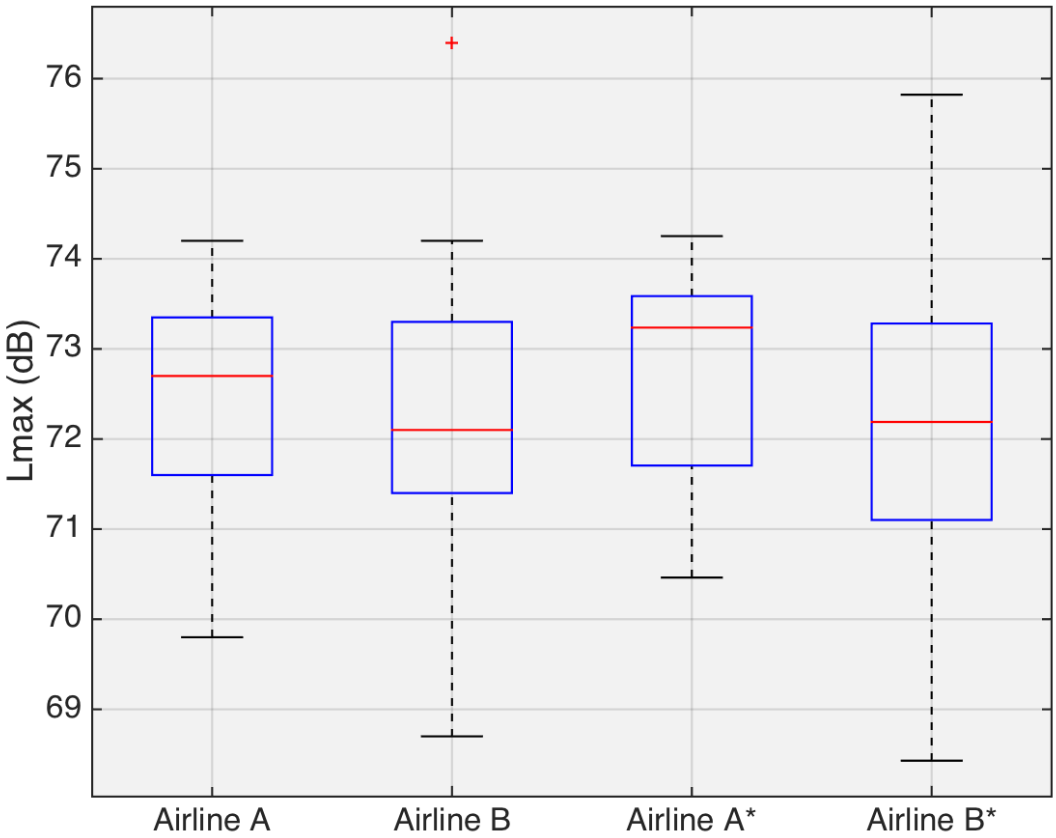

(b) Eastern routes

Figure 8.9: Box plot of the MLRA. The sign '*' indicates the corrected values

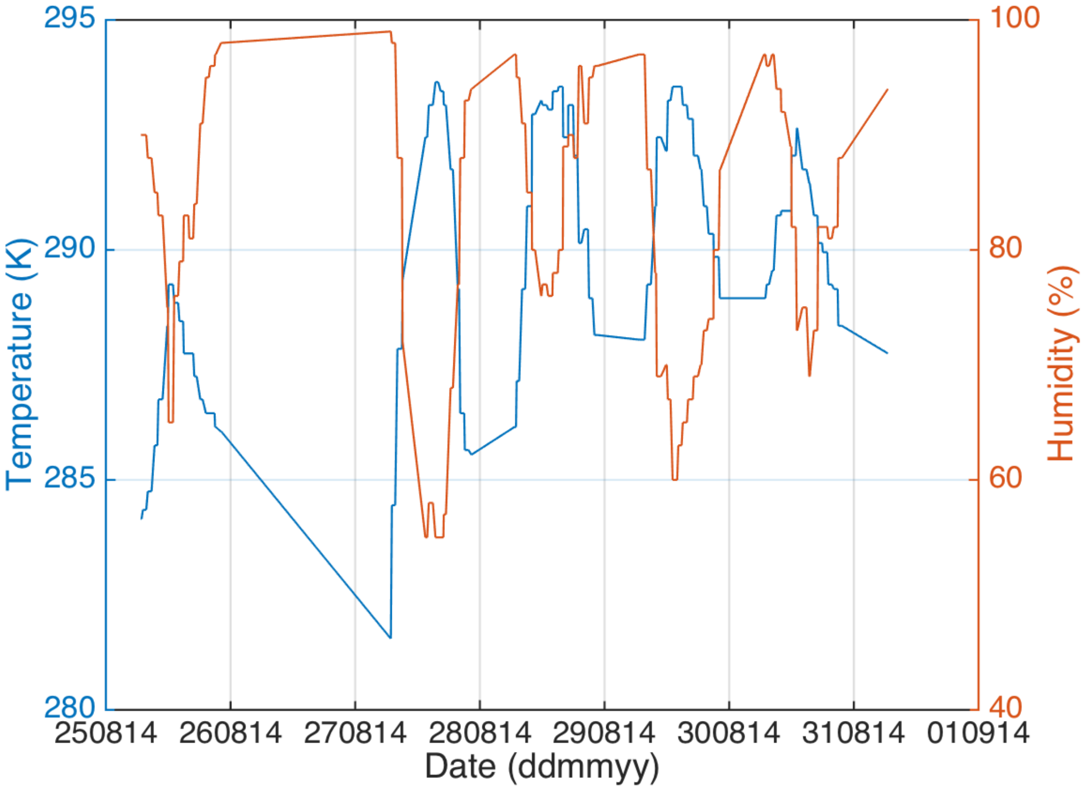

Figure 8.10: Meteo overview: Temperature and relative humidity

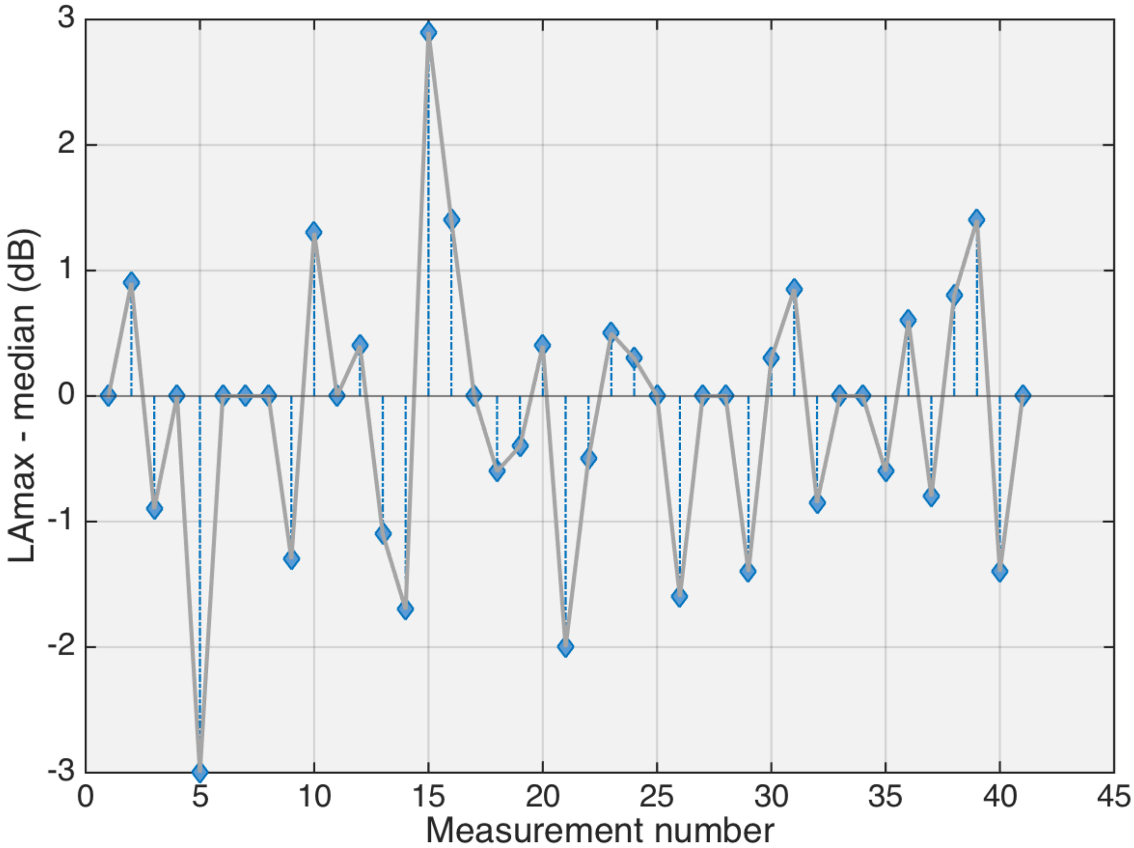

Figure 8.11: Difference between L_{max} and median L_{max} for the Boeing 737-800

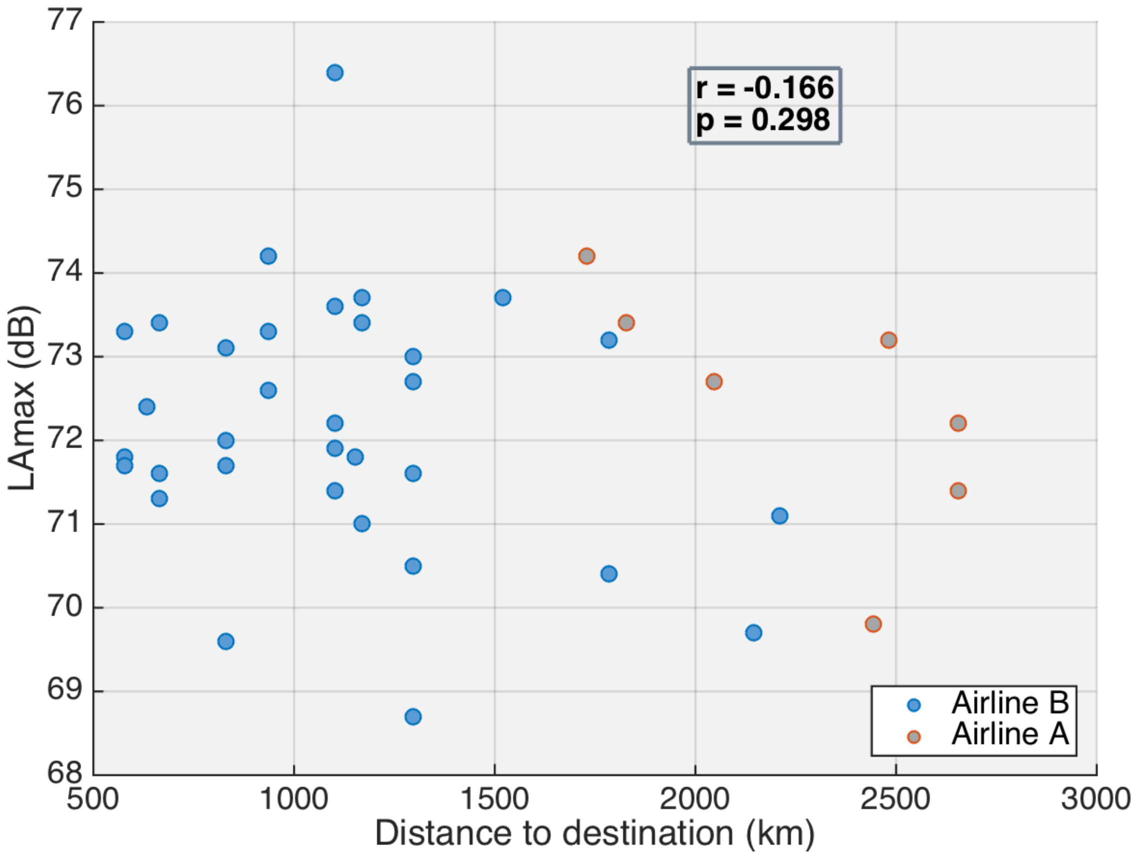

(a) Southern and western routes

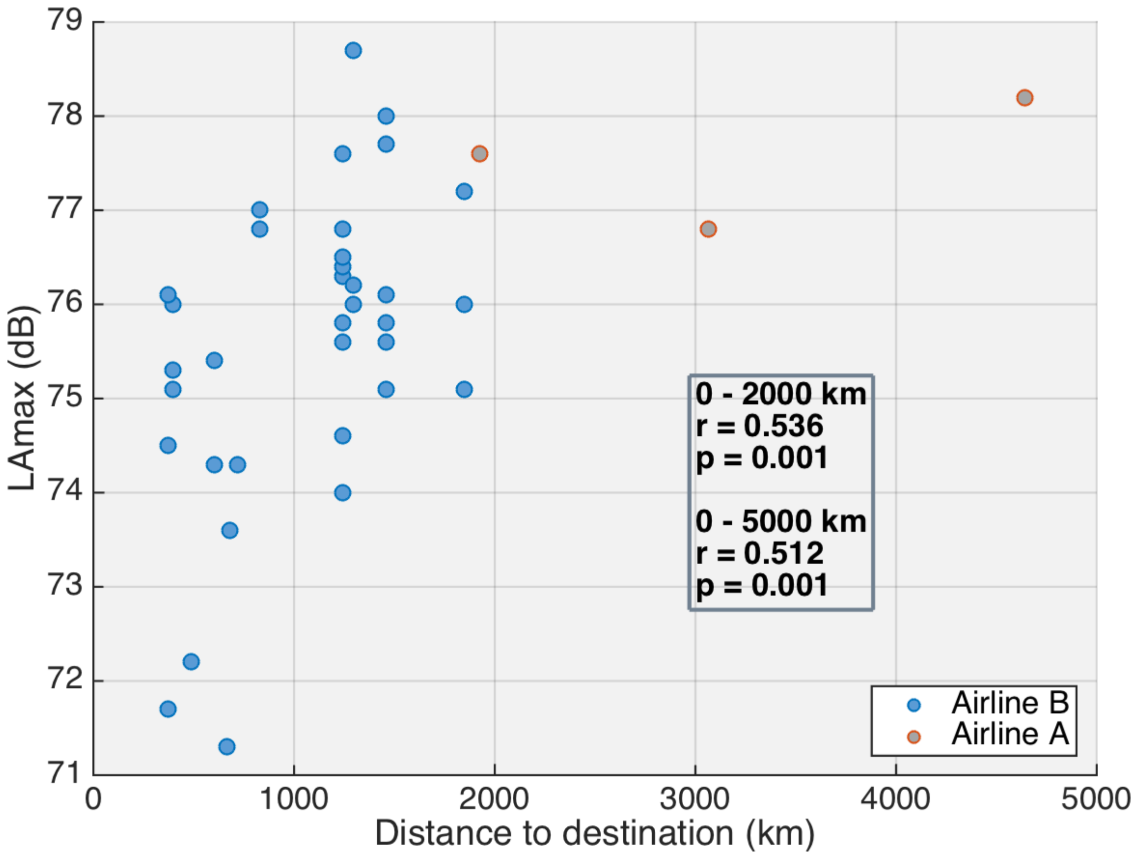

(b) Eastern routes

Figure 8.12: Distance from AAS to destination versus L_{max}

[Page intentionally left blank]

Chapter 9

Conclusions & Recommendations

This chapter draws the conclusions based on the results previously obtained. Next, given the results, recommendations are drawn for future research to improve the earlier obtained results and to continue the investigation in the field of aircraft noise classification.
First, general information is given regarding the measurement location and the dataset acquisition. Second, the results as obtained during this research are reviewed and conclusions are drawn. Last, recommendations, gained during this research, are stated to improve the overall results.

9.1 General

In general the following situation holds regarding the measurement set-up and dataset acquisition:

Chosen operational procedure: The general interest of this research is to visualize the effect of a difference in flown operational procedure to the measured noise level on the ground. Recently, AAS tried to assess the effect to L_{max} as caused by a difference in a variant of Noise Abatement Departure Procedure 2, hence this noise abatement departure procedure is chosen for the assessment.

Measurement location: NOMOS station 10 (NMT10) was chosen as the station to provide the necessary noise measurements (time series and L_{max} levels), because it was found that there exists a difference in height directly above NMT10 as caused by the flown variant of NADP2. Hence, NMT10 is a suitable station to provide the necessary noise measurements.

Departures and/or landings: Only departures are treated because the difference in operational procedure as treated in this research only occurs at departures and not at landings.

Runway choice: Since the nearest by runway with respect to NMT10, is runway 18L (the 'Aalsmeerbaan') this runway is chosen as departure location. No other runways are treated because the routes from the other runways are to far away from NMT10 and hence no measurements are conducted by NMT10 from aircraft leaving from other runways.

Route combinations: The evaluation regarding aircraft mass, aircraft engine setting and noise level is carried out by using two route combinations, since there exist seven different routes from 18L but three routes and four routes initially follow the same track when the sound level is measured by NOMOS.

Airline(s): It is investigated which airlines fly a variant of the same operational departure procedure and it appeared that two airlines fly most frequently and hence the most noise measurements from these two airlines could be conducted. Because of highly classified information revealed in this report, these airlines are abbreviated as airline A and airline B. Airline A flies the departure procedure with a height of acceleration of 1000 feet and airline B flies the same operational departure procedure with an acceleration height of 1500 feet. Theoretically, airline A flies over NMT10 lower compared to airline B and hence it is expected that airline A causes a higher maximum noise level L_{max} compared to airline B.

Aircraft type(s): To be able to assess the noise levels as caused by aircraft, it is chosen to use only one aircraft type because the shape of an aircraft as well as the engine types mounted under the aircraft influences the noise levels as measured by NMT10. Therefore, one and the same aircraft type has to be treated. Of course, multiple aircraft types departure from 18L but solely aircraft types must be investigated which are both part of the fleet of airline A as well as part of the fleet of airline B. It appeared to no other aircraft type than the Boeing 737-800 is part of the fleet of airline A as well as part of the fleet of airline B, therefore solely this aircraft type is investigated.

Dataset size: Taking all the above into consideration resulted in a dataset size of 263 flights/measurements: 41 for airline A and 222 for airline B.

9.2 Conclusions

This research is set-up in the following individual parts being:

1. Aircraft engine setting $N1$ determination and $N1$ versus L_{max} relation;
2. Aircraft mass m determination and m versus L_{max} relation;
3. Relation between $N1$ and m;
4. Relation between $N1$ and m versus L_{max};
5. Development of a model based on these two predictors to estimate L_{max}.
6. Alternative mass representative 'distance to destination' D.

The purpose of item 5 is to improve the distinctive capabilities between noise measurements by subtracting the contribution of the two predictors to L_{max} from L_{max}, hence visualizing the effect of a difference in flown operational procedure.

The results of these individual parts will be treated consecutively.

9.2.1 N1 determination and N1 versus $\mathbf{L_{max}}$ relation

During the development of the *N1* Determination Algorithm two alternative algorithms have been investigated from which one method, called the Peak Find Method (PFM), appeared to show the best results as it searches for the maximum negative derivative of the SPL and does not necessarily have to come up with a result: it could also be the case

that $N1$ could not be determined for a measurement and hence the algorithm reject the measurement.
The following conclusions regarding $N1$ as a potential predictor can be drawn:

Results of the PFM: The PFM shows good results for the B738 because of a clearly visible first BPF harmonic. However, when one of the harmonics is not clearly visible (for example with the Fokker 70), the PFM rarely determines $N1$. These aircraft spectrograms show a high level of broadband noise which masks the tonal noise BPF.

Number of occurrences of N1 for both airline A and B: When both measurements are assessed in perspective, it can be concluded that airline A operates with a slightly lower $N1$ compared to airline B ($N1 = 90\%$ versus $N1 = 93\%$). This result appeared not to be statistically significant because the Two-Sample t-Test (TStT) resulted in a p value of 0.1689 and thus the set significance level of 5% was exceeded. However, if the TStT showed statistical significance, this can be the direct result of a difference in operational procedure because airline B is climbing at the moment the noise measurement is conducted and airline A is continuing its climb into the acceleration phase hence decelerates from climb thrust to acceleration thrust.

N1 versus $\mathbf{L_{max}}$: $N1$ versus L_{max} showed a high degree of scattering which results in a low correlation coefficient and a high probability value. Therefore, two conclusions can be drawn with respect to this result: [1] the measurement set-up of aircraft versus NMT10 disturbs the L_{max} measurements so that no qualitative conclusions can be drawn of $N1$ with respect to L_{max}, or [2] $N1$ does not show a linear relation with L_{max}.

N1 versus $\mathbf{L_{max}}$ for airline A and B: Taking into account a high degree of scattering in the $N1$ versus L_{max} plot and knowing that all measurements of airline A and airline B are flown by following their company procedures, $N1$ for airline A at the southern and western route combinations seems to be negatively correlated, which is very unlikely to occur since a higher $N1$ setting increases engine noise and hence is expected to result in a higher measured L_{max} level. Airline B for both route combinations shows a very high degree of scattering and hence no correlation between airline B $N1$ settings versus L_{max} exists.

9.2.2 m determination and m versus $\mathbf{L_{max}}$ relation

It appeared to be very difficult to determine aircraft mass m directly from aircraft performance theories. Therefore, it was chosen to determine an m representative and use this parameter as predictor in the development of the model as mentioned in item 5.
The m representative was chosen to be the speed of the aircraft at lift-off: hence the speed V_{lof} where height $h > 0$ for the first time. Research showed that this speed is based on the weight of the aircraft and the chosen flap setting. The flap setting was assumed to be constant for all $B738$ aircraft. Internal information of AAS showed that flap setting 5 is the standard flap setting for airline A in normal conditions. Airline B uses flap setting 5 in standard conditions as well, followed from internal contact between AAS and airline B. The term 'normal conditions' in this case means no heavy cross-wind and/or heavy rain or snow conditions. This is assured by the fact that in case of heavy weather conditions, NOMOS cannot measure aircraft noise accurately and rejects and noise event from saving it to the internal server of AAS. Because the speed V is related quadratically to m, V_{lof}^2

is used as predictor.
The following conclusions can be drawn based on the results related to V_{lof}:

$\mathbf{V^2_{lof}}$ versus aircraft mass m: A weak correlation of 0.385 exists between V^2_{lof} and m, meaning that only 15% of the total variation in m can be described by V^2_{lof}. Nevertheless, the p value shows that there is a very low chance of obtaining this correlation by chance. Hence, although far from being an ideal m representative, due to a lack of time V^2_{lof} was chosen to be used in the development of the MLRA model. The low correlation is most likely caused by the fact that there are many more involved to be able to predict m for a given V^2_{lof}.

Number of occurrences of $\mathbf{V_{lof}}$ in total dataset for Airline A and B: Figure 8.3 showed that V_{lof} is typically higher for airline A compared to airline B. This can be caused by the difference in business models between airline A and B. Airline B flies more frequent compared to airline A and does not necessarily always have to be fully booked, while airline A flies less frequent and is very focussed on getting their aircraft fully booked.

$\mathbf{V^2_{lof}}$ versus $\mathbf{L_{max}}$: The southern and western route combination showed to have some correlation. However, this is caused by the outlier at $(V^2_{lof}, L_{max}) = (7500, 84)$. Thus, both route combinations show no correlation and therefore it can be concluded that either V^2_{lof} is not a good m representative, or V^2_{lof} does not have any influence on the noise level as measured by NOMOS. Also, the possibility exists that V^2_{lof} is a good m representative, but not a good predictor to explain variation in L_{max}. This relation should be further investigated in future research.

9.2.3 Relation between N1 and m representative $\mathbf{V^2_{lof}}$

$N1$ and m representative V^2_{lof} individually showed no promising results since both were non correlated with respect to L_{max}. Nevertheless, to continue the comparison the ultimate goal is to assess the relation of $N1$ and V^2_{lof} versus L_{max} and thus first it is investigated whether or not $N1$ and V^2_{lof} are correlated. If this is the case, it is better to use one of both as a predictor because otherwise both predictors would explain the same linearity with respect to L_{max}.
However, $N1$ and V^2_{lof} showed to have a negative and positive correlation for the southern and western route combinations and eastern route combinations, respectively. It can reasonably be concluded that both predictors are not correlated, also supported by the fact that the associated p values are significant. Hence, a comparison is made using both parameters as a predictor.

9.2.4 Relation between N1 and m versus $\mathbf{L_{max}}$

$N1$ and V_{lof} versus L_{max} as expected show no relation with each other as already predicted since both individual assessments appeared to have no correlation.
However, this assessment is largely dependent upon the individual assessments of both predictors with respect to L_{max} since a high correlation between the individual predictors versus L_{max} automatically results in a higher correlation when this comparison is carried out.
Hence, it is expected that in the case the correlation factor between one of the predictors versus L_{max} improves, this comparison also improves. Thus, no firm conclusions can

be drawn since the quality of the individual comparisons can not be guaranteed. It is expected that many more factors have to be taken into account than only V_{lof}^2 to estimate m and/or the L_{max} values are disturbed by environmental factors.

9.2.5 Model development based on N1 and m-representative $\mathbf{V_{lof}^2}$ to estimate $\mathbf{L_{max}}$

A Multivariate Linear Regression Analysis model has been constructed based on the noise levels measured by NMT10 in combination with the determined $N1$ settings and V_{lof}^2 speeds. The following conclusions regarding this model and its results can be drawn:

Model result expectations in advance: The model is based on two predictors from which earlier was proven to show a low correlation with L_{max}. The development of a model also brings its own shortcoming and L_{max} residuals. It was therefore expected in advance that correcting L_{max} for the effects of $N1$ and V_{lof}^2 would not show the effect of a difference in flown operational procedure as desired.

Using Multivariate Linear Regression Analysis to construct a model: MLRA is used to calibrate a L_{max} prediction model based on $N1$ and V_{lof}^2 as predictors. This model showed only to be able to explain 7% of the total variation in L_{max}.

Using a reference situation to compare $\mathbf{L_{max}}$ levels: A reference situation is used to be able to compare the set of L_{max} levels at the same reference values for $N1$ and V_{lof}. The median of $N1$ and V_{lof} were determined and used to determine a reference $L_{max,ref}$ level. The reference values and reference L_{max} level were $91.8\%, 83.8$ m/s and 76 dB, respectively.

Results of the $\mathbf{L_{max}}$ prediction model: The addition of two predictors appeared to worsen the results. The situation in which no correction is applied for the effect of both predictors, show better results and a smaller variation compared to the situation in which the correction is applied. This also argues that in this case there was no correlation between the individual predictors and L_{max}, whatsoever. For the southern and western routes combination there already existed a clearly visible difference in L_{max} levels and so it was not necessary to add the extra two predictors. Nevertheless, it must be mentioned that the total dataset size for airline A in the comparison was only 5 flights/measurements compared to 36 flights/measurements for airline B. Taking this into consideration puts the results in perspective and argues whether there can be drawn quantitatively good conclusions based on such a small dataset for airline A because the change of obtaining the same results by random in that case increases significantly. The correction of L_{max} levels using the model as previously obtained for eastern routes combination resulted in a wider spread over the total set of results for airline A and exactly the opposite was the case for airline B: the spread decreased after correction. The difference in upper and lower boundaries after correction for both airlines slightly increased, which generally improved the distinctive capabilities. But however, still a large overlap after correction between both airlines exist and hence it can be concluded that the distinctive capabilities between both airlines did not improve. Note that the total dataset size of airline A and B were again relatively small: 7 for airline A against 34 for airline B.

9.2.6 Alternative mass representative 'distance to destination' d

At the end of the research the idea came up of an alternative mass representative: the great circle distance from AAS to each flight destination. It can generally be stated that aircraft travelling greater distances carry more fuel and hence should generally be heavier. This is investigated on a small scale by calculated the great circle distance D between AAS and each flight its destination.
Given this assessment, the following conclusions can be drawn:

Results: Although the southern and western routes combination does not show any improvement, the results for the western routes combination does. The correlation coefficient r for this route combination is high ($r = 0.512$) with a low probability value p ($p = 0.001$), hence this dataset shows an increase in L_{max} level when the distance to the destination D increases. In other words, taking the previous assumption into account, when the aircraft is heavier it causes a higher maximum noise level.

Results in perspective: However, it can not readily be stated that D is a better m representative than V_{lof}^2, although the results are better for one routes combination. It can only be concluded that for this specific routes combination it is better to use D as a predictor to assess L_{max}. For the time being, this is left as a potential better predictor for future research regarding this thesis topic of interest.

9.3 Recommendations

Given the approach as used during this MSc thesis research, the following recommendations can be drawn:

Dataset size: Some of the conclusions were drawn an a dataset which was very small. To be able to draw fundamental conclusions it is better to collect a larger dataset. To assure approximately the same weather conditions it would therefore be better to collect measurements over one entire season.

Varied dataset: From this dataset only one aircraft type could be studied. In future research it would be better not only to study one aircraft type. Hence, a varied dataset is recommended.

Runway versus measurement location: NOMOS possesses multiple stations which measure aircraft noise. As the route flown provided to significantly influence the measured maximum noise levels this would advocate to use an other runway versus measurement location combination.

RADAR versus ADSB: RADAR determines the position of an aircraft with a sample frequency of approximately four seconds (0.25 Hz). The spectrograms for the PFM are corrected for the Doppler effect by using position data originating from RADAR (TAR4). To improve position data it would be better to use ADS-B data since ADS-B provides position data with a sample frequency of a half of a second (2 Hz) which takes care of a smaller distance over which there should be interpolated between two data points.

NOMOS versus other measurement methods: NOMOS has its great advantage that it measures aircraft noise continuously and does not require anyone from assisting during its measurements. Nevertheless, the purpose of NOMOS is to provide information regarding the level of aircraft noise in an inhabited area, hence the locations are often not very close to the runway. To improve the noise measurements of this study, it is recommended to perform the same study with qualitatively better aircraft noise measurements which have been obtained closer to the runway to assure the less background noise as possible. For example, placing a mobile microphone in the extension of runway 36L of AAS (the 'Polderbaan') provides much better noise measurements since the area surrounding runway 36L is uninhabited and located in the farmland.

Relation between NOMOS times and RADAR times: From this research followed that there is an off-set between the times of NOMOS samples and the starting times of RADAR data. The variability between these times were not constant and hence it should be studied extensively how these times between these two data sources are related.

Noise abatement measure: In this study a difference in acceleration height is studied and its effect on the measured maximum noise level. For future research and for development purposes it is advised to study a noise abatement measure from which the difference in measured maximum noise level is expected to be significant, because the expected difference in this study was only 2 dB. Also, other noise abatement measures could involve the possibility to include landings as well as departures, which enlarges the dataset.

Static harmonic: In this study the expected visible harmonic for each aircraft has been set in advance. For future study, it would be better to use a dynamic harmonic finder to check which harmonic is visible in each spectrogram, in stead of predetermining which harmonic will be visible.

Image processing: To find the actual engine setting $N1$, improvements can be made in the method used. For example, image processing has already been used for multiple other purposes as for example car sign recognition [5] and 3D-trajectory tracking of a moving car [12]. In fact, one is looking for a tonal noise component at one of the frequencies of the spectrogram.

Other representative for aircraft mass: No qualitatively good representative has been found for the aircraft mass m. Hence, to judge whether or not aircraft mass is a good predictor, a better aircraft mass representative has to be found or, when the data is available, aircraft mass has to be investigated. In this study, aircraft mass has not been investigated extensively and requires extra research to be able to conclude on the predictive capabilities of aircraft mass on the maximum noise level L_{max}.

Gauging the algorithms and draw fundamental conclusions: To be able to gauge the algorithms and to check for the quality of the methods it is better to use the Cessna Citation of the TU Delft, for example, and to perform noise measurements from which the aircraft engine setting and mass are known. Multiple flyovers with variation in aircraft mass and engine setting provides the possibility to draw fundamental conclusions. Also, the quality of the algorithms can be checked very easily because the setting and configuration is known in advance.

Cooperation with a large airline: A partnership with a large airline provides more data which was found to be necessary for this research. More data provides the possibility to be able to exclude more parameters from the dataset, hence could improve the distinctive capabilities between noise measurements. Also, the PFM can be validated on its quality for a large dataset. Since in this research no real-time

$N1$ data was available, only a small dataset was tested on its quality by manually determining $N1$ and comparing these to the outcome of the PFM. However, a large dataset provides the possibility to draw fundamental conclusions regarding the quality of the PFM.

Bibliography

[1] AIP Netherlands. Schiphol rwy 18l standard departure chart-instrument. Technical report, Air Traffic Control The Netherlands, 2014.

[2] Schiphol Amsterdam Airport. Effecten op de omgeving. URL: http://noiselab.casper.aero/ams/#menu=g_effect_op_de_omgeving/page=g_geluidbelasting/target=subcontent [cited 7th April 2014].

[3] Schiphol Amsterdam Airport. Stakeholder strategy and development. Online, n.d.

[4] H. Alders. Wat doet de alderstafel? [online]. n.d. URL: http://www.alderstafel.nl [cited 13th March 2014].

[5] Yuji Aoyagi and Toshiyuki Asakura. A study on traffic sign recognition in scene image using genetic algorithms and neural networks. In *Industrial Electronics, Control, and Instrumentation, 1996., Proceedings of the 1996 IEEE IECON 22nd International Conference on*, volume 3, pages 1838–1843. IEEE, 1996.

[6] Michael Arntzen. *Aircraft noise calculation and synthesis in a non-standard atmosphere*. PhD thesis, Delft University of Technology, 2014.

[7] G. D. Bergland. A guided tour of the fast fourier transform. *IEEE*, 1969.

[8] M. M. Boone, T. C. V. D. Dool, P. Sijtsma, and U. Stelwagen. Microphone array technology for aircraft noise measurements. *InterNoise 2000*, August 2000.

[9] Chris Bradly. The 737 technical site. Website, 1999. URL: http://www.b737.org.uk/vspeeds.htm#Take-Off_Speeds_.

[10] Capt. P. Boone. *Noise Abatement Procedures*. Boeing 737 Management Reference Guide, June 2006.

[11] W. Dobrzynski, L. C. Chow, P. Guion, and D. Shiells. A european study on landing gear airframe noise sources. *AIAA*, 1971.

[12] Leonie Dreschler and H. H. Nagel. Volumetric model and 3d-trajectory of a moving car derived from monocular tv-frame sequences of a street scene. In *Proceedings of the 7th international joint conference on Artificial intelligence-Volume 2*, pages 692–697. Morgan Kaufmann Publishers Inc., 1981.

[13] Louis J. J. Erkelens. Research into new noise abatement procedures for the 21st century. *American Institute of Aeronautics and Astronautics*, 2000.

[14] A. Filippone. Aircraft noise prediction. *Progress in Aerospace Sciences*, 68:27–63, March 2014.

[15] M. R. Fink. Noise component method for airframe noise. *AIAA*, (1271), October 1977.

[16] Global Virtual Airlines Group. *Delta Virtual Airlines*. Delta, 4th edition, April 2013.

[17] Schiphol Group. Geluidmeetgegevens schiphol actueel te bekijken. URL: http://www.geluidnieuws.nl/2005/juli2005/schiphol.html [cited 6th April 2014].

[18] M. F. Heidmann. Interim prediction method for fan and compressor source noise. Technical Report TMX-71763, National Aeronatics and Space Administration, 1979.

[19] ICAO. *Aircraft Noise*, n.d.

[20] International Civil Aviation Organization. Review of noise abatement procedure research and development and implementation results. Online, 2007.

[21] KNMI. Daggegevens van het weer in nederland. URL: http://www.knmi.nl/klimatologie/daggegevens/index.cgi.

[22] LDS-Group, editor. *Understanding FFT windows*, number 14, 2003. URL: http://www.physik.uni-wuerzburg.de/~praktiku/Anleitung/Fremde/ANO14.pdf.

[23] Y. Liu and A. Dowling. Assessment of the contribution of surface roughness to airframe noise. *AIAA*, 45(4):855–869, April 2007.

[24] NASA. How does a jet engine work? Technical report, National Aeronatics and Space Administration, n.d.

[25] J. Pan, Sun. H. M., B. S. Walsh, K. D. Do, P. O'Neill, and J. Ranasinghe. Analysis and reduction of blade passing noise of the entecho mupod. *Acoustics Australia*, 38(1):12, April 2010.

[26] William Roberson and James A. Johns. Fuel conservation strategies: Takeoff and climb, 2008.

[27] H.A. Siller and U. Michel. Buzz-saw noise spectra and directivity from fly-over tests. *American Institute of Aeronautics and Astronautics*, 2002.

[28] James R. Stone. Interim prediction method for jet noise. Technical Report TM-X 71618, National Aeronatics and Space Administration, 1974.

[29] G.L. Strang van Hees. Globale en lokale geodetsiche systemen. Technical report, Delft University of Technology, 2006.

[30] The International Council of Aircraft Owner and Pilot Associations. http://www.iaopa.eu/fuelprices. URL: http://www.iaopa.eu/fuelprices.

[31] Wikipedia. File:turbofan operation.svg. URL: http://en.wikipedia.org/wiki/File:Turbofan_operation.svg.

[32] G. S. K. Wong and T. F. W. Embleton. Variation of the speed of sound in air with humidity and temperature. *Journal of Acoustical Society of America*, 77(5):1710–1712, May 1985.

[33] Xin Zhang. Airframe noise: High lift device noise. *Encyclopedia of Aerospace Engineering*, 2010.

[Page intentionally left blank]

Appendix A

Expected Harmonic

Table A.1 indicates the expected harmonic k which will be visible in the spectrogram of the associated aircraft type. This table has been established by investigating multiple spectrogram for each aircraft type, hence assuming that k will be constant for all spectrograms of a specific aircraft type.

Table A.1: Expected harmonic per aircraft type

Aircraft	Harmonic	Aircraft	Harmonic
A306	2	B752	1
A310	2	B753	1
A318	1	B763	1
A319	1	B772	2
A320	1	B77L	3
A321	1	B77W	3
A332	2	B788	4
A333	2	CRJ9	1
A343	1	CRJX	1
A388	3	DH8D	38
AT72	26	E145	1
B712	1	E170	1
B733	1	E190	1
B734	1	F100	1
B735	1	F50	30
B736	1	F70	1
B737	1	MD11	1
B738	1	MD83	1
B739	2	RJ1H	1
B744	2	RJ85	1
B748	4		

[Page intentionally left blank]